How to Use this Test Plan & Post Access Report Template

This document provides a template for both the Test Plan and the Post Access Report. Instructions on how to use this template are as follows:

- When developing the Test Plan, please complete Sections 1-6 of the template. Sections 7-10 can be removed. Please add Appendices as needed.
- When developing the Post Access Report, please complete all sections of this template. Sections 1-6 should be based on the Test Plan that was submitted. For the Post Access Report, Sections 1-6 must be updated to reflect where actual work deviated from the Test Plan, or where additional information is needed to describe the work actually performed during testing. Any changes to Sections 1-6 in the Post Access Report must be indicated using track changes for Version 2 described below.
- The Executive Summary section of the template should only be completed for the Post Access Report and does not need to be completed for the Test Plan
- Mark all items that are considered intellectual property (IP) in the document by highlighting in yellow. IP highlighting will be reviewed to ensure consistency with the IP agreement established with the TEAMER Network Director.
- Provide two (2) versions of the finalized Post Access Report. Version 1 should include information for immediate public viewing with protected data redacted or excluded. Version 2 must include all protected data as stated by the data requirement guidelines for the award.

Notes on guiding text provided throughout this template:

- Blue text provides guidance throughout this template. All blue text must be removed prior to submitting the completed Test Plan and Post Access Report documents.
- Black text defines the structure for the Test Plan and Post Access Report. Black text should not be removed or modified without approval from the TEAMER Network Director.

TEAMER
Testing & Expertise for Marine Energy

Test Plan

Numerical modelling of a unique half submerged, biconcave buoy that extracts surge and heave motions

Awardee: Laminar Scientific Inc.

Awardee point of contact: Narayan R Iyer

Facility: AMOG Consulting Inc.

Facility point of contact: Andrew Kilner

Date: January 14 2022

EXECUTIVE SUMMARY

Laminar Scientific has designed a unique WEC system which is meant to capture energy through horizontal wave forces and vertical buoyancy forces. The system is composed of a rectangular shaped buoy with concave sides that is tethered by 4 mooring lines. Each mooring line is attached to a reel located inside of the buoy structure. As the buoy moves along with the waves, the mooring lines pay in and out of the reels which drives a series of generator mechanism to capture the wave energy and convert to electrical power.

AMOG was engaged by TEAMER to conduct a series of numerical analysis to assess the performance of Laminar Scientific's WEC design. Using PacWave South as the primary environment, AMOG performed hydrodynamic analysis on the system and investigated design parameters such as buoy size and geometry to optimize the performance of the system.

To assist Laminar Scientific, AMOG:

1. **Created an OrcaFlex model** of the Laminar Scientific WEC system. This model was built using specifications which were provided by Laminar Scientific.
2. **Performed regular wave hydrodynamic analysis** of the WEC system using PacWave South site conditions to understand the performance of the WEC for these wave conditions. The analyses were performed for the original buoy model and four subsequent iterations of the buoy considering regular wave approximations. Each iteration considered variation in buoy parameters such as overall dimensions, damping, inertia and geometry. Of the Base Model and four iterations, one iteration was chosen for irregular wave testing.
3. **Performed irregular wave hydrodynamic analysis** on the chosen iteration to investigate factors such as buoy stability and mooring line loading. The chosen iteration was assessed over a simulation period of 3 hours for a range of sea states which were determined based on the PacWave south site conditions. These simulations considered first order wave loading as well as drag and radiation damping.
4. **Assessed the system's performance** for the base model and each of the iterations. The motions and behavior of the models were compared to determine which design parameters had the most influence on the performance of the WEC system.

The following conclusions were made as a result of the work undertaken.

1. The power at the mooring line connection to the reels is driven by the surge and heave motions of the buoy, and the system performs best when the buoy follows the elliptical path of the waves.
2. The Base Model configuration, which is included the original buoy design parameters, exhibited uncontrolled buoy motion in some regular wave conditions. Typically, these conditions had small wave periods or wave periods near the heave or roll natural response periods of the system.
3. Increasing the size of the buoy resulted in an increase in the stability of the system. A larger buoy showed less uncontrolled motions than a smaller buoy for the same wave cases. Analysis of the larger buoy size also indicated that the average power at the mooring line to reel connection point is increased when the size of the buoy is increased.

4. Reducing the inertia of the internal rotational mechanisms has a significant effect on the stability of the system. As this inertia becomes smaller, it becomes easier for the system to recover from uncontrolled motion and snatch loading of the mooring lines. The reduction of inertia does not have a noticeable effect on the average power seen at the mooring line to reel connection points.
5. When the concavity of the buoy is removed and replaced with flat sides the performance of the system is similar to that of the concave buoy. However, the concave does see slightly more power at the mooring line to reel connection points than the flat sided buoy.
6. For the original range of irregular sea states tested, the buoy motions were unstable, and the mooring lines exhibited snatch loading. This resulted in line tension spikes which exceeded the MBL of the mooring lines. Additional simulations were performed for sea states with a reduced significant wave height. The results of these cases indicated that the system is more stable and that the snatch loading is reduced in smaller sea states.
7. The current mooring configuration of the system offers little resistance against yaw motions. Slight yaw motions quickly can quickly become uncontrolled, and the mooring system is unable to recover reliably.
8. While the system performed best in smaller sea states, further analysis and iteration of the system may be conducted to improve its performance. This may include investigation into reducing the inertia of the internal mechanisms and increasing the yaw resistance of the mooring system.

1 INTRODUCTION TO THE PROJECT

Laminar Scientific's unique WEC buoy is a biconcave, half-submerged system that serves to harness horizontal components (surge) of wave forces in addition to vertical buoyancy (heave) forces to capture a resultant circular wave motion. The submerged portion ensures that there is a significant amount of surface area for surge capture. However, it is not fully submerged because floating buoys capture more heave motion than fully submerged buoys for the same volume, with a greater bandwidth of energy capture due to greater possible buoyancy fluctuations. The buoy is connected to several tensile members to transmit captured forces (this statement is supported by the following paper: https://www.sciencedirect.com/science/article/pii/S0960148117301829)

In order to get half-submerged in calm seas, we add ballast weight toward the bottom of the buoy; this lowers the center of gravity and brings the buoy down to the desired submergement.

This project serves to perform numerical analysis of this design, within PACWAVE South as the primary scenario, to optimize parameters such as size, generator damping coefficient and buoy restorative forces, and further study the motion and stability optimized solution in nominal and extreme scenarios.

Note: Yellow highlighted material is patent pending by Laminar Scientific but not confidential.

Laminar Scientific has two versions of this buoy:

- Version 1 has concavity in a lateral direction only and has a more voluminous mid-section compared to its vertical ends.

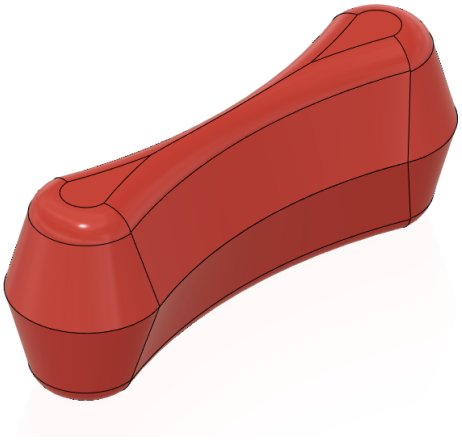

Figure 1: Buoy Version 1

  - A rudimentary test of version 1 in a small wave setting showed complexities in maintaining stability, needing CoG to be very low.
  - Response amplitude operator (RAO) simulation results are shown in Appendix A (ultimately V2 chosen over this version)

- Version 2 has concavity along lateral and vertical directions of the buoy

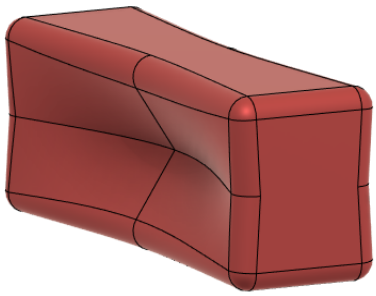

Figure 2: Buoy Version 2

- The version 2 buoy has less shape complexities
- Rudimentary tests in a small wave setting showed increased stability
- Simulations show increased surge capture and heave (Appendix A; V2 chosen)

2 Roles and Responsibilities of Project Participants

Individual project participants are listed below under their corresponding companies
Laminar Scientific Inc. - Applicant

- Narayan Iyer - Founder and CEO
- Brady Kakert - Prototype and Test Engineer
- Jian Tan - Simulation Engineer
- Madison Richard - Operations Manager

AMOG Consulting Inc. - Facility

- Andrew Kilner - Project Director
- Craig Dillon-GIbbons - Project Manager (Lead Engineer)
- Dr. Hayden Marcollo - Specialist Consultant and Director
- Jon Gumley - Lead Engineer
- Adrian Eassom - Lead Engineer
- Additional support from junior engineers.

2.1 Applicant Responsibilities and Tasks Performed

Pre-test plan: Scope discussion and planning with AMOG, understand TEAMER feedback and suggest scope accordingly.
Complete pre-test plan deliverables (see Appendix A for the resulting report):

- Initial RAO simulation using NEMOH
- Rudimentary tank test and analysis of V1 and V2
- Manufacturing Opinion
- Version Selection Opinion

Complete pre-project deliverables (post test plan):

- Convey to AMOG: expected moments of inertia and CG location based on our super buoy design, which is illustrated in a simplified manner below:

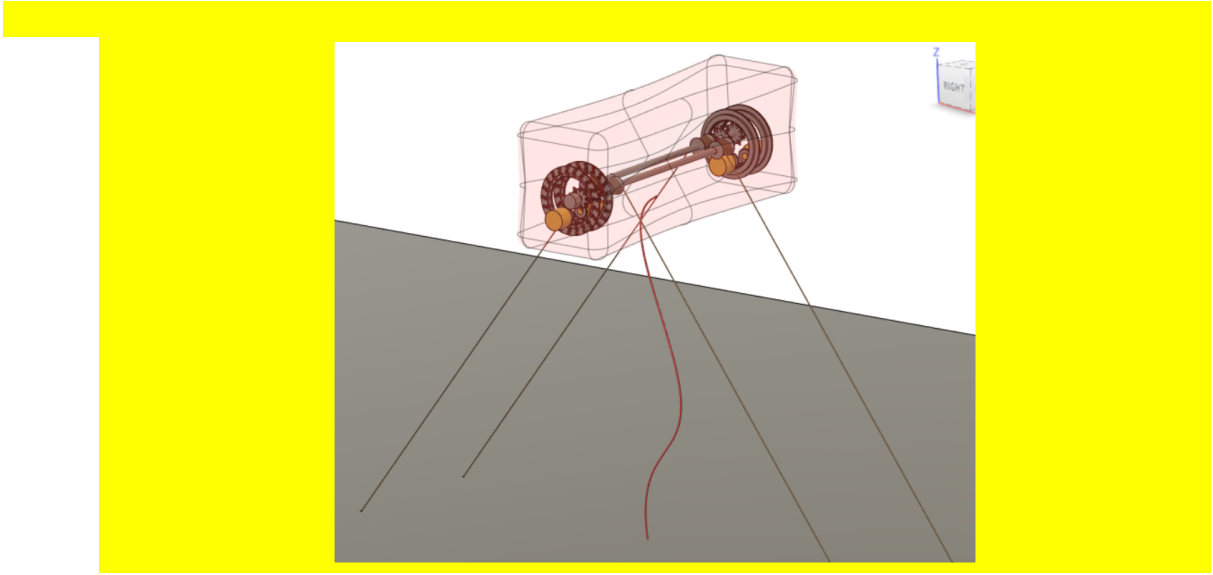

Figure 3: Super buoy design

- Send AMOG Associated CAD files for the chosen buoy version
- Discuss and set recurring meeting plans as well as milestone meetings / presentations
- Provide University of Iowa wave maker and tank details for AMOG's scaling task (last task)

During project:

- Answer any questions by AMOG at any time before and throughout project
- Attend all meetings and coordinate individual participation
- Participate in the optimization process of the buoy design including buoy geometry and mass properties, generator damping and spring configuration
- Provide design, manufacturing, and cost contexts/implications as the study proceeds
- Provide boundary conditions based on practical contexts if any solutions do not converge or occur in unrealistic ranges.

After project:

- Build the post access report along with AMOG
- Plan University of Iowa test, plan TEAMER application
- Coordinate release analysis results as soon as possible (not 5 years)

2.2 Network Facility Responsibilities and Tasks Performed

Pre-test plan: Scope discussion and planning with AMOG, understand TEAMER feedback and suggest scope accordingly.

Pre-project:

- Receive inertia metrics and CG
- Receive CAD files
- Quick sanity review in the received metrics and files
- Discuss and agree upon recurring meeting plans as well as milestone meetings / presentations

During project:

- Review and comment on Laminar's pre-project deliverables (Appendix A)
- Attend all meetings and coordinate individual participation

- Carry out the numerical analysis scope as discussed in the work plan (section 6 of this report)
- Present results as milestones are achieved
- Discuss any requirements or questions with Laminar

After project:

- Build the post access report along with Laminar

3 PROJECT OBJECTIVES

The objectives if the project are outlined below:

- The goal is to find the optimal parameters for the PACWAVE environment for the biconcave half-submerged buoy using numerical analysis. The parameters to be optimized are the buoy size, the buoy restorative forces (rotational spring or weight system to bring buoy back to an equilibrium state and keep rope taut) and finally the generator damping coefficient. Section 6 details the specific work plan. Power estimations will occur as a part of the optimization task.
- A motion and stability study of the optimal solution on nominal and extreme conditions.
- Our hypothesis on the Laminar 1 Buoy is that biconcavity allows for increased CD and therefore captures surge motion more effectively. This unique WEC has high Kc and thus importance to CD arises. Surge + Heave (through buoyancy) is captured more effectively, thus bringing down LCOE and increasing power output.
- Laminar is close to receiving manufacturing feedback on the buoy at a nominal size of 6m long at the same aspect ratio, leading to a width of 1.8m. This feedback will help understand the upfront cost impact to LCOE, and this information will be included in the project for reference and release.
    - The manufacturers will provide quotations on buoy V2 vs a simple hollow box design of 6 by 2 meters, along with a design suggestions
    - The build plan involves hollow skeletal structures and sheet metal built around it. The sheet metal will attain the flexibility to allow concavity. Rough initial estimates conveyed a buoy price increase of 17% due to the bi-concavity.
- Due to the biconcavity:
    - One can expect a slight increase in the upfront cost in building the buoy body
    - Operation costs will see no difference
    - No cost differences occur in PTO, rectifier, or other components
    - Maintenance costs might see a slight increase when skin repair needs to occur
    - However, the concavity causes an increase in drag forces. An estimated CD increase from 1.98 flat to 2.3 concave (literature for Re 10^4 -10^6) causes a greater surge force capture on both the crest and trough, and thus increased surge energy capture
    - These values are literature estimates of a flat faced prism vs a concave faced prism
    - Therefore, one can expect a decrease in LCOE compared to a boxed buoy that is also partially submerged
    - With increased surge force capture on both wave crest and trough without added mass, power-to-weight ratios should increase

This numerical analysis, coupled with the feedback from manufacturers, and further calculation of our rectifier and PTO costs (outside this project) will allow Laminar to estimate LCOE for the fully integrated system, results of which Laminar will make available to public.

We can also perform power comparisons with existing WECs for similar conditions. This data will allow anyone to compare their buoys to ours through data in MHK.

4 TEST FACILITY, EQUIPMENT, SOFTWARE, AND TECHNICAL EXPERTISE

AMOG Consulting's numerical test facility will be used to conduct this research project. AMOG will use the OrcaFlex numerical analysis software to conduct most of this analysis work. OrcaFlex is a dynamic analysis software package that is used extensively in the offshore marine systems sector. It has capabilities that allow for the modelling of complex marine systems which include the ability to model pulley systems with wave/current interaction. In combination with OrcaFlex, AMOG will use OrcaWave, a 3D panel element potential flow solver to build a numerical model of the buoy and generate response amplitude operators, (RAOs) for integration into the OrcaFlex model.

Many of AMOGs team members have used OrcaFlex and are very intimate with how it runs and how to achieve the best model representation of the Laminar's system.

Should any post processing of the OrcaFlex results files be necessary AMOG propose to use either the python/MATLAB or Julia programming languages.

The key personnel that will be used on this project include:

- Andrew Kilner - Project Director. Andrew has over 20 years of consulting experience in the offshore industry, with strengths in both project management and technical engineering. Andrew's has extensive experience in advanced numerical modeling, and his specialist expertise is used on numerous projects, including the DeepStar Joint Industry Technology Development project of which BSEE is a participant. Andrew is a registered Professional Engineer in the state of Texas.
- Craig Dillon-Gibbons - Project Manager. Craig has over 10 years of consulting experience in the offshore industry, with strengths in both project management and technical engineering. Craig has extensive experience in advanced numerical modeling, and his specialist expertise is used on numerous projects, including the management and development of the VIV specialized engineering software SHEAR7.
- Dr Hayden Marcollo - Technical Lead. Dr. Hayden Marcollo is a Director in the AMOG Group and over 15 years in the offshore energy sector. Hayden's background is a mixture of industry and research. Hayden has a PhD in Offshore Engineering and held a postdoctoral research position at M.I.T. which included both physical and numerical modelling of underwater systems. During 2017-2019 Hayden achieved international recognition (via media) for development of arguably the world's leading prospect for commercial wave energy converter (WEC) technology.
- Jon Gumley - Technical Lead. Jon Gumley is a Lead Engineer at AMOG Consulting and is the Marine Team Lead. Jon's 10 plus years of experience has come in many project roles, from technical delivery to project lead through to project management. Jon's wide range of engineering skill-sets have primarily been developed in the offshore industry including: hydrodynamic loading and response of floating offshore structures and their moorings and riser systems; monitoring of offshore installations; detailed appraisals of metocean data; and, supervision of installation works. Jon was AMOG's project manager for the design phase of AMOG's WEC technology. Jon is a registered Chartered Engineer in the UK.
- Adrian Eassom - Technical Lead. Adrian's 10+ years wealth of experience includes offshore engineering projects from pre-FEED through to detailed design, with specific emphasis in mooring and riser system design and analysis. Adrian is recognized by his clients as an expert practitioner of the industry recognized software OrcaFlex. Adrian also specializes in data analysis, machine

learning and algorithm development. These skills have been used to provide solutions and tools for clients in the Offshore Oil & Gas, Mining and Mineral Refinery industries. Adrian has programming skills in Python, MATLAB, R, Julia, C, C++, C#, Java, Javascript, PHP, SQL.

CVs of personnel assigned to lead the project can be provided upon request. To execute the work in a cost efficient manner for TEAMER, these personnel will draw upon the pool of resources in the company as required.

5 Test or Analysis Article Description

The following video briefly describes the use of this biconcave buoy in a wave energy converter: https://www.youtube.com/watch?v=OIaODebeRbo. (Pardon our lack of animation/video skills at this time).

The buoy, connected to tensile members, moves in a circular or elliptical manner due to the combination of wave surge and heave capture. The captured motion is transmitted, via tensile members, to rotating members (pulley or spool embodiments) which in turn face alternating motion, that is converted to unidirectional motion via our unique, highly efficient, patent-pending motion rectifiers. The tensile members are also coupled to restorative mechanisms (counterweight or rotational spring) that removes rope slack and brings the Buoy back to an equilibrium state after each oscillation, allowing for an efficient, repeatable cyclical motion for capturing wave motion.

Below is an early proposed open water test rig off a barge:

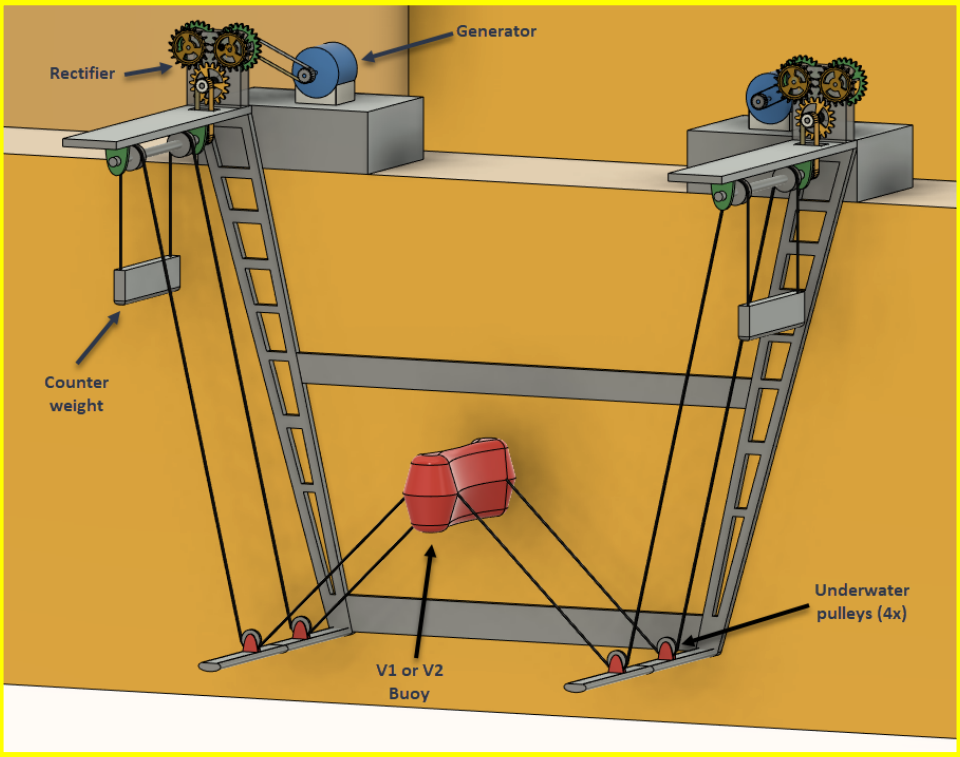

Figure 4: Proposed open water test rig

Our hypothesis on the Laminar 1 Buoy is that biconcavity allows for increased CD and therefore captures surge motion more effectively. This unique WEC has high Kc and thus the importance to CD arises. Surge + Heave (through buoyancy) is captured more effectively, thus bringing down LCOE and increasing power output. This numerical analysis not only tests the hypothesis, but also finds optimal solutions for the usage of the Buoy. This is a logical next step before any tank testing is performed. Our technology will be licensable, and will be patented in several countries, whilst allowing any profits from said license to be made in the US. Our goal later is to build a power plant with these WECs.

The Laminar Biconcave buoys can be used in several different WEC contexts: see Appendix B for use cases (offshore structure, standalone, near-shore configurations).

6 Work Plan

6.1 Numerical Model Description

6.1.1 Scope of Work

LSI has requested AMOG support with the following:

1. Hydrodynamic numerical modeling to optimize the Laminar-1 buoy, restorative forces (hang weight) and generator system for the PacWave location.
2. Identification of whether the chosen Laminar-1 buoy would experience either irrecoverable instability or over-utilization of the mooring system at PacWave in the design sea state.
3. A scaling study for the chosen Laminar-1 buoy configuration for physical model testing at University of Iowa IIHR wave basin

AMOG will conduct the following activities to meet the project objectives.

1. Develop a project Basis of Analysis & Document Review;
2. Construct a numerical model of the Laminar system;
3. Conduct numerical optimization of the Laminar system;
4. Extract and interpret the result of the Laminar system;
5. Reporting of the numerical optimization of the Laminar system
6. Preparation of Model Test Scaling report.

Each of the activities mentioned above are expanded on in the subsequent sections.

6.1.2 Basis of Analysis & Document Review

Prior to commencing any numerical modeling, AMOG will provide a Basis of Analysis to Laminar for this scope. This document will include:

- PacWave site particulars; including both ambient and design sea states, design current and the proposed water depth for the Laminar-1 system deployment.
- The proprieties of Laminar-1 buoy including geometry, mass properties and drag values.
- Laminar system general arrangement.
- Mooring line construction and properties.
- Restorative force and generator properties.
- Numerical modeling assumptions.
- Outline optimization methodology including the parameter space to be explored.

This document will be submitted to Laminar for acceptance prior to commencing any modeling activities. An allowance has been included in this task for the AMOG team to review the available research and engineering undertaken for the Laminar-1 Buoy.

6.1.3 Numerical Model Construction

A time-domain numerical model for the Laminar-1 buoy system will be constructed in OrcaFlex. The buoy and mooring lines will be modeled explicitly, while the pulleys, hang weights and generator system may be modeled as a series of equivalent springs and dampers. The OrcaFlex model can be used to simulate both regular waves and irregular sea states. Further details of the Numerical Model Construction are provided in Section 6.2.

6.1.4 Numerical Modelling Optimization

A numerical optimization study will be completed of the system which will include iteration of buoy properties (size, mass, drag properties) for pre-defined combinations of generator back-torque and effective hang weights.

For each iteration:

- The buoy properties will be calculated and implemented in the reference OrcaFlex model, including:
    - Buoy geometry and mass properties,
    - Diffraction – radiation force terms from the panel element solver, and
    - Additional drag and damping terms scaled from CFD or model tests.
- The numerical model will be subject to a series of regular wave simulations for a range wave period / wave height combination that best represent the sea states as defined in the Basis of Analysis. The regular wave analysis will be run with at least 10 complete wave cycles. Here the intent is to achieve a steady state numerical solution of the system performance.
- Permutations of up to five hang weights and five generator damping coefficients will be run for each wave period.
    - Reference constant generator damping coefficient of 68.75 Ns/m
    - Reference hang weight restorative force of 700 N.

The above process will then be iterated for each buoy design. Between each iteration, a review will be held between AMOG and Laminar to agree upon the next buoy configuration to model and give Laminar the opportunity to provide the necessary geometry and mass data for the buoy.

A total of 4 iterations of buoy design has been assumed to be sufficient to arrive at an optimal solution.

Having identified the optimal configuration of the Laminar system a series of irregular wave analyses will be conducted to further characterize the performance of the Laminar system.

6.1.5 Extract and interpret the result of the Laminar system

For each simulation outlined in Section 6.4 the following will be calculated:

- Average power in each sea state, leading to LCOE values for the optimized sea states.
- Calculated moored RAO and power generated transfer function.

In addition to the above, a design condition review will be completed for the final or otherwise directed buoy-generator-hang weight system, the design review will investigate the following:

- Irrecoverable buoy stability (capsize), and,
- Mooring line load utilization against minimum break load capacity of selected rope.

This investigation will consist of simulating a 1-year return period sea state and 100-year return period sea state in the OrcaFlex model with irregular waves. To generate meaningful statistics, five simulations of at least 100 wave cycles will be run (~30 minutes) for each sea state. It is assumed that the second order forces on the system are not significant, as such, these design simulations will only consider the following force terms:

- First order wave loading
- Drag and radiation damping
- Mean current force

6.1.6 Model Test Scaling

AMOG will provide Laminar a scaling report based on the basin depth and wave making capability of the University of Iowa IIHR wave basin.

6.2 Numerical Model Construction

As indicated in Section 6.1 AMOG propose to construct a time-domain numerical model of the Laminar-1 buoy system in the OrcaFlex software program. The buoy and mooring lines will be modeled explicitly, while the pulleys, hang weights and generator system may be modeled as a series of equivalent springs and dampers. The OrcaFlex model can be used to simulate both regular waves and irregular sea states.

AMOG has assumed that the buoy will pick up a non-negligible amount of diffraction wave loading. To calculate the diffraction force on a wetted surface, a panel element model of the buoy will be constructed and run for each buoy size iterated. AMOG will use the OrcaWave package to construct the panel element model.

The time-domain numerical model will then go through AMOG's standard checking and quality assurance processes, including time step and line segmentation, run time optimization for an efficient model to use for the optimization study below. AMOG will conduct sense checking of the model prior to conducting the optimization part of the scope. Sense check will include assessing the time step requirements and line segmentation to achieve an accurate representation of the system while maintaining a reasonable analysis run time. Through the course of the model development the boundary conditions of the system will be reviewed to ensure convergence of the model.

AMOG has conducted many highly complex analyses on a range of systems from Oil and Gas mooring and riser systems, wave energy converter systems, fish farms, and complex coupling between multiple bodies. For many of these studies AMOG has had access to physical model testing results at a range of scales. These physical model tests results have been used to validate the analysis OrcaFlex approach. AMOG can provide examples of such projects should they be necessary.

6.3 Test and Analysis Matrix and Schedule

The PACWAVE conditions have been defined, AMOG proposes to conduct the initial optimization on a range of regular wave and period combinations provided below. Should the initial base model analysis identify that the range of periods and wave heights need to be refined this will be outlined to TEAMER prior to conducting further regular wave analyses. If no modification to the selected wave period combinations are necessary AMOG will then conduct the subsequent iterations of the LSI system for the same set of conditions.

- Regular wave/period combinations:

  - H = 1.25m, T = 4 - 14 sec in 1 second increments
  - H = 1.75m, T = 4 - 14 sec in 1 second increments
  - H = 2.25m, T = 4 - 14 sec in 1 second increments
  - H = 2.75m, T = 4 - 14 sec in 1 second increments
- Irregular sea state combinations:
  - Hs = 1.75m Tp = 7. 5 sec Tp = 8.5 sec Tp = 9.5 sec
  - Hs = 2.75m Tp = 8.5 sec Tp = 10.5 sec Tp = 12.5 sec

The outline schedule for the analysis includes the following:

- Base Model Setup and running regular wave case 25 days from award.
  - Inclusive of design review, basis of design development and the initial model build
- Iteration #1 Model Setup and running regular wave case 10 days from Laminar review of base model results.
- Iteration #2 Model Setup and running regular wave case 5 days from Laminar review of iteration #1 results.
- Iteration #3 Model Setup and running regular wave case 5 days from Laminar review of iteration #2 results.
- Iteration #4 Model Setup and running regular wave case 5 days from Laminar review of iteration #3 results.
- Optimal Iteration Model to be run with Irregular wave cases 20 days from Laminar approval of optimal case to run.

Based on the proposed scope of work outlined above and the schedule AMOG propose a total budget of $149,000 and a total estimated number of man hours of 786hrs required to complete the tasks.

6.4 Safety

AMOG does not anticipate that there will be any safety related items in the numerical testing, however, should it be needed AMOG's Quality Management System applies to the provision of engineering consultancy services in the marine, offshore, mining, defence and marine environment sectors. The Quality Management System has been approved by Lloyd's Register Quality Assurance Limited to ISO 9001:2015. AMOG has maintained this accreditation since 2001. AMOG conducts all engineering to the requirements of this Quality System. A copy of our current accreditation certificate can be provided if required.

AMOGs Standard Operating Procedures (SOPs) provide detailed instructions to employees of AMOG on how to go about completing processes that affect product quality. Together, AMOG's SOPs aim to ensure that all products produced by AMOG meet both customer requirements and the requirements of applicable legislation and standards. SOPs also provide specific instructions to ensure the compliance of AMOG processes with ISO 9001:2015.

6.5 Contingency Plans

The major risk items on this Numerical Analysis project relate to the potential issues with solving and running the very complex system. Part of AMOG Standard Operating Procedures is the development of a detailed Methodology Statement, this statement will include items related to potential issues. Should the need arise AMOG will conduct internal reviews of the system and reach out to the OrcaFlex software provider to gain possible solutions. Possible solutions may require investigation or simplification of the modelling approach which may be supplemented with hand calculations. Again, with such a complex system analysis times may be long, particularly for analysis consisting of irregular waves. If model runtime

is an issue AMOG has access to further high-powered computers to assist in reducing the solution time. Should any issues occur AMOG will correspond with Laminar to work on an acceptable solution.

6.6 Data Management, Processing, and Analysis

6.6.1 Data Management

The models and subsequent data generated through this project will be saved to AMOGs internal server. AMOG anticipates that while these models and the results files may be very large, we have sufficient storage capacity for the models and results files to be stored on the AMOG server system. To assist with run times, it may be necessary to run the analyses locally on one of AMOG high powered computers, however once the run is completed it will be uploaded to the AMOG data storage systems. AMOGs data storage system is regularly backed-up to tape drives and the storage system is a RAID server.
As part of AMOGs approach to any advanced analysis is the development of an analysis run matrix which will include the logging on the runs completed and variations in the analysis.
AMOG's ISO accredited quality management system shall be followed for the management of data, including naming conventions and detailed run logs. These shall be defined in the project's Basis of Analysis.
For each simulation above, the following will be calculated:

- Average power in each sea state
- Calculated moored RAO and power generated transfer function

AMOG will provide time histories of raw key parameter output data in 'csv' format.

6.6.2 Data Processing

The numerical modelling the LSI system will produce a range of outputs, these may include:

- Displacements and rotations of the buoy, pulleys and counterweights;
- Body forces;
- Line tensions;

Each of the above parameters will be extracted at each time step of each simulation. AMOG can extract this data and post process for further interrogation. It will be important to analyze this information to understand the performance of the Laminar system. Plotting of the various parameters will provide insight into potential errors. However, as mentioned previously AMOG has a comprehensive quality management system which has been developed for identification of potential errors prior to running extensive analysis cases.
For the optimization stages, the average power calculated in each regular wave combination will be generated to give an average power generated as a function of regular wave period and regular wave height. For each simulation, the forces on the body, motions of the body and line tensions will also be available.

6.6.3 Data Analysis

In addition to the release of all raw data, graphs showing the power vs the optimization parameters in their iterated domain will be presented, likely in the form of a 3D or 4D plot. Other raw data parameters outlined above will also be graphed against time primarily. The irregular wave analysis cases will also be graphed and statistical data such as mean, standard deviation, Most Probable Maximum, will be processed.

IEC TS 62600-103:2018 “Guidelines for the early stage development of wave energy converters” will be utilised for the development of the device.

As the model will be simulated at full scale, no scaling is required for the data analysis.

As this is a numerical model, it is not anticipated that any simulations or results shall be eliminated from the data analysis.

7 PROJECT OUTCOMES

7.1 RESULTS

7.1.1 Background

The wave energy system consists of a partially submerged buoy that is anchored with 4 mooring lines made of nylon fiber to a fixed raised platform. The buoy is hollow and contains a fly wheel mechanism meant to generate power as shown in Figure 5. During the deployment, the system will be subjected to waves which cause a response motion in the buoy. The response motion is then converted to electrical energy through the internal flywheel mechanism. The flywheel is attached to a generator which converts the rotational motion of the shaft to electrical energy. Figure 6 provides an illustration of the wave energy system deployed in field along with the mooring lines and a fixed platform.

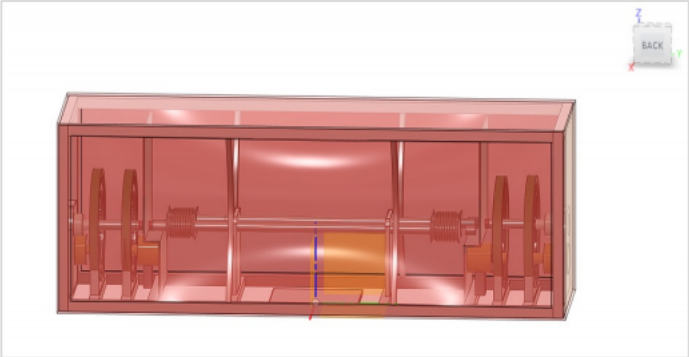

Figure 5: Buoy with interior mechanism shown

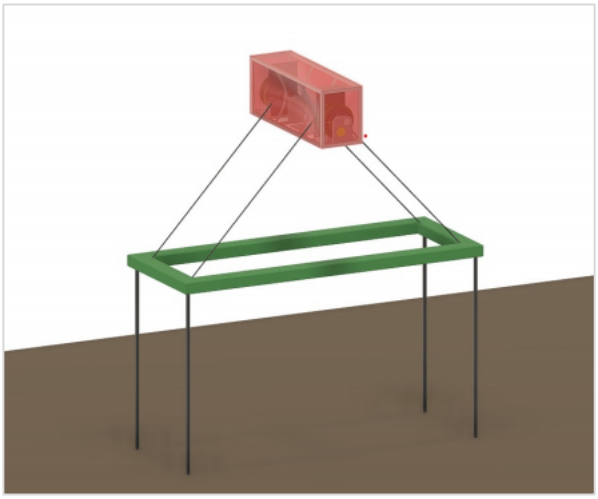

Figure 6: Buoy system deployed in field

A flywheel mechanism has been incorporated inside the buoy to convert the motions of the buoy into a rotational motion which is then used to generate power. There are 4 reels inside the buoy which act as the termination points to the mooring lines as shown in Figure 7. These reels allow for the mooring line to move as the buoy heaves and surges. The reels on the same side of the buoy are connected to a shaft which runs along the length of the buoy. These shafts in turn are connected to the 4 flywheels. The flywheels act as a planetary gear system and each rotational motion of the shaft turns one flywheel (Each shaft rotates in two ways clockwise or anticlockwise). There are two rotational springs connected to the two reel shafts. These springs provide a counter force that brings the buoy back to the equilibrium position. It is to be noted that the springs exert force only in one direction and they are modeled to always make the mooring line wound into the buoy. A gearbox is connected to each of the flywheels and the gearbox is connected to a rotor. The rotor converts the rotational motion of the flywheel into an alternating electric signal which is then passed through a rectifier to get a DC output.

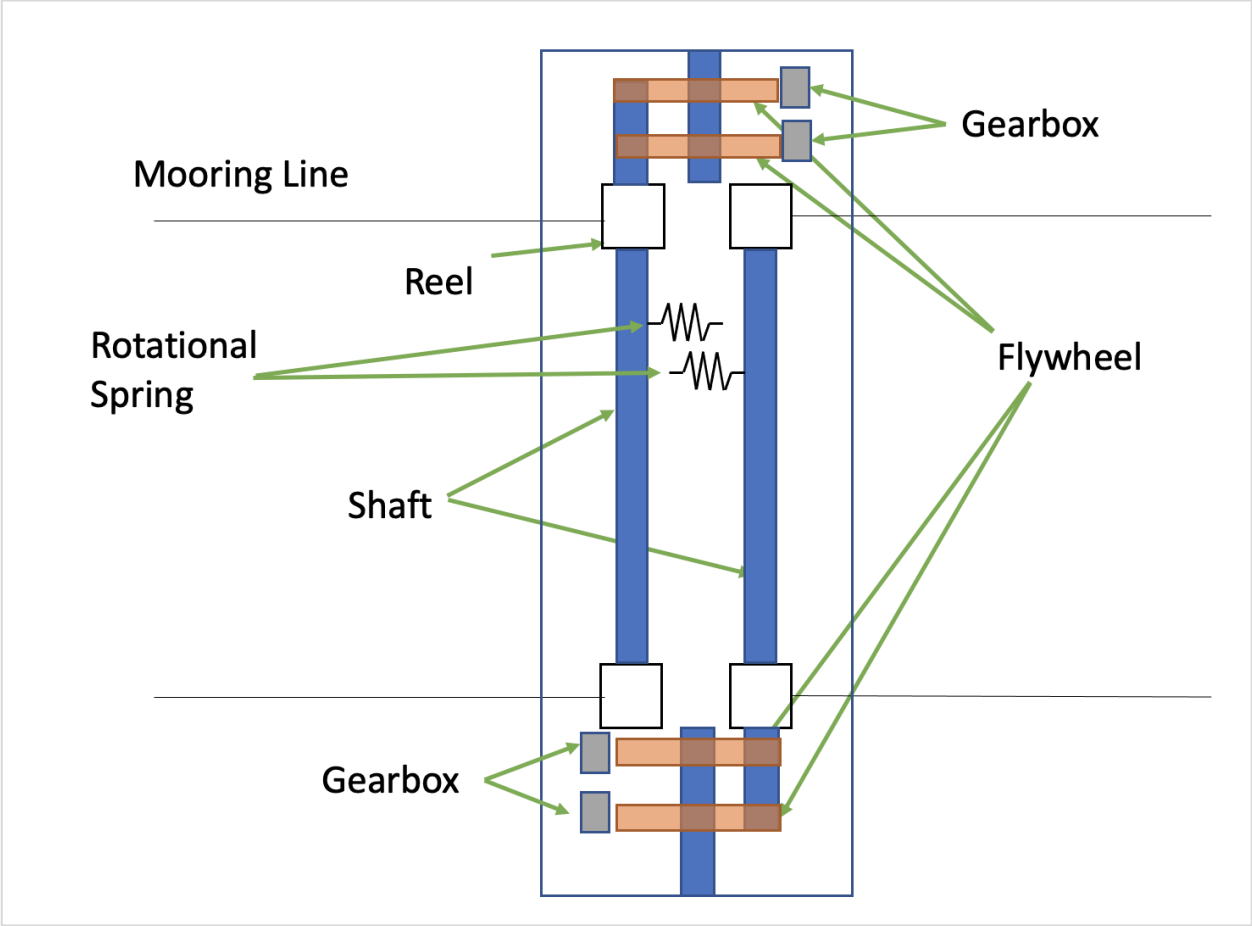

Figure 7: Internal mechanism diagram

Laminar Scientific have provided a reference table to approximate the relationship between the linear motion of the mooring line and the final RPM of the rotor. Further, it has been assumed that the power will be linearly proportional to the RPM of the rotor. The RPM of the motor will be calculated from the velocity of the mooring lines using Table 1. The reported values of the winch line velocities for all cases analyzed can be found in Appendix D.

Table 1: Motor RPM Reference Values

Absolute average rope speed [m/s]	Reel [RPM]	Flywheel [RPM]	Generator (after gearbox) [RPM]
2	121	241	1086
3	181	362	1629

7.1.2 Model Definitions

The Base Model was constructed using the CAD model of the buoy provided by Laminar Scientific. The submerged portion of the CAD model was meshed using Rhino7 and imported into OrcaWave to generate load RAOs and added mass and damping coefficients. Views of the provided CAD model are shown in Figure 8 and Figure 9 below.

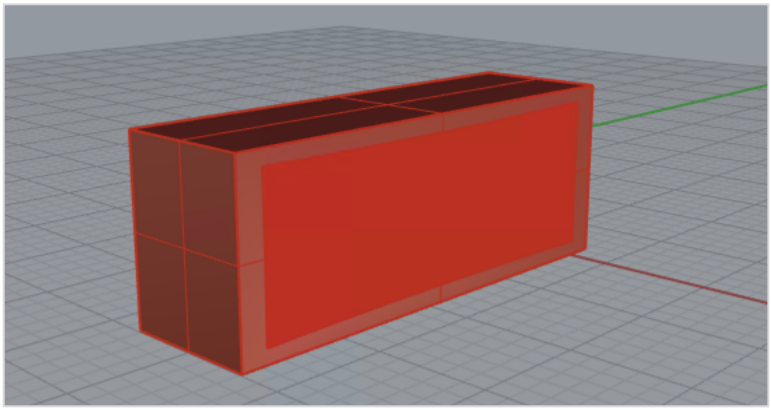

Figure 8: Buoy CAD model

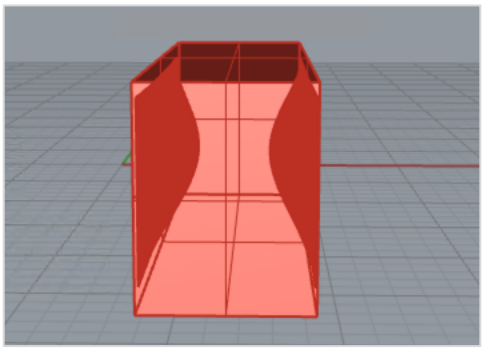

Figure 9: CAD model

To determine the influence of different parameters on the performance of the buoy, four iterations of the base model were assessed. While certain parameters differ across each iteration, the submerged depth as a percentage of the buoy height remains consistent across all models. Separate load RAOs were generated for each model which are presented in Appendix C. The Base Model and Iteration 3 model used the same load RAOs, as they both used the same buoy size and geometry for simulation. Table 2 shows the parameter changes across each iteration of the buoy. The iterations are defined as follows.

- Base Model: original sized buoy as provided by Laminar Scientific
- Iteration 1: Base Model scaled by a Froude Scale Factor of 2
- Iteration 2: Base Model scaled by a Froude Scale Factor of 3
- Iteration 3: Base Model with decoupled winches
- Iteration 4: Iteration 1 sized buoy with flat sides (curvature removed)

Table 2: Buoy Parameters

Parameter	Base Model	Iteration 1	Iteration 2	Iteration 3	Iteration 4
Mass of buoy [kg]	16,186.0	129,488.0	437,022.0	16,186.0	162,309.0
Volume of buoy [m^3]	23.94	191.52	646.38	23.94	226.85
Length of buoy [m]	6.38	12.75	19.13	6.38	12.75
Height of buoy [m]	2.39	4.77	7.16	2.39	4.77
Width of buoy [m]	1.87	3.73	5.60	1.87	3.73
Radius of the concave section [m]	0.48	0.96	1.45	0.48	N/A
Length of the concave section [m]	5.67	11.33	17.00	5.67	N/A
Height of the concave section [m]	1.99	3.99	5.98	1.99	N/A
Submerged depth of buoy [m]	1.87	3.74	5.61	1.87	3.74
Submerged depth as percentage of buoy height [%]	78.40	78.40	78.40	78.40	78.40
Mooring line outer diameter [mm]	28.58	57.15	85.73	28.58	57.15
Mooring line stiffness [kN]	96.38	385.40	867.26	96.38	385.40
Mooring line minimum breaking load (Wet – Dry) [kN]	114 – 134	455 – 535	1024 – 1205	114 – 134	455 – 535
Winch target tension [kN]	8.00	64.00	216.00	8.00	64.00
Winch inertia [kN m^2]	1,993.13	64,391.36	488,972.89	2.12	64.39

The Base Model showed instability in the buoy motions during the regular wave tests. As such the focus of Iteration 1 was to determine if a larger sized buoy would provide more stability in the same wave conditions. Iteration 1 was a 2:1 scale version of the Base Model. Scaling was performed using Froude's Law of Similitude with a λ value of 2. As a result, the mass, volume, and dimensions of the buoy were increased. For the mooring lines, the outer diameter was increased using the scale factor, and the line stiffness and minimum breaking load was determined by inputting the new line diameter into the OrcaFlex line wizard. The target tension in the mooring lines was also increased to keep a consistent ratio of submerged depth to buoy height. The winch inertias were scaled by summing the scaled inertias of each of the internal mechanisms.

The results of the Iteration 1 tests showed that the 2:1 scale buoy was more stable than the original Base Model. Iteration 2 tested an even larger sized buoy to increase the stability even further. Iteration 2 was a 3:1 scale version of the Base Model. Scaling was performed using the same method as Iteration 1 but with a λ value of 3. As with Iteration 1, the mooring line stiffness and minimum breaking load were determined using the OrcaFlex line wizard, and the mooring line target tension was increased to maintain the same ratio of submerged depth to buoy height.

The Base Model showed exceedance of the minimum breaking load in the mooring line for some of the wave cases tested. The time histories of the mooring line tensions revealed the lines were compressing and snapping back taught. This snapping motion resulted in large tension spikes which exceeded the minimum breaking load. The focus of Iteration 3 was to determine if the inertias of the internal mechanisms on the reels influenced the line behavior. The WEC system can decouple the flywheels from the reel shafts. This decoupling significantly reduces the rotational inertia that must be overcome by the mooring lines, but power cannot be generated in this state. Iteration 3 used the same scale as the Base Model but altered the winch inertias through decoupling. In this model, the winch inertia value did not include the flywheel and gearbox inertia terms. This inertia was significantly lower than that of the Base Model and was used to simulate a decoupled system.

Iteration 4 examined the effect of the concaved sides on the buoy motions. Iteration 4 used the same 2:1 scale as Iteration 1, but the curvature of the sides was removed. The flat sides resulted in a block shaped buoy with the same length dimensions as the Iteration 1 buoy. Because the curvature was removed, the Iteration 4 buoy had increased volume compared to the Iteration 1 buoy. To maintain the same submerged depth percentage and winch target tension as Iteration 1, the mass of the Iteration 4 buoy was also increased. The natural periods for surge and heave were the same as Iteration 1, but the roll natural period was increased. An image of the block CAD model is shown in Figure 10. Figure 10: Iteration 4 block CAD model

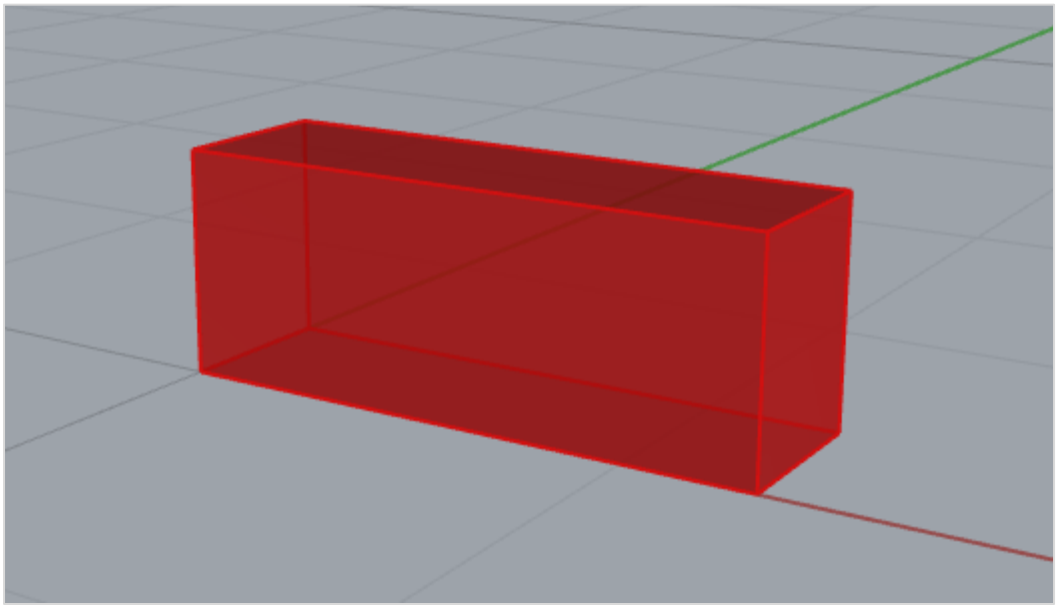

Figure 10: Iteration 4 block CAD model

Before each iteration was run, decay tests were performed to determine the surge, heave, and roll natural periods of each model. Surge, heave, and roll were determined as the 3 primary degrees of motion in line with the incoming wave. The coordinate system used describe the degrees of freedom reported is shown in the Figure 11 below.

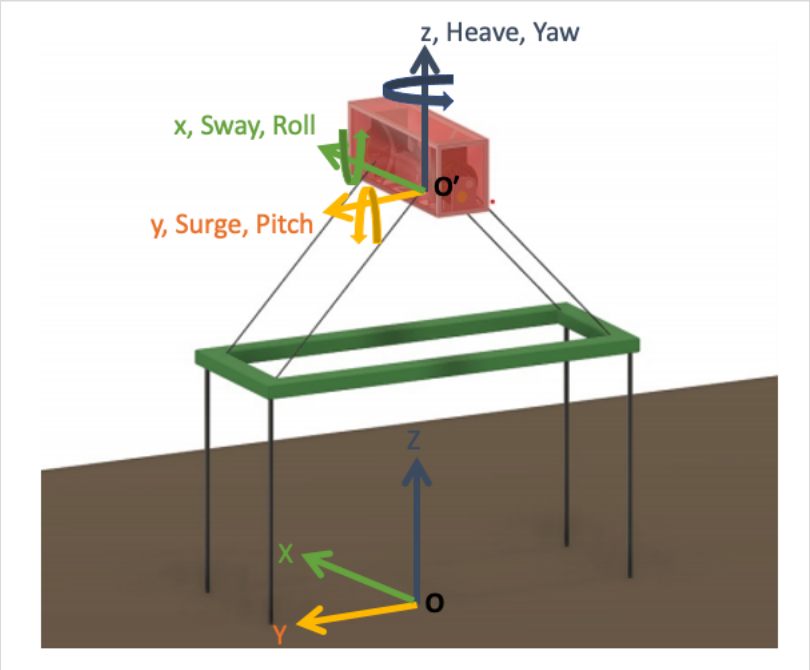

Figure 11: AMOG sign convention for buoy system

The direction of wave loading is assumed to be along the y axis for all cases. The winches are numbered such that Winch 1 and Winch 2 correspond to the winch lines on the side of the buoy on which the waves impact (wave ward). Winch 3 and Winch 4 correspond to the winch lines on the side of the buoy opposite of the wave impacts (leeward).

The changes in scale between the iterations resulted in changes in the natural periods of each model. The differences in natural period factored into the differences in behavior of each model. The surge, heave, and roll natural periods are shown in the Table 3 below.

Table 3: Natural Periods

Direction	Base Model & Iteration 3	Iteration 1	Iteration 2	Iteration 4
Roll Natural Period [s]	6.67	9.09	11.11	7.14
Surge Natural Period [s]	42.48	50.00	100.00	50.00
Heave Natural Period [s]	3.13	4.35	5.56	4.35
Yaw Natural Period [s]	20.00	33.33	33.33	33.33

In addition to the regular wave cases, each iteration was also run across five separate winch damping constants. The damping constants are as follows: 0.034, 0.068, 0.102, 0.204, and 1.020 (kN s m^{-1}). Between the four wave heights, eleven wave periods, and five damping constants, each iteration was run across a total of two hundred twenty cases.

The following equations describe the data calculation used to post process the OrcaFlex data presented in this report:

Surge Range [m]:

$$Y_{range} = Y_{max} - Y_{min} \qquad \textit{Equation 1}$$

Heave Range [m]:

$$Z_{range} = Z_{max} - Z_{min} \qquad \textit{Equation 2}$$

Roll Range [m]:

$$\theta_{range} = \theta_{max} - \theta_{min} \qquad \textit{Equation 3}$$

Accumulated Power at Reel Connection [kW]:

$$P = \sum_{n=1}^{N} \frac{F_n d_n}{t} \qquad \textit{Equation 4}$$

- F = Force in winch at buoy connection [kN]
- d = Winch line displacement [m]
- t = Length of 1 timestep [s]
- N = Number of timesteps

Average Power at Reel Connection per Wave [kW/wave]:

$$P_{avg} = \frac{P}{C} \qquad \textit{Equation 5}$$

- P = Accumulated power at reel connection [kW]
- C = Number of wave cycles over which the accumulated power was calculated

Annual Power at Reel Connection [kW/yr]:

$$P_{annual} = P_{avg} AW \qquad \textit{Equation 6}$$

- P_{avg} = Average power at reel connection per wave [kN/wave]

- A = Number of hours a given wave occurs in 1 year [hr/yr]
- W = Number of periods of a given wave that occur in 1 hour [wave/hr]

7.1.3 Regular Wave Analysis

7.1.3.1 Model Comparison

The following tables show the changes in surge, heave, and roll motions of the buoy across each model. The data for the Base Model, Iteration 1, and Iteration 2 represents the effect of the buoy scaling from 1:1, 2:1, and 3:1, respectively. Iteration 3 was the same scale as the Base Model, but it used different winch inertias. As such, it is best compared to the Base Model. Likewise, Iteration 4 is best compared to Iteration 1, as it is the same scale as Iteration 1. The differences in response between Iteration 1 and Iteration 4 are due to the changes in the buoy geometry. The data is presented for regular waves with a height of 1.75m and with a winch damping constant of 0.068 kN s m^{-1}. The 1.75m waves had the most frequent occurrence according to the PacWave document provided by Laminar Scientific, so those cases are considered to be most representative at the site. The 0.068 kN s m^{-1} damping constant was the original magnitude of generator damping provided by Laminar Scientific. Since the buoy motions did not depend on the damping constant, this value was considered representative. All data presented in this section was collected over the first five wave cycles of each simulation.

Table 4: Regular Wave Buoy Surge Comparison by Model

Wave Height [m]	Wave Period [s]	Surge range [m]				
		Base Model	Iteration 1	Iteration 2	Iteration 3	Iteration 4
1.75	4	2.30	3.71	4.73	2.23	3.90
1.75	5	1.45	1.81	2.99	1.46	1.39
1.75	6	1.64	1.90	1.78	1.64	1.21
1.75	7	2.26	1.52	1.90	2.27	1.63
1.75	8	2.22	1.25	1.61	2.22	2.29
1.75	9	2.09	1.79	1.44	2.09	2.13
1.75	10	2.07	2.36	1.31	2.07	2.01
1.75	11	2.08	2.04	1.53	2.08	1.96
1.75	12	2.11	1.96	2.44	2.11	1.94
1.75	13	2.17	1.93	2.07	2.14	1.95
1.75	14	2.20	1.93	1.94	2.17	1.94

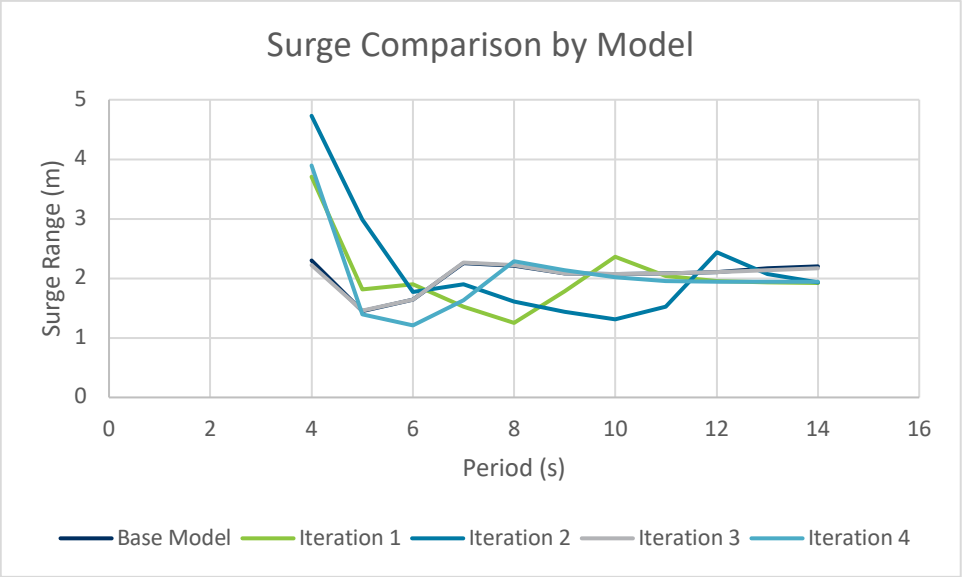

Figure 12: Surge comparison by model

Table 4 and Figure 12 show the surge range for each model across the full regular wave period range, wave height of 1.75m, and damping constant of 0.068 kN s m^{-1}. The maximum surge response occurs during the 4s period waves for all models. The maximum surge range of each model occurs for 4s period waves. The 4s period waves are short enough that the winches do not have enough time to recover the surge displacement of the buoy before the next wave impact. This results in the buoy having to reach an offset position in the direction of the wave loading before it begins to follow the orbital path of the waves. In the 4s wave scenario, it takes more than five wave cycles for the buoy to reach the offset position. Since the data presented above is collected over the first five wave cycles of the simulation, it shows the buoy drifting in the direction of the wave loading for all five wave cycles. This results in an increased surge range compared to the scenarios with longer wave periods in which the buoy follows a more orbital motion. The 5s and 6s period waves also reach an offset position, but it is closer to the buoy origin, and the system reaches the offset position within the first five wave cycles. There is a second peak in the surge range which occurs for waves which have a period near the roll natural frequency of each model. This suggests that the increased roll motions during the roll excitation causes additional surge motions. After the second peak, the surge range flattens out and slightly increases as the wave period increases. This is the result of the motion of the buoy following the orbital motion of the longer waves. When comparing Iteration 3 to the Base Model, the surge ranges are very similar. This is expected as the buoy size and geometry are the same for both models. Iteration 1 and Iteration 4 have similar magnitudes of surge motion, but the peak in surge motion due to the roll excitation occurs during waves of different periods. This is due to the difference in roll natural period between the two buoys.

Table 5: Regular Wave Buoy Heave Comparison by Model

Wave Height [m]	Wave Period [s]	Heave Range [m]				
		Base Model	Iteration 1	Iteration 2	Iteration 3	Iteration 4
1.75	4	2.20	1.69	0.51	2.18	1.69
1.75	5	1.81	2.46	1.96	1.81	2.45
1.75	6	2.05	2.03	2.74	2.05	1.99
1.75	7	1.84	1.83	2.17	1.84	1.89
1.75	8	1.72	1.78	1.90	1.72	1.78
1.75	9	1.71	1.80	1.80	1.71	1.79
1.75	10	1.72	1.76	1.78	1.72	1.73
1.75	11	1.72	1.72	1.80	1.72	1.72
1.75	12	1.72	1.72	1.76	1.72	1.72
1.75	13	1.72	1.72	1.72	1.72	1.72
1.75	14	1.72	1.72	1.72	1.72	1.72

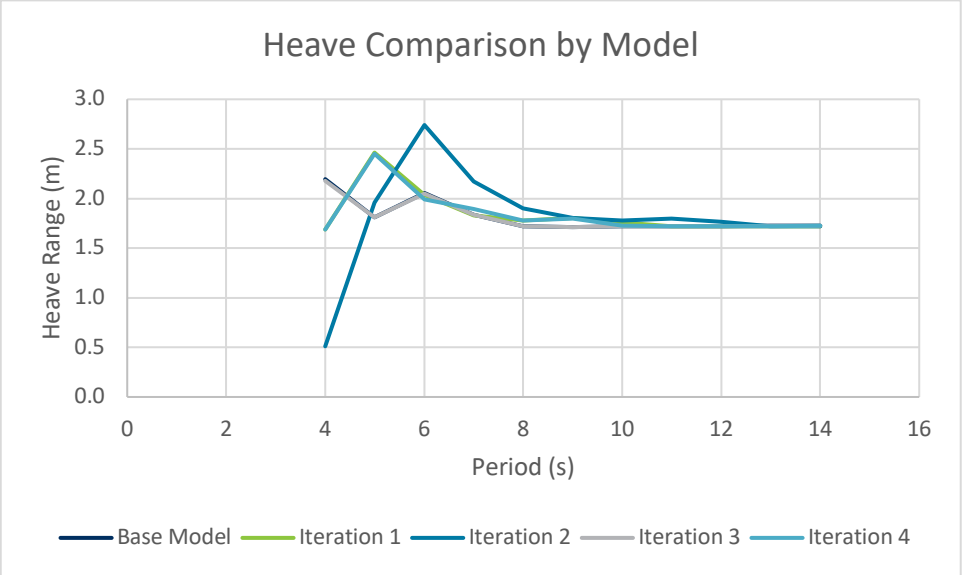

Figure 13: Heave comparison by model

Table 5 and Figure 13 show the heave range for each model across the full regular wave period range, wave height of 1.75m, and damping constant of 0.068 kN s m^{-1}. For each model, the maximum heave range occurs during waves which have a period close to the heave natural period for each buoy. As seen in the surge motions, the Base Model and Iteration 3 have very similar responses. Iteration 1 and Iteration 4 also have nearly identical responses, as the heave natural frequency is the same for both models.

Table 6: Regular Wave Buoy Roll Comparison by Model

Wave Height (m)	Wave Period (s)	Roll Range [deg]				
		Base Model	Iteration 1	Iteration 2	Iteration 3	Iteration 4
1.75	4	95.75	6.01	4.49	94.82	8.07
1.75	5	35.24	11.34	4.09	35.09	13.99
1.75	6	60.69	8.63	4.74	60.26	20.69
1.75	7	46.05	10.45	4.89	45.80	36.13
1.75	8	19.47	19.25	5.12	19.41	21.49
1.75	9	9.15	28.03	6.34	9.14	11.44
1.75	10	5.20	19.94	10.24	5.20	6.47
1.75	11	3.10	6.85	18.63	3.09	4.21
1.75	12	1.87	3.39	16.51	1.90	2.96
1.75	13	1.53	1.91	5.21	1.47	2.18
1.75	14	0.38	1.06	2.47	0.37	1.94

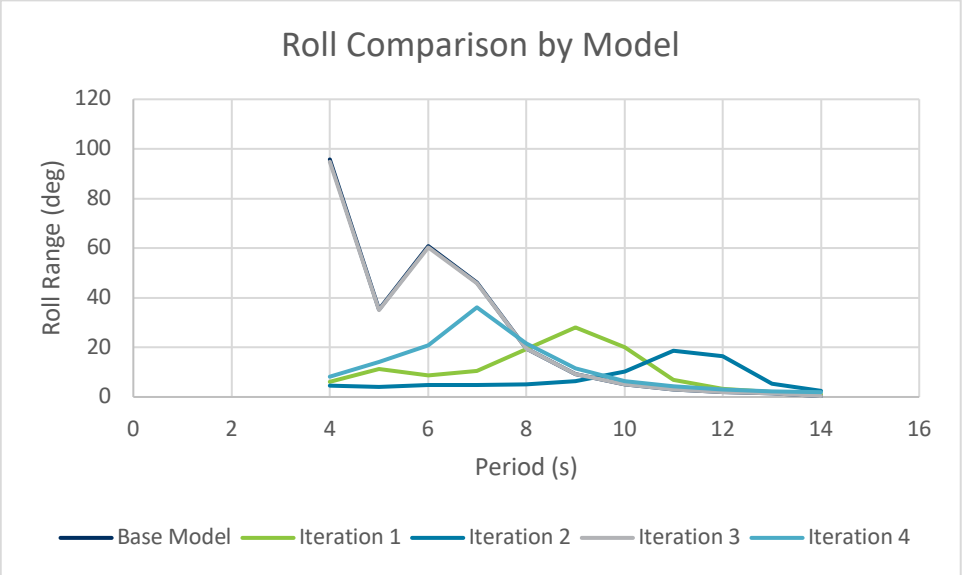

Figure 14: Roll comparison by model

Table 6 and Figure 14 show the roll range for each model across the full regular wave period range, wave height of 1.75m, and damping constant of 0.068 kN s m^{-1}. The Base Model and Iteration 1 show a spike in roll range for 4s and 5s period waves. The roll load RAOs for both buoys have an amplitude peak in the 4-5s period range. Iteration 2 also has a roll load RAO peak around the same period range, but there is no noticeable peak in the roll response like that seen in the Base Model and Iteration 1. When comparing the Base Model, Iteration 1, and Iteration 2, the size of the buoy appears to diminish the roll response during the 4s and 5s period waves, as the peak in roll excitation decreases as the scale of the model increases. There is a peak in roll range at the natural period for all models. As before, the Base Model

and Iteration 3 have similar motions. Because Iteration 4 has a shorter natural period than Iteration 1, the roll excitation of each model occurs during different wave periods.

7.1.3.2 Wave Height Effect

Larger wave heights resulted in greater response in the buoy. The following tables show the surge, heave, and roll response of the Iteration 1 buoy with a 0.068 kN s m^{-1} damping coefficient across each of the wave heights simulated. All data presented in this section was collected over the first five wave cycles of each simulation.

Table 7: Regular Wave Buoy Surge Comparison by Wave Height Iteration 1

Wave Period [s]	Surge Range [m]			
	Wave Height [m]			
	1.25	1.75	2.25	2.75
4	2.38	3.71	4.95	6.49
5	1.34	1.81	2.41	4.00
6	1.31	1.90	2.41	2.80
7	1.05	1.52	1.98	2.41
8	0.91	1.25	1.54	1.79
9	1.24	1.79	2.32	2.82
10	1.75	2.36	2.94	3.49
11	1.45	2.04	2.62	3.21
12	1.40	1.96	2.52	3.08
13	1.38	1.93	2.49	3.04
14	1.38	1.93	2.48	3.03

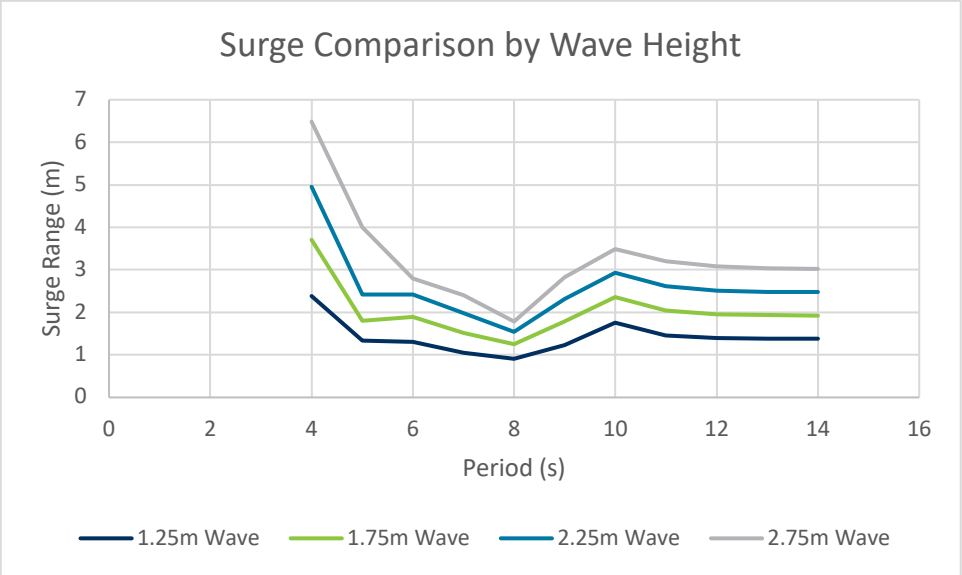

Figure 15: Surge comparison by wave height Iteration 1

Table 7 and Figure 15 show the surge range across the full regular wave period range, full wave height range, and damping constant of 0.068 kN s m^{-1}. The surge maximum occurs during the 4s wave periods, and a second peak in the surge range occurs near the natural period of the buoy. An increase in the wave height for the same period results in an increase in surge range, the increase is consistent across the wave period range.

Table 8: Regular Wave Buoy Heave Comparison by Wave Height Iteration 1

Wave Period [s]	Heave Range [m]			
	Wave Height [m]			
	1.25	1.75	2.25	2.75
4	1.27	1.69	2.05	2.97
5	1.90	2.46	2.97	3.65
6	1.46	2.03	2.59	3.13
7	1.31	1.83	2.35	2.87
8	1.27	1.78	2.31	2.87
9	1.29	1.80	2.34	2.91
10	1.25	1.76	2.27	2.79
11	1.23	1.72	2.21	2.70
12	1.23	1.72	2.21	2.70
13	1.23	1.72	2.21	2.70
14	1.23	1.72	2.21	2.70

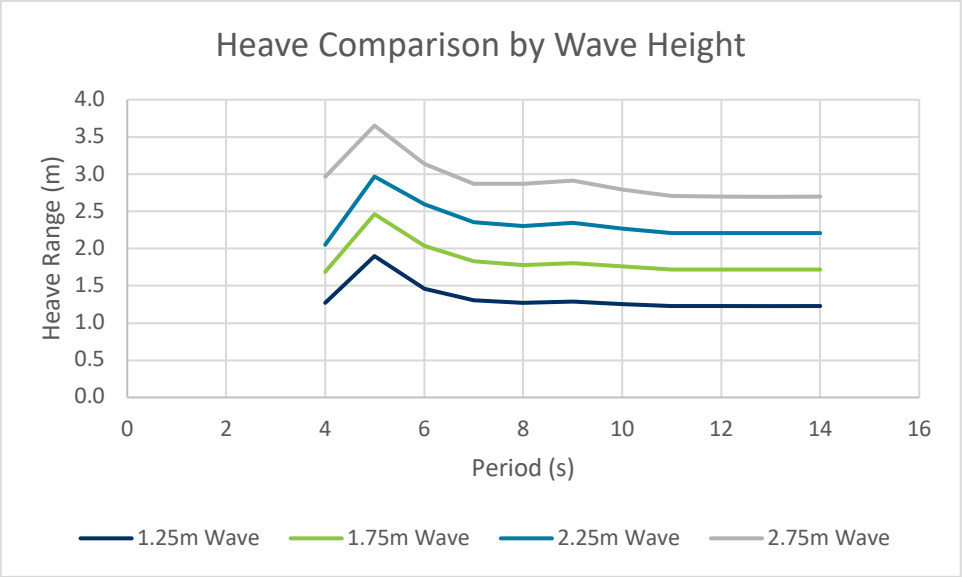

Figure 16: Heave comparison by wave height Iteration 1

Table 8 and Figure 16 show the heave range across the full regular wave period range, full wave height range, and damping constant of 0.068 kN s m^{-1}. The maximum heave range occurs during the 5s period waves which is near the natural frequency for the buoy. The maximum always occurs over 5s period waves regardless of the wave height indicating that the wave height does not affect the excitation of the model. The wave height does affect the magnitude of the heave response, as the heave range for each wave period increases with increase in wave height.

Table 9: Regular Wave Buoy Roll Comparison by Wave Height Iteration 1

Wave Period [s]	Roll Range [deg]			
	Wave Height [m]			
	1.25	1.75	2.25	2.75
4	5.09	6.01	5.09	96.36
5	6.05	11.34	42.34	107.69
6	6.15	8.63	11.13	15.00
7	7.34	10.45	13.79	17.43
8	12.37	19.25	27.78	37.97
9	22.71	28.03	33.24	38.48
10	15.16	19.94	24.70	29.27
11	4.82	6.85	8.97	11.19
12	2.41	3.39	4.40	5.43
13	1.36	1.91	2.47	3.04
14	0.76	1.06	1.38	1.70

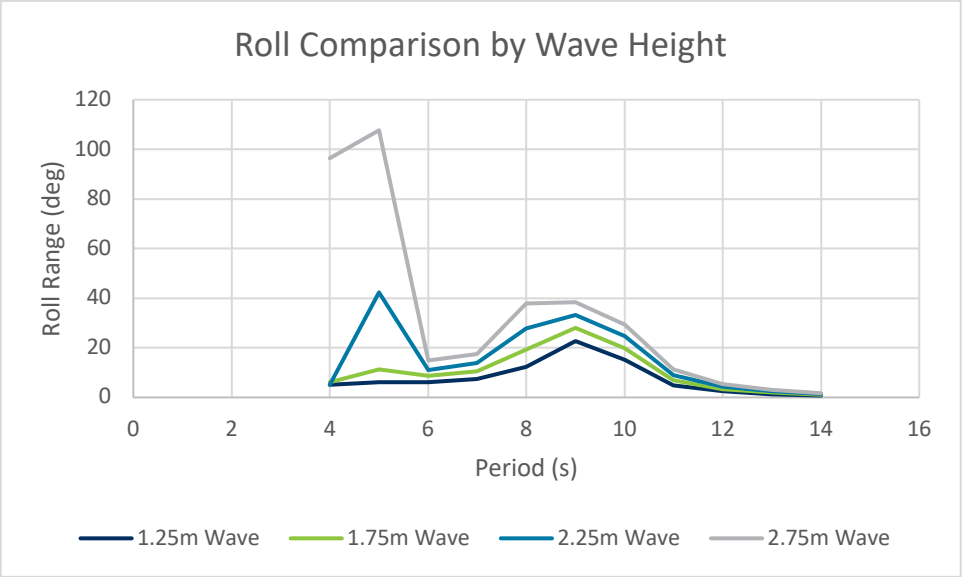

Figure 17: Roll Comparison by Wave Height Iteration 1

Table 9 and Figure 17 show the roll range across the wave period range, wave height range, and damping constant of 0.068 kN s m^{-1}. The peak in roll range occurs at the buoy heave natural period of 5s, as expected the peak roll increases with wave height increase. The second roll peak seen in Figure 17 occurs at the 9s waves period which is near the roll natural frequency of the buoy. They roll range increases with increase in wave height.

7.1.3.3 Winch Damping Effect

Each model was run for five winch damping constants. The following tables show the surge, heave, and roll motions of Iteration 1 for 1.75m waves across each damping constant. All data presented in this section was collected over the first five wave cycles of each simulation.

Table 10: Regular Wave Buoy Surge Comparison by Damping Constant Iteration 1

Wave Period [s]	Surge Range [m]				
	Damping Constant [kN s m^{-1}]				
	0.034	0.068	0.102	0.204	1.02
4	3.71	3.71	3.70	3.70	3.67
5	1.81	1.81	1.81	1.79	1.70
6	1.90	1.90	1.89	1.88	1.82
7	1.52	1.52	1.52	1.52	1.49
8	1.25	1.25	1.25	1.25	1.23
9	1.79	1.79	1.79	1.78	1.77
10	2.36	2.36	2.36	2.36	2.36
11	2.04	2.04	2.04	2.04	2.04
12	1.96	1.96	1.96	1.96	1.96
13	1.93	1.93	1.93	1.93	1.93
14	1.93	1.93	1.93	1.93	1.93

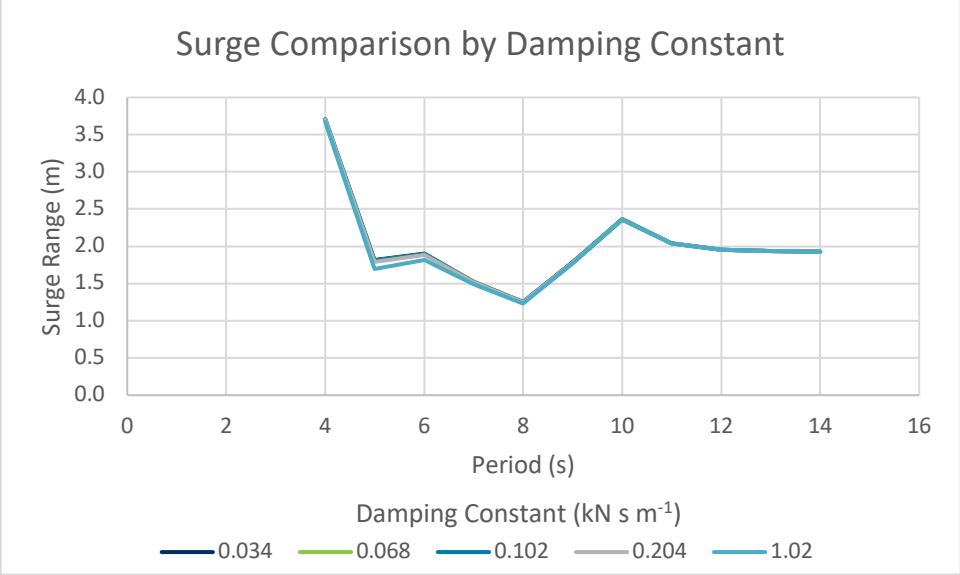

Figure 18: Surge comparison by damping constant Iteration 1

Table 10 and Figure 18 shows the influence of damping constant on the surge range across the full regular wave period range at a wave height of 1.75m. The surge range for each wave period is almost identical across the damping constants considered which suggests that the damping constant has a minimal effect on the surge response.

Table 11: Regular Wave Buoy Heave Comparison by Damping Constant Iteration 1

Wave Period [s]	Heave Range [m]				
	Damping Constant [kN s m^{-1}]				
	0.034	0.068	0.102	0.204	1.02
4	1.69	1.69	1.69	1.69	1.69
5	2.46	2.46	2.46	2.46	2.46
6	2.03	2.03	2.03	2.03	2.03
7	1.83	1.83	1.83	1.83	1.83
8	1.78	1.78	1.78	1.78	1.78
9	1.80	1.80	1.80	1.80	1.80
10	1.76	1.76	1.76	1.76	1.76
11	1.72	1.72	1.72	1.72	1.72
12	1.72	1.72	1.72	1.72	1.72
13	1.72	1.72	1.72	1.72	1.72
14	1.72	1.72	1.72	1.72	1.72

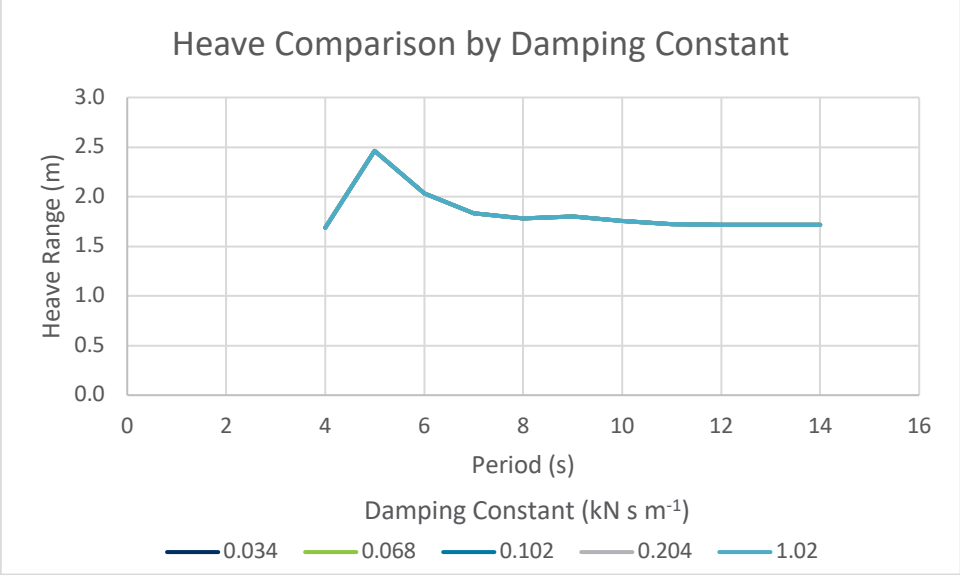

Figure 19: Heave comparison by damping constant Iteration 1

Table 11 and Figure 19 shows the influence of damping constant on the heave range across the full regular wave period range with a wave height of 1.75m. Again, this figure shows that across the damping constants considered there is no impact on the heave range for each wave period.

Table 12: Regular Wave Roll Comparison by Damping Constant Iteration 1

Wave Period [s]	Roll Range [deg]				
	Damping Constant [kN s m^{-1}]				
	0.034	0.068	0.102	0.204	1.02
4	6.02	6.01	6.00	5.97	5.70
5	11.34	11.34	11.34	11.33	11.33
6	8.64	8.63	8.63	8.63	8.59
7	10.45	10.45	10.45	10.45	10.44
8	19.25	19.25	19.25	19.25	19.28
9	28.03	28.03	28.03	28.03	28.03
10	19.94	19.94	19.94	19.94	19.96
11	6.85	6.85	6.85	6.85	6.85
12	3.39	3.39	3.39	3.39	3.39
13	1.91	1.91	1.91	1.91	1.91
14	1.06	1.06	1.06	1.06	1.06

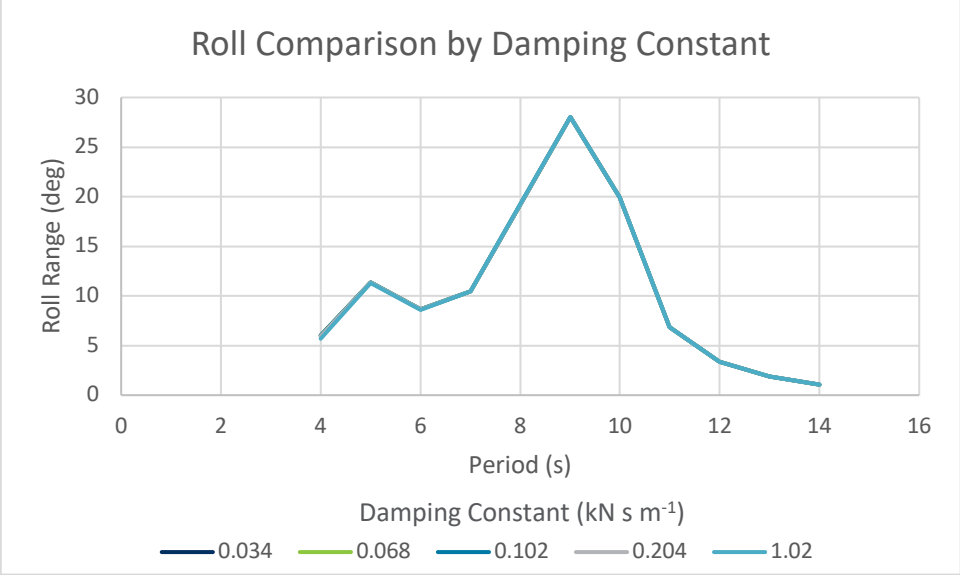

Figure 20: Roll comparison by damping constant Iteration 1

Table 12 and Figure 20 shows the influence of damping constant on the roll range across the full regular wave period range with a wave height of 1.75m. Again, consistent with the surge and heave responses, over the damping constants considered there is no impact on the roll range for each wave period.

7.1.3.4 Decoupling Effect

Iteration 3 was designed to simulate a scenario in which the Base Model reels had decoupled from the generators. To model the decoupled buoy, the winch inertias for Iteration 3 only considered the inertia contribution from the reel shafts. The following table compares the maximum tensions between the Base

Model and Iteration 3 for the wave ward (Winch 1) and leeward (Winch 3) winches for regular wave cases where the MBL was exceeded at least one winch of the Base Model. The data shown is collected from cases using the 0.068 kN s m^{-1} damping constant. All data presented in this section was collected over the first five wave cycles of each simulation.

Table 13: Decoupling Effect on MBL Exceedance

Wave Height [m]	Wave Period [s]	Damping Constant [kN s m^{-1}]	Winch1 Tension [kN]		Winch3 Tension [kN]	
			Base Model	Iteration 3	Base Model	Iteration 3
2.75	12	0.204	69.04	8.15	60.40	8.15
2.75	12	1.020	61.83	8.73	79.59	8.71
2.75	13	0.034	73.73	8.04	37.50	8.04
2.75	13	0.068	73.50	8.05	38.73	8.06
2.75	13	0.102	73.27	8.07	41.25	8.08
2.75	13	0.204	72.55	8.14	82.07	8.14
2.75	13	1.020	66.93	8.69	82.17	8.67
MBL is 68.26 kN including 1.67 safety factor						

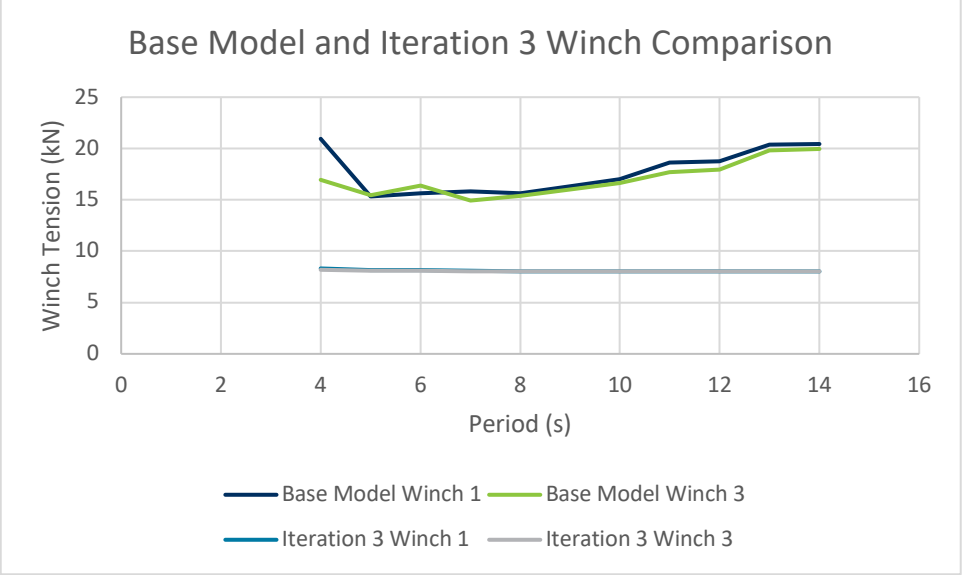

Figure 21: Reduced line tension from decoupling

Table 13 and Figure 21 show that the tension in the winches on either side of the buoy is significantly decreased when the inertia is reduced. For the Base Model and Iteration 3, the target tension of the system was 8 kN. These results show that the decoupled model sees little deviation from the target tension compared to the Base Model over the same wave conditions.

7.1.3.5 Average Power at the Reel Connections

The average power at the reel connections for each wave was determined using Equation 5. The accumulated power was determined by summing the power at each time step across the first five wave cycles of the simulation. The accumulated power was then divided by 5 to produce an "Average Power" over one wave cycle. The average power over one wave at the reel connections is shown in Table 14, this is reported for a wave height of 1.75m and over the full wave period range considered. Note that the Average Power presented is the power seen at the connection points of the winches and is not representative of the power that is produced by the generators. The Average Power for the Iteration 3 model is not presented, as the decoupled system would not generate any power. The benefits of the decoupled system or reduced inertia are seen in the performance of the winches and the overall stability of the buoy which is discussed Section 7.2.

Table 14: Average Power at the Reel Connections by Model

Wave Height [m]	Wave Period [s]	Average Power [kW/wave]			
		Base Model	Iteration 1	Iteration 2	Iteration 4
1.75	4	2,834	17,531	29,953	17,347
1.75	5	2,942	25,976	63,680	26,172
1.75	6	3,206	23,629	94,701	23,930
1.75	7	2,878	22,787	82,187	23,932
1.75	8	2,796	23,483	76,969	21,322
1.75	9	2,874	23,823	76,217	21,350
1.75	10	2,928	21,294	77,888	21,865
1.75	11	2,975	21,979	80,888	22,181
1.75	12	3,024	22,411	71,565	22,485
1.75	13	3,070	22,725	73,683	22,743
1.75	14	3,107	22,927	74,985	22,922

The Base Model achieved maximum Average Power at a 6s period wave. This is near the roll natural period of the Base Model. As shown previously in Table 6 and Figure 14, the Base Model and Iteration 3 had noticeably larger roll ranges at the roll natural period compared to the other models, so it is sensible that the roll motions contribute the most average power. Iteration 1 and Iteration 4 both have a maximum in the average power for 5s period waves. This is near the heave natural frequency of both models. Each model also has a second peak in power at waves near their respective roll natural period. For Iteration 1 this second peak occurs for the 9s period waves, and for Iteration 4 this occur for the 7s period waves. Iteration 2 shows maximum average power for 6s period waves which is near its heave natural period and a second peak in average power for 11s period waves which is near its roll natural period. For all models, the average power slowly increases with the wave period for waves with period larger than the roll natural period. The buoy follows the orbital motion of the waves more closely for longer period waves. As the waves get longer, the surge motions of the buoy also increase. The increasing surge motions result in the increasing average power.

At the 4s period waves, the average power is low for the Base Model and at a minimum for the other models. This is due to the surge motions of the buoy discussed in Section 7.1.3.1. As the size of the buoy

increases, it takes more time for the buoy to reach the offset position before it begins to follow the orbital motion of the waves. Since the buoy performs best when following an orbital path, the average power presented for the 4s period waves is lower, for a few reasons, 1) over the five wave cycles range considered the buoy has not reached the surge equilibrium point (ie still drifting), and 2) the buoy is not able to respond to the small period wave, here it is worth nothing that the base model responds to the smaller wave periods better than the larger buoy models, hence there is not as much difference in the average power when going from 4 to 5 s waves.

Table 15: Average Power at the Reel Connections by Wave Height

Wave Period [s]	Average Power [kW/wave]			
	Wave Height [m]			
	1.25	1.75	2.25	2.75
4	12405	17531	22419	28157
5	19723	25976	31511	34879
6	16929	23629	30236	36713
7	16268	22787	29311	35833
8	16620	23483	30527	37686
9	17173	23823	30594	37518
10	15004	21294	27735	34305
11	15692	21979	28277	34590
12	16004	22411	28825	35246
13	16227	22725	29228	35741
14	16375	22927	29480	36036

Table 15 shows the average power over one wave for the Iteration 1 model across each of the four wave heights. The table is colored such that the lowest magnitudes of power are in Red, and the largest magnitudes of power are in Green. As seen in the table, the wave height influences the average power, as the average power increases along with the wave height for waves of the same period. As illustrated previously, the average power only marginally increases with wave period.

Table 16: Factored Average Power at the Reel Connections

Wave Period [s]	Factor			
	Wave Height [m]			
	1.25	1.75	2.25	2.75
	1.0	1.4	1.8	2.2
4	1.0	1.4	1.8	2.3
5	1.6	2.1	2.5	2.8
6	1.4	1.9	2.4	3.0
7	1.3	1.8	2.4	2.9
8	1.3	1.9	2.5	3.0
9	1.4	1.9	2.5	3.0
10	1.2	1.7	2.2	2.8
11	1.3	1.8	2.3	2.8
12	1.3	1.8	2.3	2.8
13	1.3	1.8	2.4	2.9
14	1.3	1.8	2.4	2.9

Table 16 presents the same data as Table 15, but the values are a factor of the lowest power which occurred for the 1.25m height and 4s period waves. The coloring of the table is the same as in Table 15. The factors at the top of each column which are not colored represent the wave heights as a factor of the lowest wave height (H = 1.25m). As seen in the table, the difference in wave height factor is similar to the difference in average power when comparing waves of different heights.

7.1.3.6 Annual Power

The annual power contribution was determined by taking the average power of an individual model across each wave height, wave period, and damping coefficient combinations and factoring it by the annual occurrence of that wave as shown in Equation 5 and Equation 6. The annual powers for each wave were summed to form the total annual power. This power is the rate of work done on the buoy by the winches taken at the reel connection point and is not representative of the power that is generated by the internal mechanism. All data presented in this section was collected over the first five wave cycles of each simulation.

Table 17: Annual Power Contribution Iteration 1

Wave Height [m]	Wave Period [s]	Wave Annual Occurrence [hrs/yr]	Annual Power [MW/yr]				
			Damping Constant [kN s m^{-1}]				
			0.034	0.068	0.102	0.204	1.02
1.75	4	0.0	0	0	0	0	0
1.75	5	7.5	140,272	140,270	140,268	140,261	140,211
1.75	6	102.0	1,446,144	1,446,114	1,446,084	1,445,993	1,445,321
1.75	7	286.0	3,351,606	3,351,600	3,351,595	3,351,580	3,351,484
1.75	8	455.5	4,813,460	4,813,484	4,813,509	4,813,583	4,814,152
1.75	9	504.0	4,802,707	4,802,765	4,802,822	4,802,994	4,804,367
1.75	10	392.5	3,008,810	3,008,841	3,008,871	3,008,962	3,009,693
1.75	11	234.5	1,686,778	1,686,782	1,686,785	1,686,794	1,686,865
1.75	12	127.0	853,877	853,878	853,878	853,881	853,903
1.75	13	64.0	402,748	402,748	402,748	402,749	402,756
1.75	14	26.5	156,230	156,230	156,230	156,230	156,234

Table 17 shows the annual power contribution of the 1.75m waves across all wave periods for the Iteration 1 model. The waves with a period of 8s and 9s have the largest magnitude of annual power contribution, as the annual wave occurrence is highest for waves with those periods. Even though 8s period waves have a slightly lower annual occurrence, they contribute slightly more annual power than the 9s waves. This is due to differences in the average power between the 8s and 9s waves.

Table 18: Total Annual Power at the Reel Connections

Model	Total Annual Power [MW]				
	Damping Constant [kN s m^{-1}]				
	0.034	0.068	0.102	0.204	1.02
Base Model	7,823,522	7,824,616	7,825,806	7,829,733	7,869,674
Iteration 1	61,275,270	61,275,571	61,275,870	61,276,776	61,284,087
Iteration 2	210,384,308	210,384,255	210,384,194	210,384,034	210,382,966
Iteration 4	59,418,706	59,418,782	59,418,857	59,419,096	59,421,083

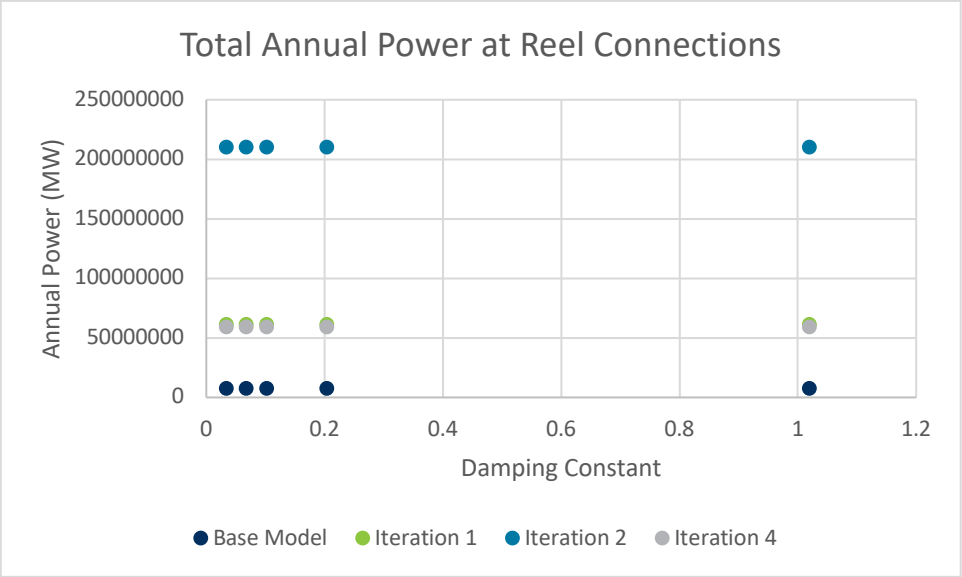

Figure 22: Total annual power

Table 18 and Figure 22 show the power at the winch connections for the Base Model and each iteration. There is a noticeable increase in the power between the Base Model and Iteration 1 and between Iteration 1 and Iteration 2. This indicates that the power acting on the winch connections increases as the size and mass of the buoy increases. Iteration 4 has similar power at the winch connections as Iteration 1. This is sensible since Iteration 4 is of a similar size and mass as Iteration. All models showed very little change in power over change in winch damping constant.

7.1.4 Irregular Wave Analysis

The Iteration 1 model was chosen for the irregular wave analysis, so all irregular wave simulations were performed using that model. The model showed instability in both buoy motions and winch performance for all original irregular sea states tested as per the test plan. The instability was most prevalent in cases with the largest significant wave height (2.75m) or shortest peak period (7.5s) with the Hs = 2.75m and Tp = 7.5s sea state being the worst scenario. The 7.5s peak period waves had an average period of about 5.3s which was near the heave natural period and the surge and roll load RAO peak responses for the Iteration 1 model. The following sections list the results from these simulations as well as results from a few additional simulations which were run to determine the limiting sea state for the buoy's stability. All data presented in the following sections was collected over a three-hour simulation for each case.

7.1.4.1 Wave Height and Winch Damping Effect

The buoy showed significant instabilities and struggled to keep station under the irregular sea states tested. This was due to the excitation of the buoy at its natural periods and peaks in load RAO amplitude in combination with other hydrodynamic instabilities. Additionally, the winch lines in all cases saw compression and tension spiking. The magnitudes of tension were above the minimum breaking load for all cases. The large magnitudes in buoy motions and line tensions suggest that the sea states tested are too large for the buoy to perform effectively. The following tables show the surge, heave, and roll motions of the buoy in each irregular sea state across each damping constant. All cases shown are over the original sea states as mentioned in the Test Plan. Further discussion on the stability of the buoy can be found in Section 7.2.

Table 19: Irregular Wave Buoy Surge Range Iteration 1

Significant Wave Height [m]	Peak Period [s]	Surge Range [m]				
		Damping Constant [kN s m^{-1}]				
		0.034	0.068	0.102	0.204	1.02
1.75	7.5	8.73	8.81	8.66	8.65	9.50
1.75	8.5	7.96	7.96	7.99	7.79	12.03
1.75	9.5	4.93	4.90	4.89	4.93	12.68
2.75	7.5	38.21	37.26	34.73	36.20	29.50
2.75	8.5	15.27	15.22	15.35	15.01	14.63
2.75	9.5	9.47	9.57	9.39	9.45	9.33

Table 19 shows the surge range data for the irregular wave cases. The maximum surge range typically occurs for the Tp = 7.5s sea states. The average period (Tz) of these sea states is approximately 5.3s which is near the 5s period at which the surge and roll load RAO amplitude peaks occur.

Table 20: Irregular Wave Buoy Heave Range Iteration 1

Significant Wave Height [m]	Peak Period [s]	Heave Range [m]				
		Damping Constant [kN s m^{-1}]				
		0.034	0.068	0.102	0.204	1.02
1.75	7.5	3.90	3.91	3.91	3.92	3.87
1.75	8.5	4.05	4.05	4.05	4.05	4.00
1.75	9.5	3.59	3.59	3.59	3.60	3.86
2.75	7.5	5.89	5.65	6.29	5.73	6.54
2.75	8.5	5.99	5.99	6.00	5.89	5.59
2.75	9.5	5.67	5.67	5.69	5.66	5.70

Table 20 shows the heave range data for the irregular wave cases. The maximum heave range typically occurs on the Tp = 8.5s sea states which have an average period (Tz) of about 6s. The heave range did not see significant changes in magnitude across the winch damping constant over the same significant wave height and peak period. There was less than half a meter of heave range difference between the heave responses over each peak period for the same winch damping constant. These results indicate that the heave response is most dependent on the wave height.

Table 21: Irregular Wave Buoy Roll Range Iteration 1

Significant Wave Height (m)	Peak Period (s)	Roll Range [deg]				
		Damping Constant [kN s m^{-1}]				
		0.034	0.068	0.102	0.204	1.02
1.75	7.5	91.05	91.13	90.57	91.13	86.77
1.75	8.5	72.75	72.86	73.04	74.02	84.68
1.75	9.5	68.90	68.98	68.92	68.85	102.17
2.75	7.5	126.24	122.19	127.89	136.64	148.20
2.75	8.5	100.53	100.56	100.45	100.56	127.14
2.75	9.5	93.40	93.45	92.22	92.70	90.23

Table 21 shows the roll range data for the irregular wave cases. The trend of the roll range follows that of the surge range, as the maximum roll range of each case occurs over the same sea states as the maximum surge range. The maximum roll range typically occurred over the Tp = 7.5s sea states. These sea states had an average period (Tz) of about 5.3s which is near the 5s period at which the roll load RAO amplitude peaks occur.

7.1.4.2 Reduced Wave Height

Since the model showed winch line compression and buoy instability across all cases for the original sea states in the Test Plan, four additional simulations were run at sea states with a reduced significant wave. These sea states were generated with the following parameters:

- Hs = 0.5m, Tp = 7.5s Tp = 9.5s
- Hs = 1.0m, Tp = 7.5s Tp = 9.5s

In the reduced wave height sea states, the winch tensions were much lower, and the line compression only appeared in the Hs = 1.0m and Tp = 7.5s sea state. The buoy motions and average power at the reel connection of the buoy in the reduced wave height sea states is compared to the buoy motions and average power at the reel connections of the buoy of the H = 1.25m regular waves in the Table 22 and 23. The following cases were all run with the 0.068 kN s m^{-1} winch damping constant.

Table 22: Regular and Irregular Wave Buoy Motion Comparison Iteration 1

Wave Height [m]	Period [s]	Surge Range [m]	Heave Range [m]	Roll Range [m]
Regular Waves				
1.25	4	2.38	1.27	5.09
1.25	5	1.34	1.90	6.05
1.25	6	1.31	1.46	6.15
1.25	7	1.05	1.31	7.34
1.25	8	0.91	1.27	12.37
1.25	9	1.24	1.29	22.71
1.25	10	1.75	1.25	15.16
1.25	11	1.45	1.23	4.82
1.25	12	1.40	1.23	2.41
1.25	13	1.38	1.23	1.36
1.25	14	1.38	1.23	0.76
Irregular Waves				
0.5	7.5	1.46	1.28	23.10
0.5	9.5	1.14	1.03	17.79
1.0	7.5	3.29	2.30	52.43
1.0	9.5	2.47	2.02	35.17

Table 22 compares the surge, heave, and roll ranges of the buoy in the reduced wave height irregular sea states with the surge, heave, and roll ranges of the buoy under the 1.25m regular wave case. The peak periods of the reduced wave height simulations were Tp = 7.5s and Tp = 9.5s. These peak periods have a corresponding average period (Tz) of 5.3s and 6.7s, respectively. The magnitudes of the surge, heave, and roll ranges of the buoy over the reduced irregular sea states are similar to or larger than the surge, heave, and roll ranges of the 1.25m regular waves despite having a smaller wave height. In the irregular sea states, the buoy will see a range of wave periods some of which will be extremely close to the natural periods of the buoy. While some of the regular waves have periods that are near the natural periods of the buoy, they do not excite the buoy motions to the same degree.

Table 23: Regular and Irregular Wave Average Power Comparison

Wave Height [m]	Period [s]	Average Connection Force Power [kW/wave]
Regular Waves		
1.25	4	12404.55
1.25	5	19723.38
1.25	6	16928.54
1.25	7	16267.70
1.25	8	16619.60
1.25	9	17173.27
1.25	10	15003.85
1.25	11	15691.78
1.25	12	16003.92
1.25	13	16227.14
1.25	14	16375.44
Irregular Waves		
0.5	7.5	4275.27
0.5	9.5	4383.70
1.0	7.5	7945.86
1.0	9.5	8354.27

Table 23 compares the average power at the reel connection of the buoy under the reduced wave height irregular seas states to the average power at the reel connection of the buoy under the 1.25m regular wave case. There is noticeably more average connection force power for the regular waves than the irregular waves. This is due to the average energy in the waves being a function of the square of the wave height. Since the regular waves presented are larger in height than the irregular waves presented, the regular wave will contain more energy on average than the irregular waves. The largest magnitude of average power in the regular wave cases occurs for the 5s period wave. This case had the highest maximum and minimum winch displacements compared to the other wave periods. As each case had comparable magnitudes of connection force, the larger displacements resulted in more average power based on the equation shown previously. The winch displacements were largest over the 5s period wave as that is where the maximum heave range and the second largest surge range of the buoy occurred. There is a second peak in the average power at the 9s period wave. The maximum roll range occurs at the 9s regular wave which results in increased winch displacements. For the reduced irregular wave cases, the average power for the 1.0m significant wave height sea states was larger than the average power for the 0.5m sea states. This is expected since the average energy per wave is dependent on the square of the wave height. It is important to note that the Hs = 1.0m and Tp = 7.5s sea state showed winch line compression and tension spiking. This behavior will have an influence on the values for surge, heave, and roll range and the resultant average connection force power.

7.1.5 Model Scaling Report

The Iteration 1 model was also selected for wave tank testing which is to be performed in the wave tank at the University of Iowa. The documents outlining the wave tank criteria can be found in Appendix E. The model scaling factor was determined based on the wave tank's maximum achievable wave amplitude of 250mm and wave period of 2.5s. In order to cover the full range of irregular waves, the wave period is the limiting parameter. Table 24 shows the Iteration 1 model parameters scaled by a factor of 14.5. At this factor, the maximum peak period of 9.5s is equal to the maximum achievable wave tank period of 2.5s. Due to the limited depth of the wave tank, the geometrical dimensions of the mooring lines are not scaled using the scaling factor. Instead, the vertical separation of the mooring frame from the base of the buoy maintains the same percentage of the buoy length as in Iteration 1. All other parameters were scaled using Froude's law of similitude with a scaling factor of 14.5.

Table 24: Wave Tank Scaling

Parameter	Iteration 1	Wave Tank Model
Buoy		
Mass [kg]	129,488.00	42.47
Volume [m^3]	191.52	0.06
Density [kg/m^3]	676.23	676.23
Length [m]	12.75	0.88
Height [m]	4.77	0.33
Width [m]	3.73	0.26
COG from buoy base [m]	1.88	0.13
COG as % of buoy height	41.06	41.06
Submerged idle depth [m]	3.74	0.26
Submerged idle depth as % of buoy height	78.40	78.40
Vertical separation of frame from buoy base (150% of length)	19.13	1.32
Environment		
Significant wave height [m]	2.75	0.19
Peak wave period [s]	9.50	2.50
Water depth [m]	67.40	3.00
Mooring		
Distance between frame and sea floor [m]	44.54	1.42
Depth of frame [m]	22.87	1.58
Axial stiffness [kN]	385.40	0.13
Line tension [kN]	64.00	0.02

7.2 Lessons Learned and Test Plan Deviations

7.2.1 Buoy Instability

The buoy showed uncontrolled motions in one or more degrees of freedom and struggled to keep station in the irregular sea states mentioned in the Test Plan. These motions, along with continued wave activity, do not allow the buoy to return to following the orbital motion of the waves. The cause of the instability was a combination of multiple factors including: natural period excitation and mooring parameters. In the irregular sea states, the effect on the buoy by these factors resulted in mooring line compression and tension spikes that exceeded the minimum breaking load. These effects are discussed further in the following sections. Additionally, the mooring system provided little resistance to yaw motion. As such any asymmetries in the wave load on the buoy caused yaw motions that the winches were unable to resist effectively. The yaw motions affected the performance of the buoy in the other degrees of freedom and contributed to the instability of the system. In the reduced wave height irregular sea states, the yaw motion of the buoy was greatly reduced, and the minimum breaking load of the mooring lines was not exceeded. These results suggest that the original irregular sea state cases were too large for the current design of the system to perform correctly, but it has the potential to perform as intended in a sea state with smaller waves. It should be noted that the conclusions are based on the Iteration 1 model only.

7.2.2 Buoy Drift

When subjected to consecutive, low period waves, the mean point of the buoy moves in the direction of the wave loading over time. This is most noticeable in the regular wave cases as presented in Section 7.1.3.1. This data shows that the surge range is maximum during the 4s period regular wave train for all iterations of the buoy. This occurs because, when the wave period is low, the system does not have enough time to recover back to its original equilibrium position in between wave impacts. Repeated impacts from low period waves causes the mean position of the system to slowly drift in the direction of the wave loading. As the wave period increases, the drift of the system becomes less significant. Due to this behavior, the surge range is largest over the 4s period wave train even though the orbital motion of the buoy is smaller than the orbital motion during longer period waves. The buoy drift is also possible during an irregular sea state, but it is dependent on the sequence of waves which interact with the system. A group of consecutive, low period waves will cause the buoy to drift in the direction of the loading, but longer period waves will give it a chance to recover to its original mean position.

7.2.3 Diffraction Effects

Considering the dimensions of the buoy and the sea state conditions, a regime check was conducted as per Figure 23 [Det Norske Veritas (2010). *"Environmental Conditions and Environmental Loads"*. Recommended Practice DNV-RP-C205, April 2014.]. The Base Model and Iteration 1 fell into Region III; however, Iteration 2 fell under Region II. Based on the regime check and preliminary OrcaFlex models, it was determined that the diffraction effects on the Iteration 2 model were significant. To account for the diffraction, load RAOs were generated for Iteration 2. Load RAOs were also generated for the Base Model and Iteration 1 to maintain consistency across the model construction.

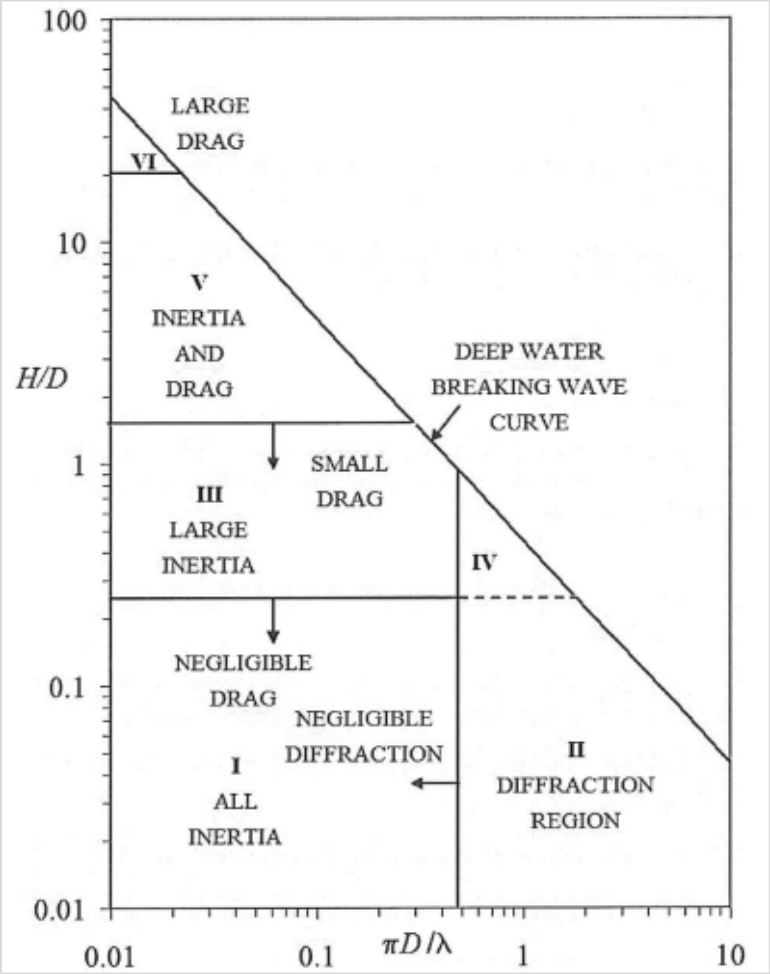

Figure 23: Limits of application for small vs large structures

7.2.4 Natural Periods and Peak Load RAO Periods

The surge, heave, and roll natural periods of the buoy change depending on the geometry, mass, and moments of inertia. As the buoy is scaled up from the Base Model to Iteration 1, the natural periods also increase. The same is true when comparing Iteration 1 to Iteration 2. Further, the slight change in geometry between Iteration 1 and Iteration 4 resulted in a change in the roll natural period. Since the waterplane areas of the buoy were the same, the surge and heave natural periods were unaffected. Refer to Table 3 in Section 7.1.2 for the surge, heave, and roll natural periods.

For all models, the load RAO amplitude for roll showed a peak response around the 4-5s. This caused excitation in the roll response of the buoy for waves with a period between 4-5s. The size of the buoy impacted the magnitude of the excitation, as a smaller buoy model showed more roll excitation than a larger buoy model across the same wave period range.

There was also a peak in the surge load RAO amplitude in the 4-5s. The result of this peak was a low frequency response in the system for 4-5s period waves. When looking at the regular wave surge data reported previously, the surge range of the buoy is largest over the waves with a 4s period. Likewise, for the irregular waves, the surge range is largest for sea states with a 7.5s Tp (5.3s Tz). This effect can be seen in the time histories of the winch tensions shown below.

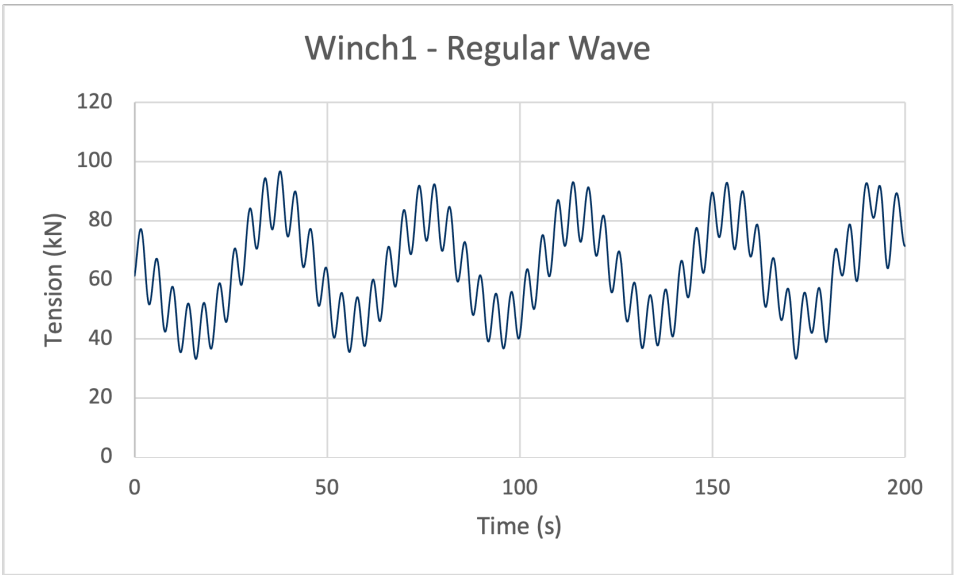

Figure 24: Winch1 time history for regular wave H = 1.25m, T = 4s

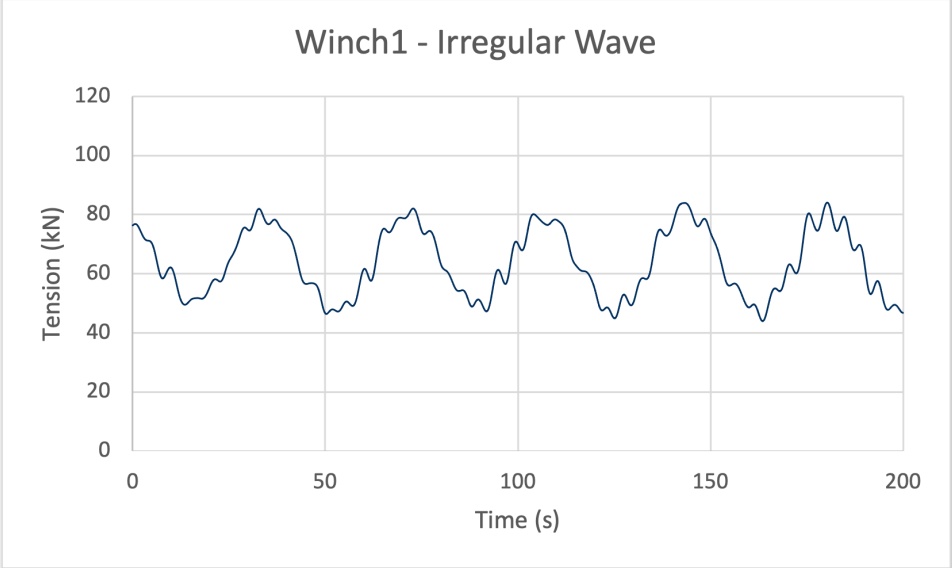

Figure 25: Winch1 time history for irregular wave Hs = 0.5m, Tp = 7.5s

Figure 24 and Figure 25 show the time history of the tension in Winch 1 which is located on the wave ward side of the buoy. Figure 24 is the time history of the Iteration 1 model over a wave of 1.25 height and 4s period. Figure 25 is the time history of the Iteration 1 model over an irregular sea state with significant wave height of 0.5m and peak period of 7.5s. Across both plots, a high frequency and low frequency response is seen. In the regular wave case, the high frequency response occurs at 4s which is in line with the 4s period waves of that case. The 4s period is also near the model's heave natural frequency of 4.35s. In the irregular wave case, the high frequency response occurs at around 5s. The average period for this sea state is 5.3s. Since this is only about a second off the heave natural frequency, there will be waves in

the irregular sea state that have a period at or very close to the heave natural frequency. Both plots show a low frequency response on the order of 45s which is near the surge natural frequency of the model. The low frequency response in both the regular and irregular wave cases is diminished when the period and peak period are increased.

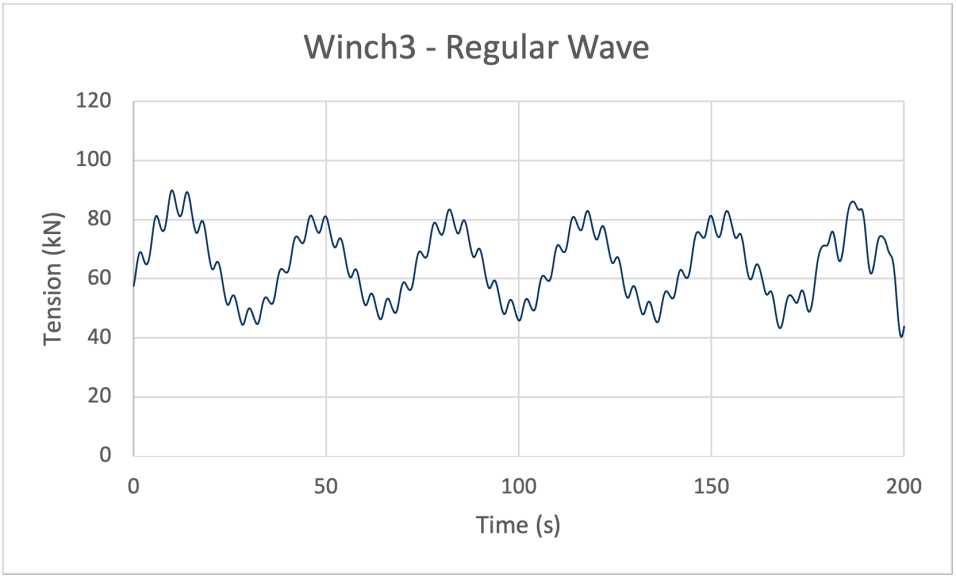

Figure 26: Winch3 time history for regular wave H = 1.25m, T = 4s

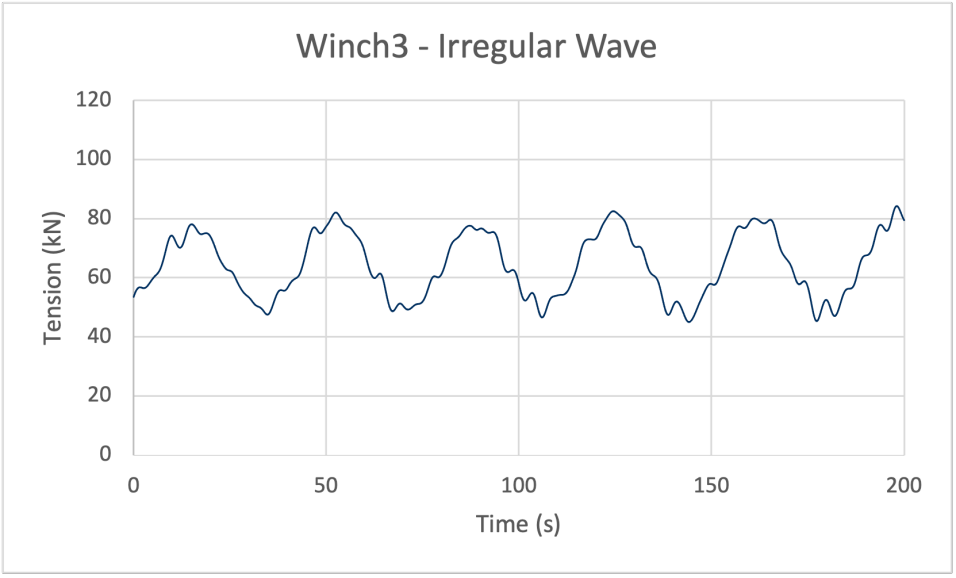

Figure 27: Winch3 time history for irregular wave Hs = 0.5m, Tp = 7.5s

Figure 26 and Figure 27 show the time history of the tension in Winch 3 which is located on the leeward side of the buoy. The plots represent the same wave conditions as the previous plots of Winch 1. Like Winch 1, Winch 3 shows a high frequency response at around 4-5s and a low frequency response at

roughly 45s. The plots of both Winch 1 and Winch 3 suggest that the tension in the winch lines is driven by a combination of the heave and surge responses of the buoy

7.2.5 Winch Inertia

As discussed previously, Iteration 3 was run using a decreased winch inertia which showed a significant decrease in winch tensions compared to the larger winch inertia used in the Base Model. Based on these results, a single decoupled test was run for Iteration 1 over the irregular sea state which showed the highest winch tensions. For this simulation, the winch tensions were considerably reduced, and there was no occurrence of tension spiking in the leeward winches.

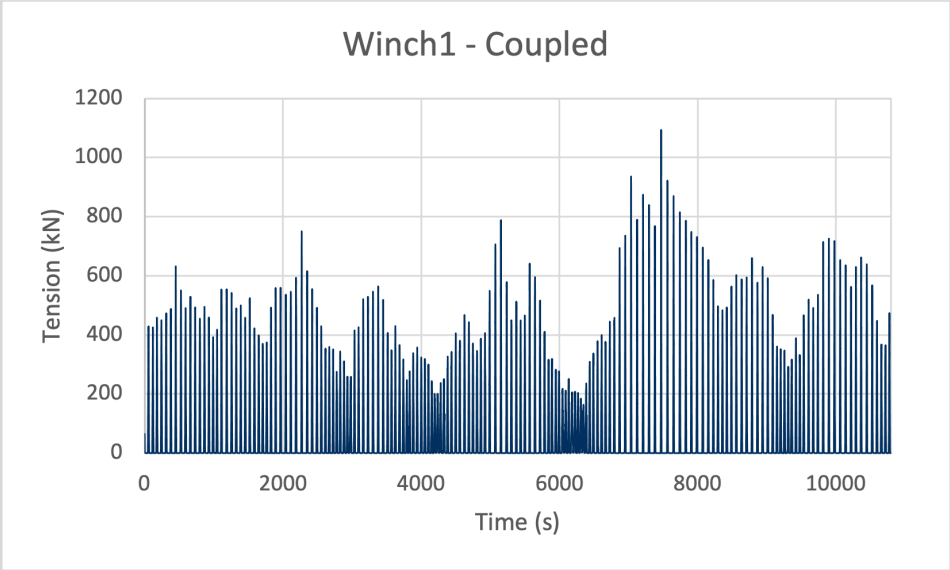

Figure 28: Winch1 time history for irregular wave Hs = 2.75m, Tp = 7.5s

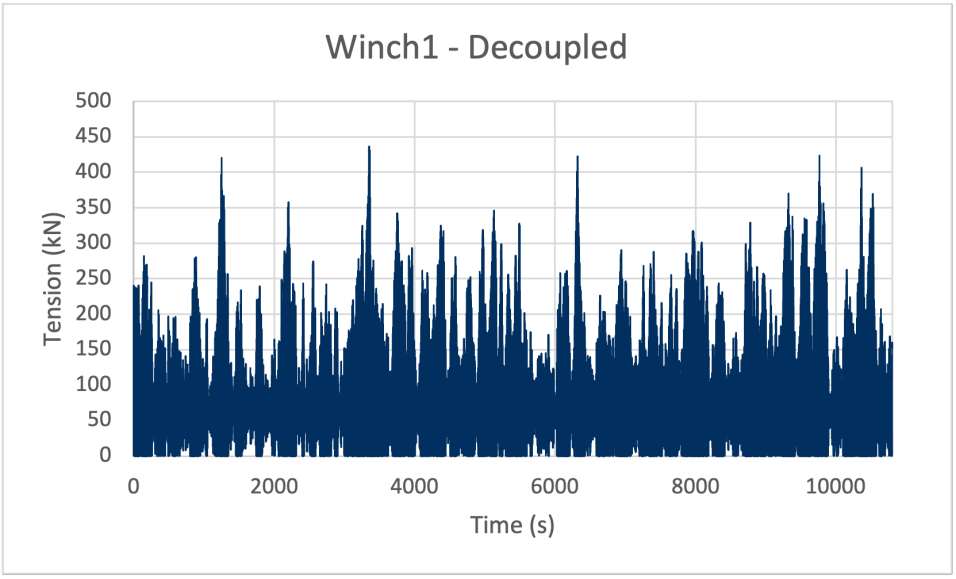

Figure 29: Decoupled Winch1 time history for irregular wave Hs = 2.75m, Tp = 7.5s

Figure 28 and Figure 29 show the time history of the tension in Winch 1 (wave ward). Both cases were run in an irregular sea state with significant wave height of 2.75m and peak period of 7.5s. This sea state was chosen because it showed the highest magnitude of winch line tensions across all tested sea states. Figure 28 shows the original Iteration 1 run while Figure 29 shows the decoupled Iteration 1 run. There is winch compression in both cases; however, the magnitude of tension in the winch line is much smaller in the decoupled case. Additionally, the decoupled case shows less time between tension spikes. This indicates that the periods of compression in the winch line are shorter in the decoupled case.

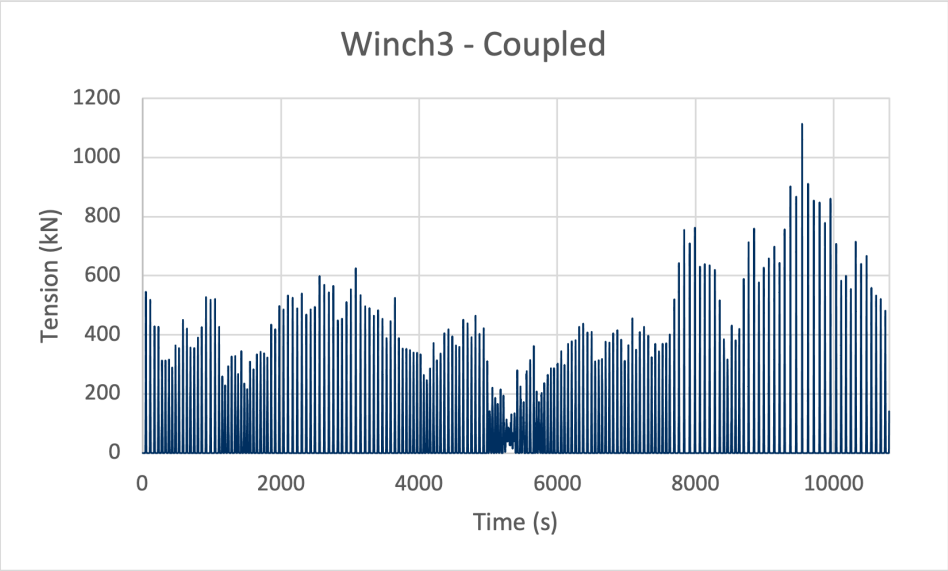

Figure 30: Winch3 time history for irregular wave Hs = 2.75m, Tp = 7.5s

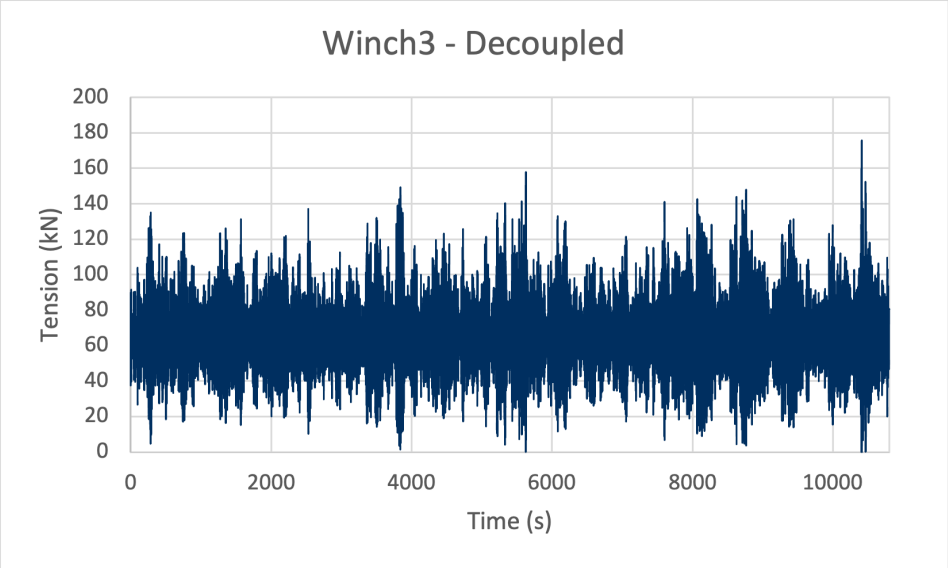

Figure 31: Decoupled Winch3 time history for irregular wave Hs = 2.75m, Tp = 7.5s

Figure 30 and Figure 31 show the time history of the tension in Winch 3 (leeward). The time histories are for the same simulations as shown in the previous plots of Winch 1. Like Winch 1, Winch 3 shows lower magnitudes of tension in the decoupled case. The decoupled Winch 3 case does not show the line compression and tension spiking seen in the original case. The differences in the tension in both Winch 1 and Winch 3 between the original and decoupled cases suggest that the winch inertia has a significant impact on the performance of the system. Larger inertias result in longer time in compression of the winch lines and larger tension spikes. Reducing the inertia lowers both the time in compression and magnitude of tension in the lines.

7.2.6 Increased Target Tension

Additional irregular wave cases were run to determine the effect of the torsional spring stiffness on the system. To achieve this, the irregular wave model was updated by increasing the target tension in the winches by 50%. This version of the model was run using the 0.068 kN s m^{-1} damping coefficient for 1.75m Hs across 7.5, 8.5, and 9.5s Tp. The results showed reduced surge, heave, and roll motions of the buoy and increased maximum tensions in the winches. There was no noticeable impact on the winch compression. The following plots show the Winch 1 (wave ward) and Winch 3 (leeward) tensions for the original Iteration 2 model with a 64 kN target tension and the modified Iteration 2 model with a 96 kN target tension.

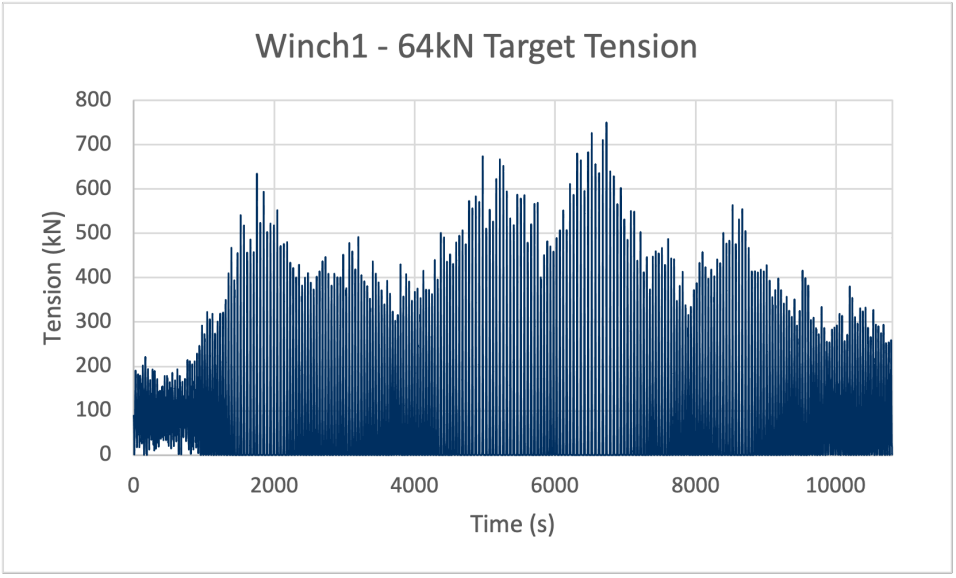

Figure 32: Winch1 time history for irregular wave Hs = 1.75, Tp = 9.5

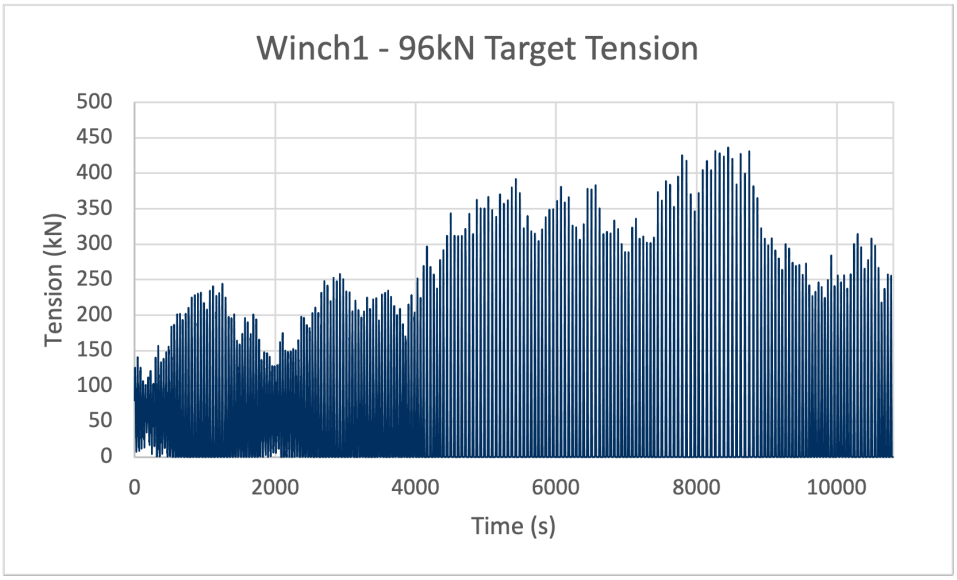

Figure 33: Winch1 with increased target tension time history for irregular wave Hs = 1.75, Tp = 9.5

Figure 32 and Figure 33 show the time history of the tension in Winch 1 (wave ward) for an irregular sea state with a significant wave height of 1.75m and a peak period of 9.5s. Figure 32 is the original run of Iteration 1 with a winch target tension of 64kN. Figure 33 shows the case with an increased target tension of 96kN. Both plots show winch line compression and tension spiking for most of the simulation. The case with increased target tension also shows in increase the magnitude of the tensions.

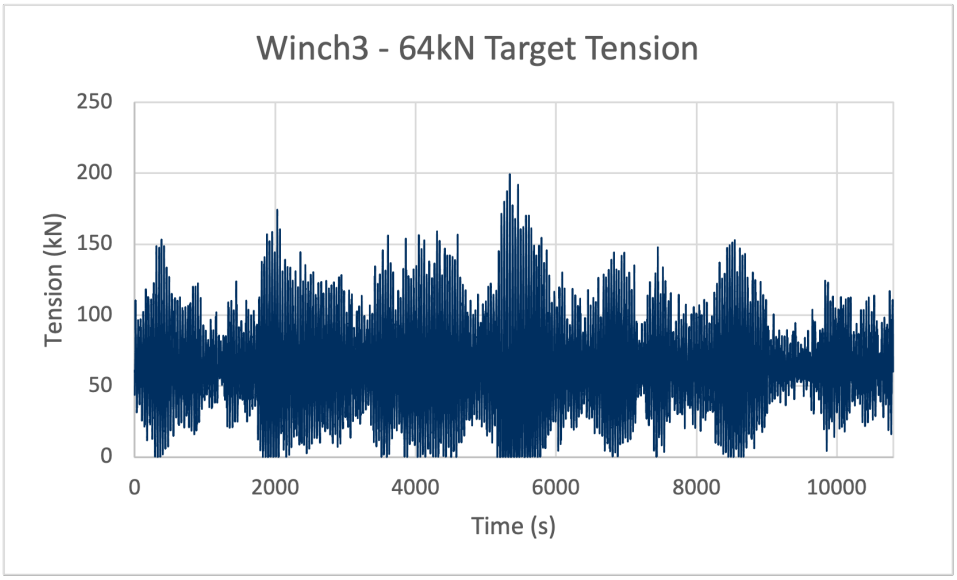

Figure 34: Winch3 time history for irregular wave Hs = 1.75, Tp = 9.5

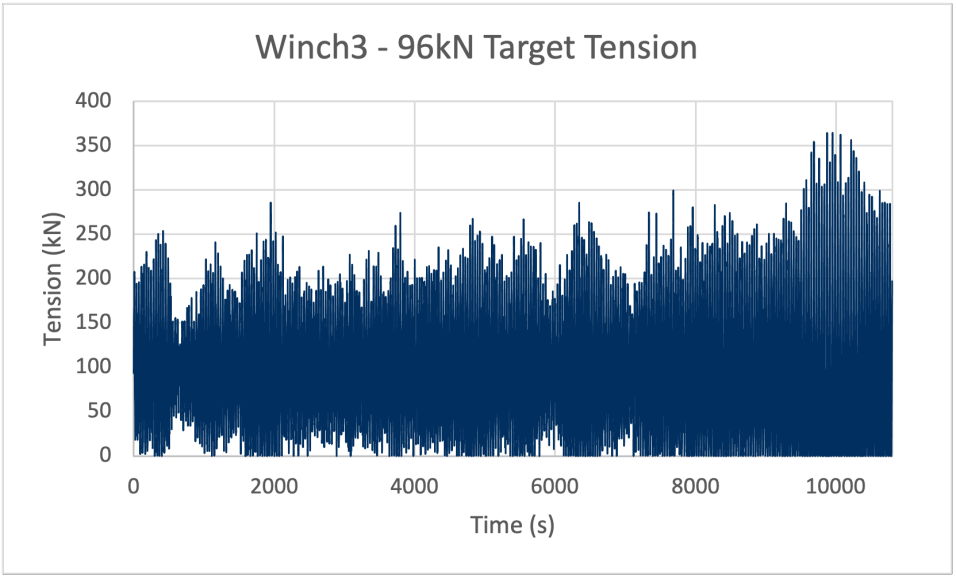

Figure 35: Winch3 with increased targe tension time history for irregular wave Hs = 1.75, Tp = 9.5

Figure 34 and Figure 35 show the time history of the tension in Winch 3 (leeward) for an irregular sea state with a significant wave height of 1.75m and a peak period of 9.5s. Figure 34 is the original run of Iteration 1 with a winch target tension of 64kN. Figure 35 shows the case with an increased target tension of 96kN. As seen in Winch 1, Winch 3 shows an increase in tension magnitude when using a larger target tension. The previous plots indicate that increasing the stiffness of the torsional spring does not reduce the amount of compression in the winch lines.

7.2.7 Increased Winch Damping

Iteration 1 was also run through the full range of regular wave cases with an increased winch damping. As shown previously, the winch damping did not have much impact on the response of the buoy. For these additional cases, the largest winch damping was increased by a factor of 100 to determine if a large magnitude damping constant would result in any changes in the buoy motions. Plots of the surge, heave, and roll motion are shown below. These are the same plots shown in Section 7.1.3.3 but with the results of the 102 kN s m^{-1} damping constant cases included. All data presented following three plots was collected over the first five wave cycles of each simulation.

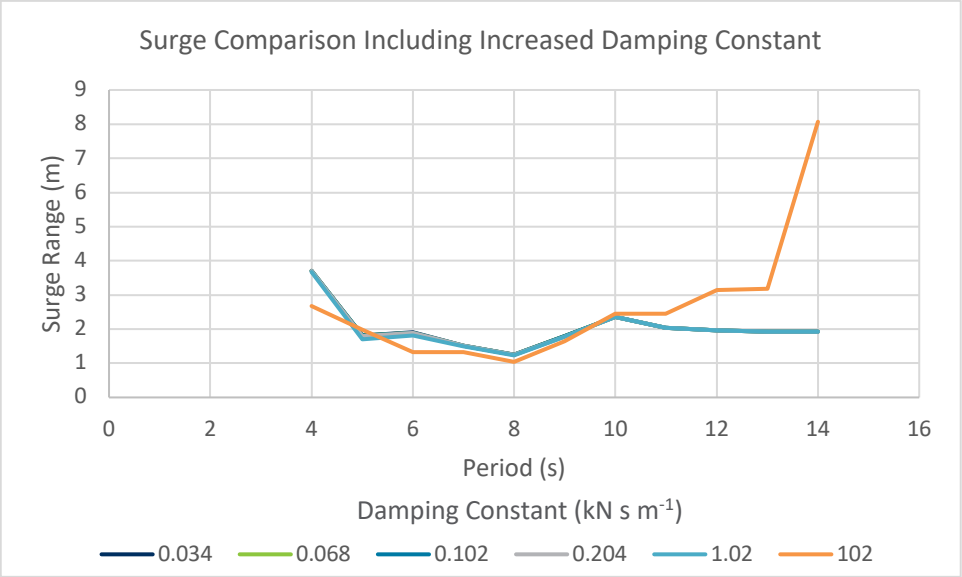

Figure 36: Increased damping constant surge comparison

Figure 36 shows the surge range of the buoy for 1.75m regular waves across the original five damping constants in addition to the 102 kN s m^{-1} damping constant. The surge response of the higher damping constant case is comparable to the previous cases until the 11s wave periods. From this point through the 14s wave periods, the surge range of the high damping case increases considerably while the surge ranges of the previous cases flatten out.

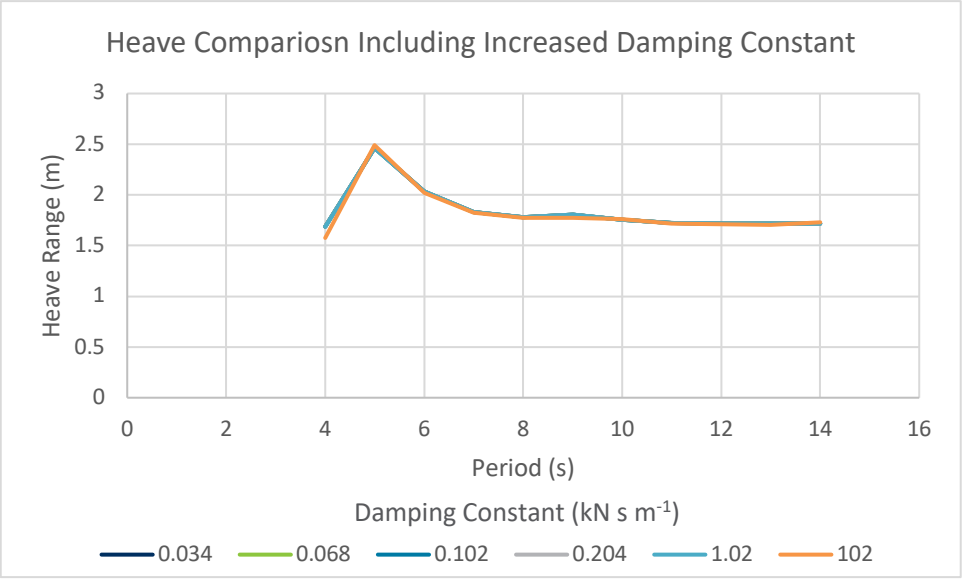

Figure 37: Increased damping constant heave comparison

Figure 37 shows the heave range of the buoy for 1.75m regular waves across the original five damping constants in addition to the 102 kN s m^{-1} damping constant. The heave range is insensitive to increased damping constant.

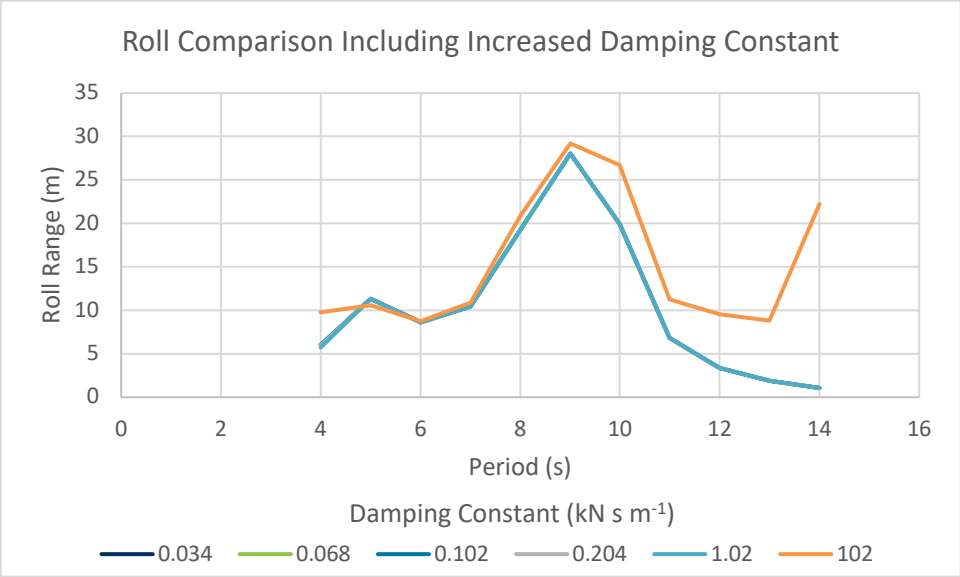

Figure 38: Increased damping constant roll comparison

Figure 38 shows the roll range of the buoy for 1.75m regular waves across the original five damping constants in addition to the 102 kN s m^{-1} damping constant. As with the surge range, the roll range increases over the higher period waves. However, the increase in roll range is not to the same degree as the increase in surge range.

The increase in surge and roll motions is a result of the increased damping in the winches. As the simulation time increases, the winches begin to dominate the response of the buoy over the waves. This can be seen in the time history of the surge motion shown below.

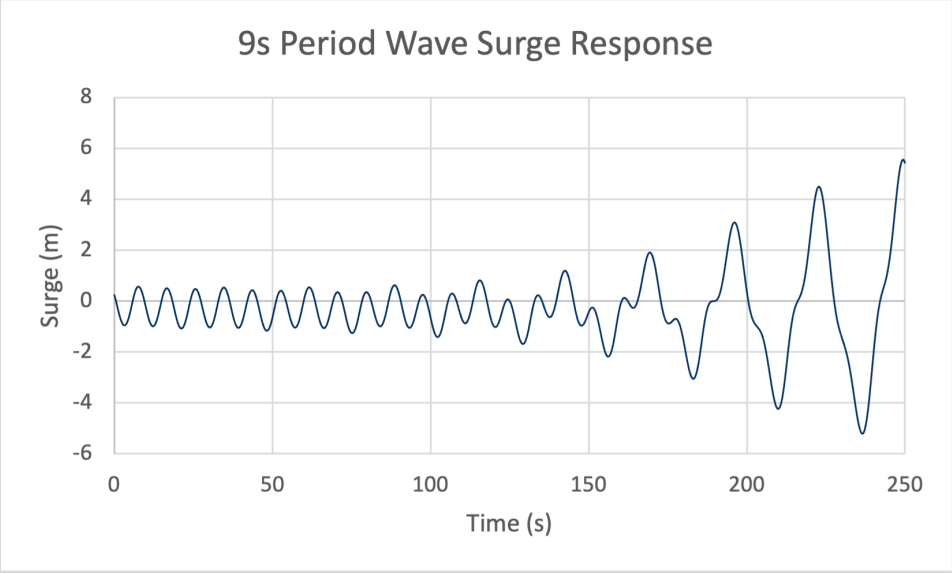

Figure 39: Increased damping constant surge time history for regular wave H = 1.75m, T = 9s

As seen in Figure 39 above, the amplitude of the surge response begins to increase about 100s into the simulation. Before 100s, the period of the surge response is 9s which is the same as the wave period. As the amplitude increases, the 9s period of the wave influence is still noticeable, but there is a longer period response which begins to dominate. By 250s, the 9s response is negligible compared to the longer response. This longer response is driven by the winches, and it has a period of roughly 28s. This increased response is not present in the previous plot of the surge range, because the long period response does not begin to dominate within the first five wave cycles of the simulation. For a 9s wave period, the first five wave cycles occur within the first 45s of the simulation. This is well before the 100s point where the long period response starts to dominate. When referencing the previous plot of the surge range, the surge response of the high damping case begins to deviate starting at the 10s waves. This is due to the long period response dominating earlier in the simulation for longer period waves. This can be seen in the time history for the surge over a 14s period wave.

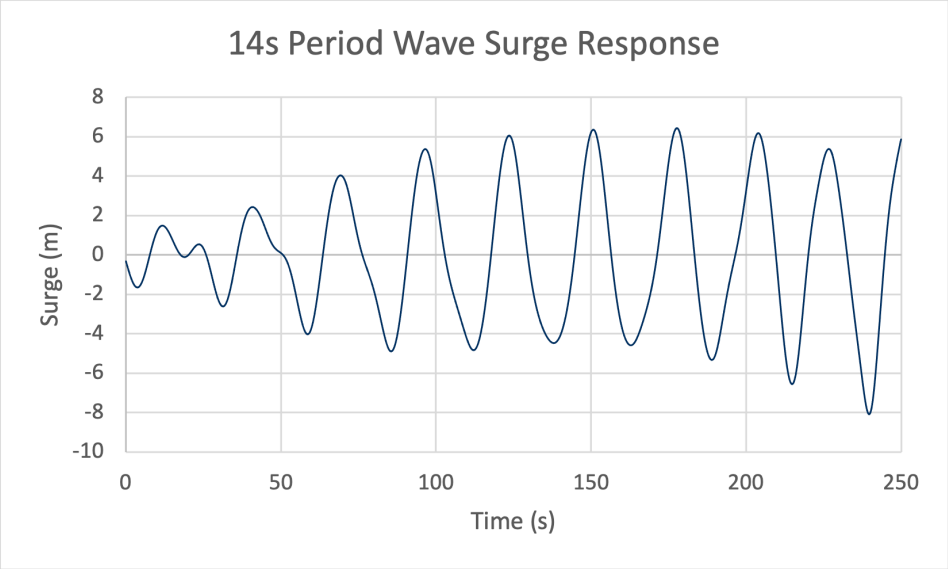

Figure 40: Increased damping constant surge time history for regular wave H = 1.75m, T = 14s

Figure 40 is taken over the same time period as the Figure 39. As shown, the long period response is already beginning to dominate the buoy motion at time 0s which is the end of the wave ramp up period. The long period response for the 14s wave is roughly 28s which the same as the long period response for the 9s wave. Since the 14s wave period is half of the 28s long period response, the system reaches the long period response much quicker over the 14s period waves compared to the 9s period waves. This explains the increase in surge range presented in the beginning of this section. As the wave periods increase from 9s, the winch driven, long period response begins to dominate earlier in the simulation. Since the data is collected over the first five wave cycles, the increase in surge range becomes apparent in the higher wave period cases. The winches have a similar effect on the roll motion, but to a lesser degree than the surge motion.

The long period response in the surge motion at 28s is near the yaw natural period of the buoy. Once the surge motions become dominated by the winch, the yaw becomes excited, and the buoy loses stability. Increased yaw motion causes the wave loading on the buoy to be asymmetrical which increases the yaw

motion even further. At this point, the winches are unable to recover the system and the buoy stability is lost.

The annual power at the reel connections over the high damping constant cases was also examined. As seen in Figure 41 below, the higher damping constant did not have much effect on the total annual power of the system. The data presented in this plot was taken over the first five wave cycles of each case, and the x axis (damping constant) is in log scale.

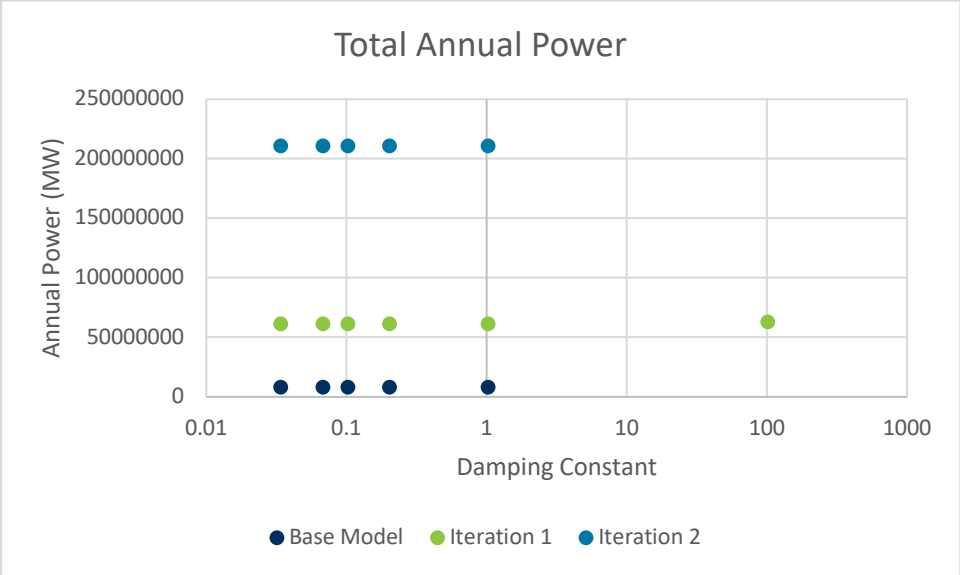

Figure 41: Total annual power comparison with increased damping constant

8 CONCLUSIONS AND RECOMMENDATIONS

The purpose of this study was to assess the performance of the Laminar Scientific Wave Energy Converter system as described in Section 7.1. The Base model configuration which consisted of a concave buoy shape, two iterations on buoy size, one iteration considering reduced inertia, and one considering, non-concave buoy shape were assessed. Each of these iterations considered initially regular wave analyses and a further assessment considered the damping. After conducting the initial regular wave studies, a selected iteration was subjected to irregular waves. The main conclusions from this study identified the following:

- The study has indicated that the power of this arrangement is closely linked to the surge and heave response of the buoy to the waves, best performance is for stable motion that follows the elliptical path of the wave.
- The Base Model configuration in regular wave conditions indicated that in some conditions the buoy motion became uncontrolled, this was typically associated with small wave periods or when the incoming wave period closely matched one of the natural response periods of the buoy.
- Consideration of a larger buoy size indicated that with increased size the buoy motion became more stable and indicated that the larger buoy has the potential to create more average power than the base model configuration. The increase in power is approximately to the cubic of the scaling. That is the 1:3 buoy produced approximately 27 time more energy than the base model.

- Assessment of the damping in the system indicated that the buoy performance was insensitive to this parameter.
- Assessment of the inertia drive systems suggest that reducing the inertia as much as possible has the effect of stabilizing the system, however this does not impact the average power at the reel connections.
- When the concave buoy is replaced with a rectangular shaped buoy the buoy performance is relatively similar to the concave buoy however for the same buoy size the concave buoy does see slightly more power at the reel connections.

The following conclusions outline the effect of specific parameters on the performance of the system.

1. The buoy showed uncontrolled motions in one or more degrees of freedom and struggled to keep station in the irregular sea states mentioned in the Test Plan. These motions, along with continued wave activity, do not allow the buoy to return to a steady orbital motion of the waves. The instability was the result of a combination of natural period excitation, load RAO effects, winch line compression and tension spiking, and low yaw resistance in the mooring system. The sea states defined in the test plan are too large for the current buoy design to perform effectively. The buoy performed best in irregular sea states with the 9.5s peak period compared to the 7.5s and 8.5s peak period sea states. This is due to the 9.5s peak period sea states having longer waves on average which allows the buoy to more closely follow the orbital path of the wave. However, even in the 9.5s period sea states, the system was not stable and showed considerable winch line compression and tension spikes. The current design would need to be implemented in a smaller sea state to perform as intended.
2. The wave diffraction effects on the buoy will become more significant as the buoy size increases. When modelling a buoy sized greater than 2:1 scale of the Base Model, load RAOs should be included.
3. The heave and roll natural periods fell within the period ranges of both the regular and irregular waves defined in the Test Plan. Peaks in both heave and roll motions occurred during waves with a period near the respective natural periods of the buoy. Increasing the size of the buoy increases the heave and roll natural periods. Removing the curvature of the buoy decreases the roll natural period, but it does not change the heave natural period.
4. The roll load RAOs had a peak in amplitude in the 4-5s period range, and peaks in the roll motion of the buoy occurred during wave which had a period in this range. The influence of the roll load RAOs on the buoy was more significant for wave of larger wave height. Buoy models which were larger in size (mass, moment of inertia, and volume) were less influenced by the roll load RAOs than smaller sized buoy models.
5. The surge load RAOs had a peak in amplitude in the 4-5s range, and the winch line tensions had a long period response during waves which had a period in this range. The long period response in the winches occurred near the surge natural period, and peaks in surge motions occurred.
6. Winch inertia had the most noticeable effect on the winch line compression and tension spiking. In both the regular and irregular wave cases, the winch line tensions were considerably decreased. In cases where winch line compression and tension spiking were observed, the decoupled winches reduced the time in compression and the magnitude of the tension spikes. Additionally, cases with decoupled winches showed less extreme buoy yaw motions. Average winch line velocity was increased in cases with decoupled winches.

7. Changes in winch damping constant which were of a factor of 0.5-15 times the reference generator damping constant of 0.068 kN s m^{-1}, did not have significant influence on the buoy performance. When the reference damping constant was increased by a factor of 1500, the buoy showed an increase in both surge and roll response. With the increased damping constant, the winches began to dominate the surge response of the buoy. This surge response occurred over a period near the yaw natural period of the system, and the buoy quickly lost stability.

The following recommendations are made based on the results of the analysis:

1. Lowering the winch inertia had the most significant effect on reducing the winch line compression and tension spiking. The value used for the winch inertia was calculated based on the inertia of the internal mechanisms of the buoy (shaft, flywheels, and gearbox). If the inertia of these components can be reduced, the mooring lines can recover more quickly in unfavorable conditions. Investigating potential ways to lower this inertia will help to improve the performance of the system.
2. The current mooring configuration provides little resistance against yaw motion. Slight yaw motions can quickly become uncontrollable, and the mooring system is unable to recover reliably. If the mooring system can be altered to provide greater resistance against yaw motion, the stability of the system can be improved. One potential change to the mooring system would be to investigate the stability reduction effect of changing the constant torsional force spring to a non-constant force spring where the spring force increases with extension.
3. When the target tension was increased, the magnitudes of winch line tension over the simulation also increased. If the mass of the buoy is increased, the buoy will become less buoyant, and the target tension could be reduced. Additionally, the increased mass of the buoy could provide more stability in unfavorable conditions., as larger sized buoy models with greater mass and moment of inertia were more stable than smaller sized buoy models.

9 APPENDIX

9.1 APPENDIX A: LAMINAR PRE-TEST PLAN ANALYSES

The Analysis of Hydrodynamic Performance of Laminar Scientific V1 and V2
Contract with Laminar Scientific Inc.
Prepared primarily by: Jian Tan
September 2021
Delft, the Netherlands

1. Introduction

This task is intended to analyse the hydrodynamic performance of two versions of the buoy provided by the Laminar Scientific company. The objective of this report is to help the decision maker to choose the more promising design of the buoy.

The two designs of the buoy are shown in the Figure 1 and 2. These two designs of the buoy are semi-submerged in still water. In this task, their mass are assumed to be evenly distributed over the surface, which means the gravity center (GC) is located at the geometry center (Origin O).

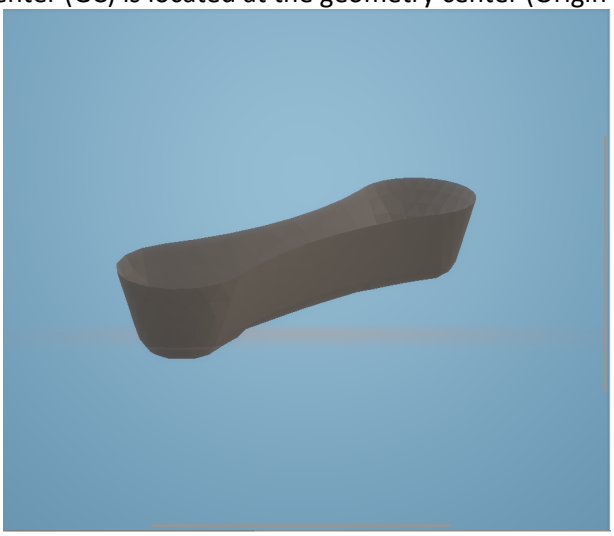

Figure 1. Schematic of wetted surface of version 1

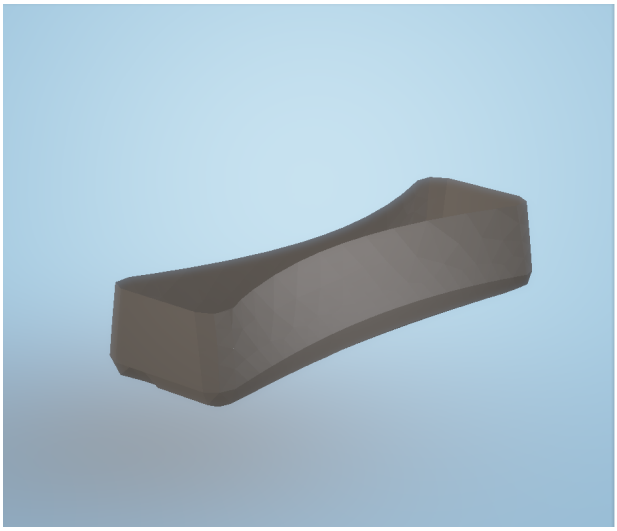

Figure 2. Schematic of wetted surface of version 2

2. Methodology

In this task, the frequency domain model is applied to analyse the performance of the two designs. According to Newton's second law, the dynamics of the buoy can be described as

$$\hat{\xi} = A_w(\omega)\hat{\mathrm{f}}_{\mathrm{e}}[-\omega^2(M+A)+G+K_{pto}+K_m+\mathrm{i}\omega(\mathrm{R}+\mathrm{B}_{\mathrm{pto}})]^{-1} \quad (1)$$

where $\hat{\xi}$ is the matrix of complex amplitude of the displacement, A_w is the wave amplitude, $\hat{\mathrm{f}}_{\mathrm{e}}$ is the matrix of complex matrix of the excitation force, M and A are mass matrix and added mass matrix, G is the matrix of hydrostatic restoring coefficients, K_{pto} and K_m are the matrix of PTO (power take-off) spring stiffness and mooring spring stiffness matrix, R and $\mathrm{B}_{\mathrm{pto}}$ are the matrix of radiation damping and PTO damping.

The hydrodynamic related coefficients $\hat{\mathrm{f}}_{\mathrm{e}}$, $\mathrm{B}_{\mathrm{pto}}$ and A are calculated by the open source boundary element method code Nemoh (Penalba et al., 2017). As an important input, the mesh is performed in the environment of open source software Salome. The number of mesh grids for V1 and V2 are 775 and 889, in which the maximum size of the grid is controlled with 0.2. This is considered to be sufficient for boundary element method. The mass of the buoy is calculated by the Archimedes' law, which indicates that the mass of the buoy is equal to be mass of displaced water. As the mass is assumed to be distributed on the surface, the moment of inertia in mass matrix can also be calculated as

$$I_{ij} = \rho V r_{ij}\left|r_{ij}\right| \quad (2)$$

where ρ is the density of the buoy and r_{ij} is the corresponding radius of gyration. In addition, the K_{pto}, K_m and $\mathrm{B}_{\mathrm{pto}}$ are set to be zero matrices in this task since they are not in the scope of hydrodynamic analysis. However, they are significant to the optimization of PTO parameters and identification of power

performance, which can be investigated in following phases. Therefore, as all the coefficients have been obtained explicitly, the response amplitude operators (RAOs) are then derived as

$$\frac{\hat{\xi}}{A_w(\omega)} = \hat{f}_e[-\omega^2(M+A)+G+i\omega R]^{-1} \tag{3}$$

RAO is a commonly used dimensionless measure in hydrodynamic analysis, and it is calculated by dividing the amplitudes of the motion in one of the degrees of freedom by the amplitudes of the incoming the waves. It effectively indicates how strongly the system responds to the incoming waves. The higher the value of the RAO, the larger motion the system is associated with.

The limitation of the frequency domain modelling could be divided into three parts:

1) The frequency domain model is based on the assumption of linear wave theory, and the nonlinearity of ocean waves is not considered, such as the higher order strokes waves;
2) The frequency domain model is based on the linear potential theory, in which the nonlinear force components resulting from wave-structure interaction could be included, such as nonlinear Froude-Krylov force and viscous force;
3) The frequency domain model is not able to model time-dependent external forces, such as nonlinear PTO force and displacement/force/velocity saturation.

3. Results and analysis

3.1. Results presentation

The hydrodynamic coefficients of these two designs are presented in Figure 3 and 4.

Figures 3. Hydrodynamic coefficients of V1 buoy

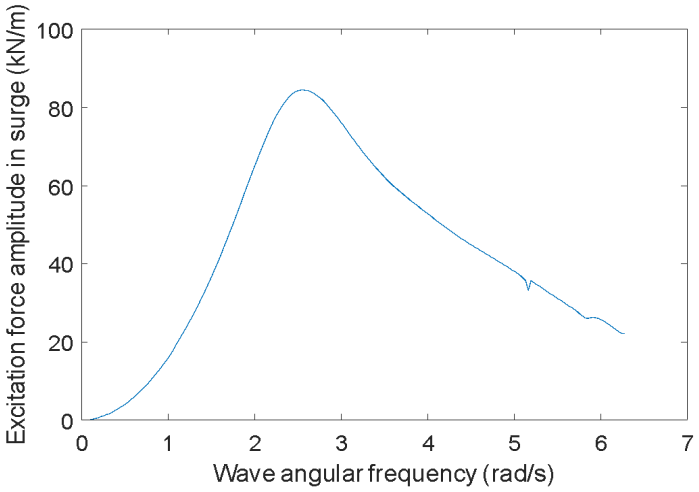

3. (a) Excitation force coefficient in surge V1

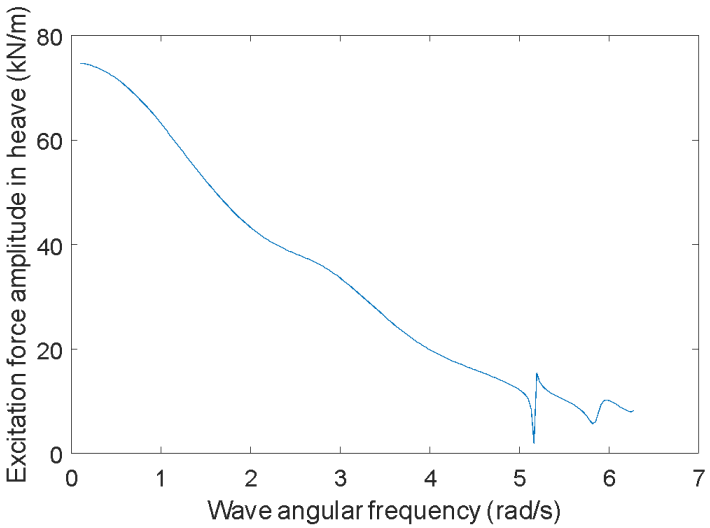

3. (b) Excitation force coefficient in heave V1

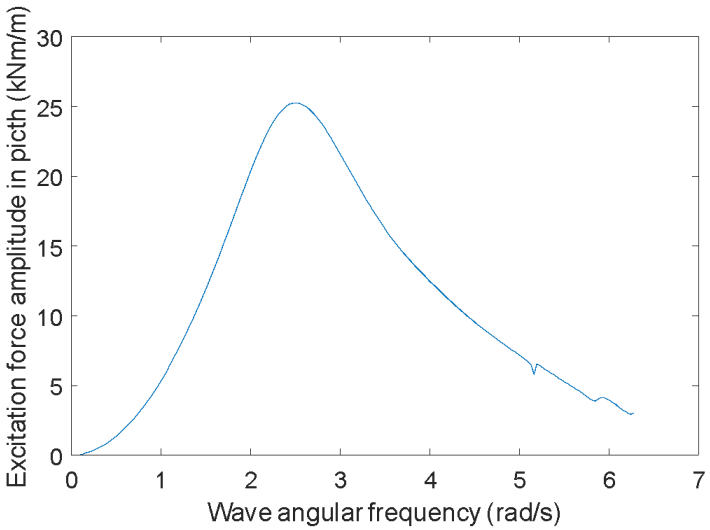

3. (c) Excitation force (torque) coefficient in pitch V1

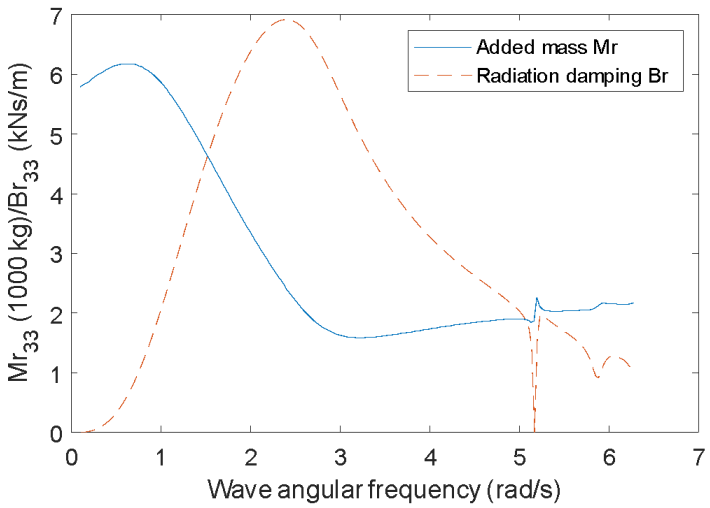

3. (d) Added mass and radiation damping in heave V1

Figures 4. Hydrodynamic coefficients of V2 buoy

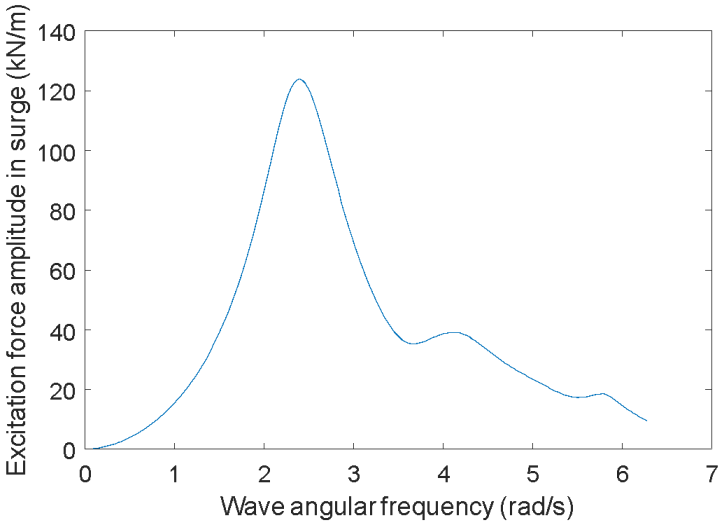

4. (a) Excitation force coefficient in surge V2

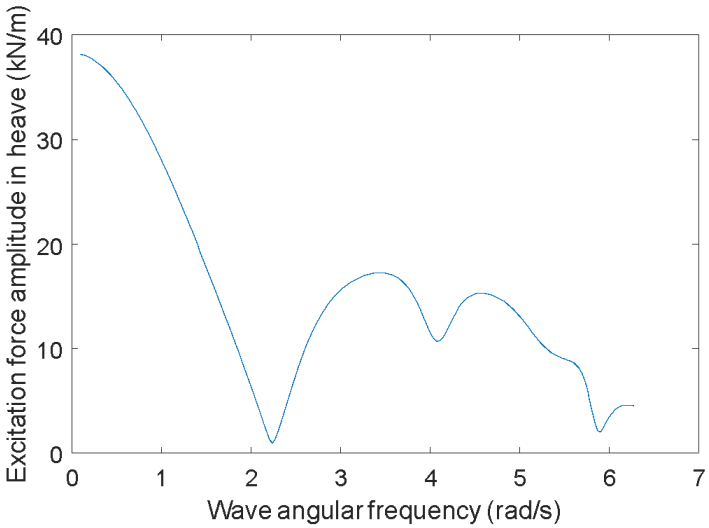

4. (b) Excitation force coefficient in heave V2

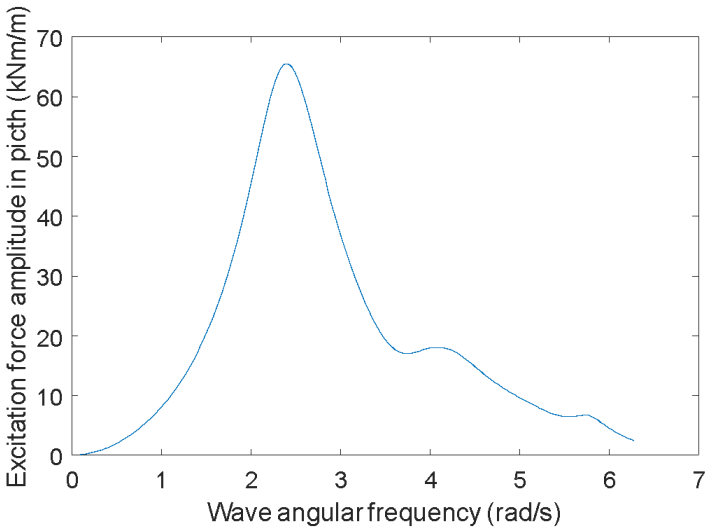

4. (c) Excitation force (torque) coefficient in pitch V2

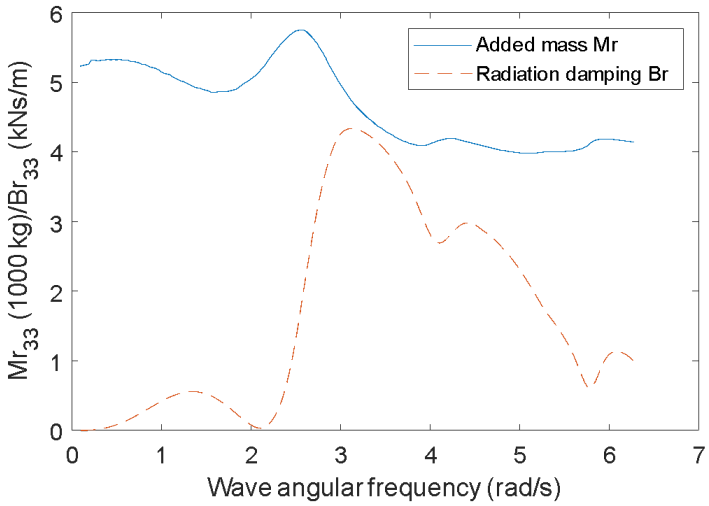

4. (d) Added mass and radiation damping in heave V2

The RAOs of the two designs are presented in figures 5(a) through (c).

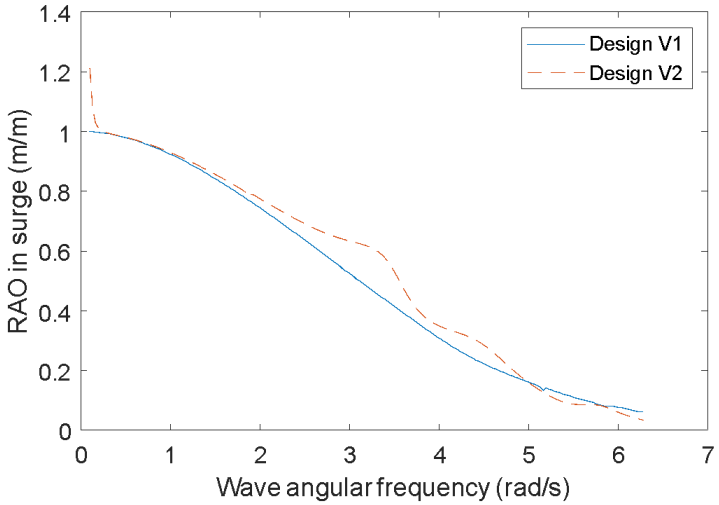

5. (a) In Surge

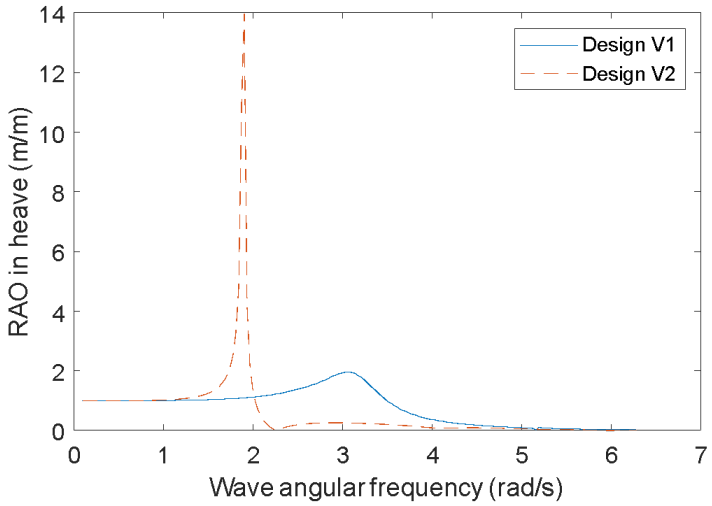

5. (b) In Heave

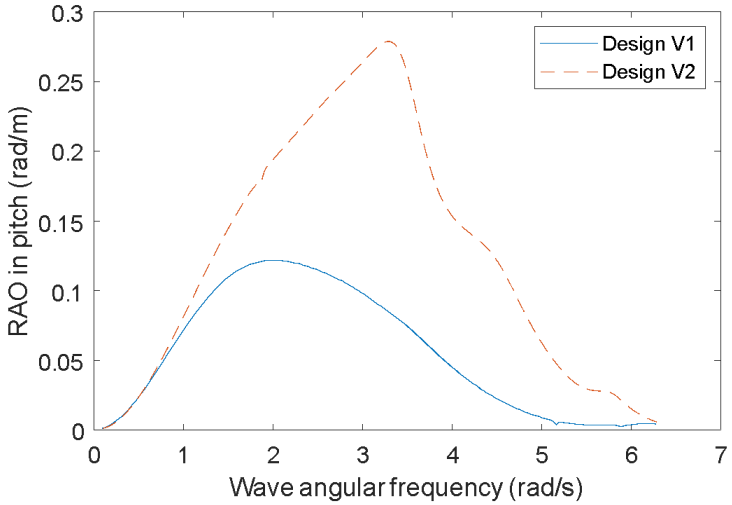

5. (c) In pitch

3.2. Discussion

A comparison the RAOs of these two designs is made, and it is shown in Figures 5(a) through (c). However for PACWAVE South, a frequency range between 0.3 to 1.5 is the only applicable range.

RAO for surge shows that the two buoys are very similar, however since this buoy design is a drag heavy system, it is more applicable to use Morrison equation where the drag coefficient is considered. V2 is expected to have a greater drag coefficient than V1 because V2 has concavity about a horizontal and vertical axis.

From Figure 5 (b), it demonstrates that the peak RAO of V2 in heave is significantly higher than that of V1. For instance, the peak value of V1 is around 2 while it is 14 for V2. However, the power absorption bandwidth of V2 is obviously narrower than V1. In the PACWAVE range however, V2 and V1 are very similar. If the buoy was brought closer to the shore, where the frequency increases, V2 will have a lesser bandwidth of operation. The limitation of this analysis however does not consider the fact that the buoy will sink further than 50% (at calm seas) during a wave, therefore another quick analysis step was undertaken for V2 for heave with the wetted area of 70%:

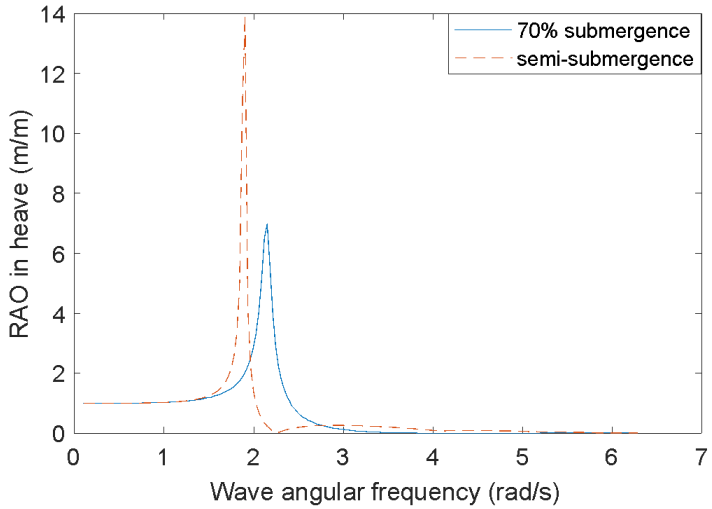

This above plot for V2 conveys that the bandwidth will change dynamically with level of submergence. 70% is a more likely scenario within a wave crest.
With heave and surge, using just RAO, a difference between V1 and V2 is not seen for the PACWAVE conditions. Surge is expected to be larger for V2 due to drag effects.
As for pitch motion, it is observed from Figure 5 (c) that the V2 shows a clearly larger response than V1 over all the considered wave frequencies. If the pitch motion is designed to make the main contribution, then V2 is considered to be a better solution. Pitch motion can positively contribute to energy capture if the mooring point is away from CG, such that the rotation of the buoy will lead to translation of the mooring points.
V2 is also much easier to build, without complex contours except for the concave faces.
Using CFD in SimScale, it was found that V2 had a greater CD than V1 for seawater at 3m/s as a scenario for calculation. CD for V2 in this environment (and Re) is 1.24 and CD for V1 is 0.79. This suggests that the surge capture due to drag forces will be significantly higher for V2.
Therefore a decision to pursue V2 buoy is made due to factors summarized below:

- Greater expected surge
- Easier to build
- Greater pitching
- Same heave as V1

Follow up task: Brief Initial Comparison of Laminar V2 to a simple cylindrical half submerged buoy.

RAO in surge showed negligible difference since CD is not considered. CD for a cylinder in 10^7 was found in literature to be approximately 0.8 [2], whereas V2 CD is estimate to be 1.24, which infers a greater surge capture with V2. RAO in pitch was extremely low as expected. RAO in heave is shown below:

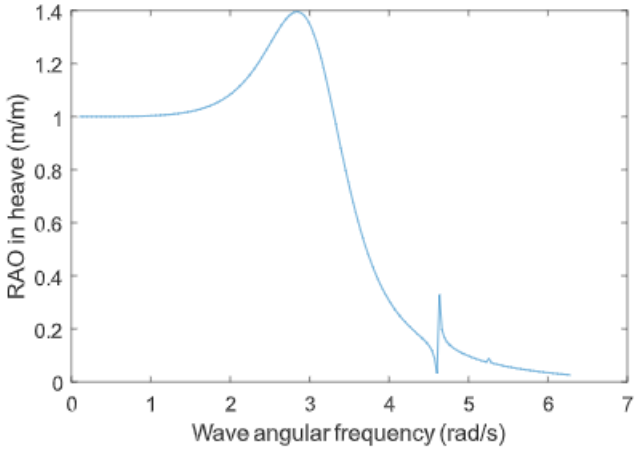

Compared to V2, the cylindrical buoy attains significantly less heave, but comprises a greater bandwidth. Our next follow up would be to attain heave RAO for a fully submerged cylindrical buoy for comparison with V2.

References:

[1] Penalba, M., Kelly, T., & Ringwood, J. V. (2017). Using NEMOH for Modelling Wave Energy Converters : A Comparative Study with WAMIT. 12th European Wave and Tidal Energy Conference, 10.
[2] Experimental data from Incompressible Flow, Wiley-Interscience, New York, 1984

9.2 APPENDIX B: LAMINAR BI-CONCAVE BUOY USE CASES

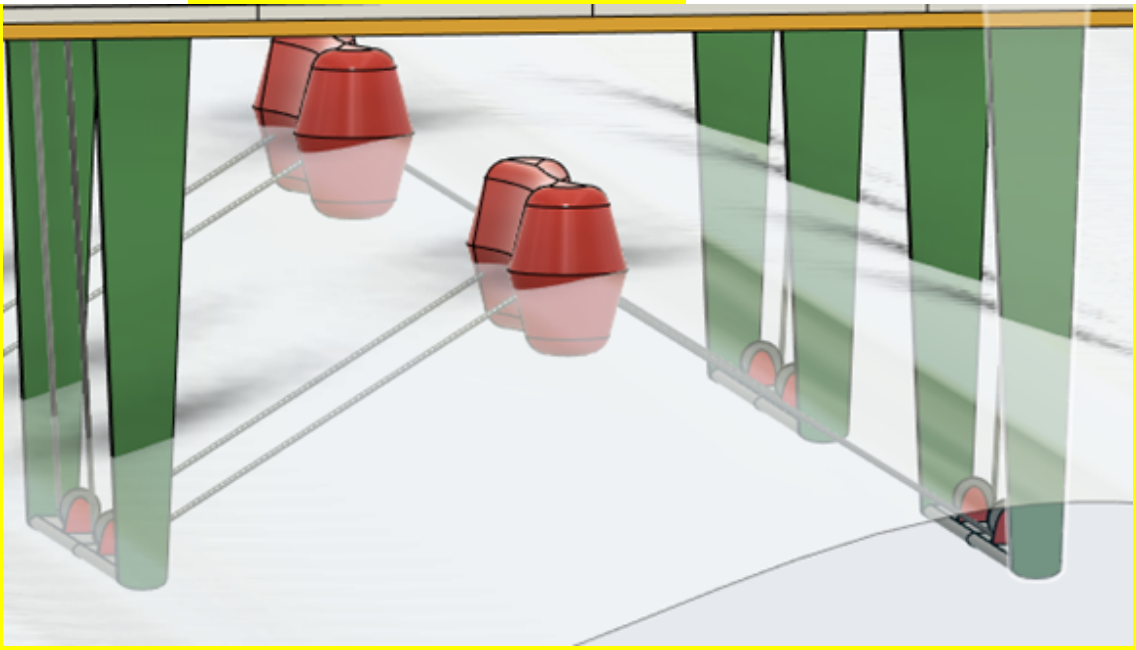

Figure 1: Zoomed in to offshore hybrid structure's biconcave buoy configuration

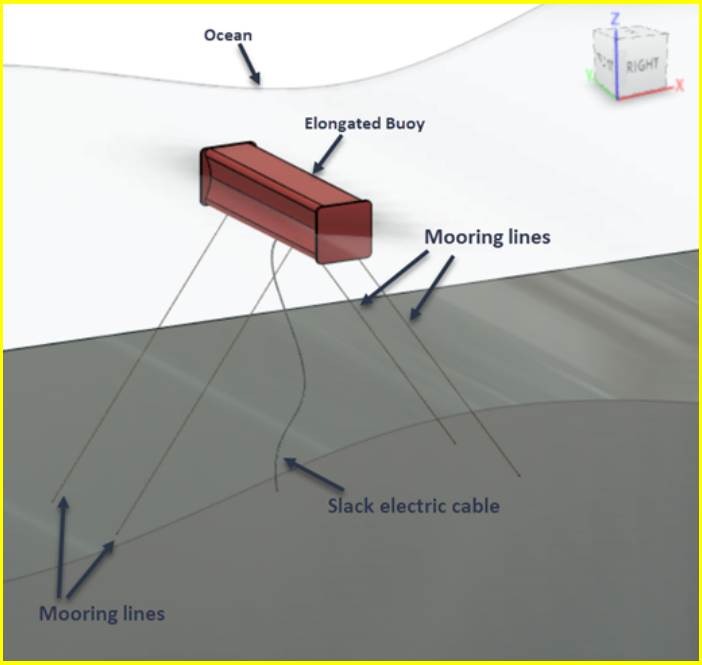

Figure 2: Standalone biconcave buoy configuration

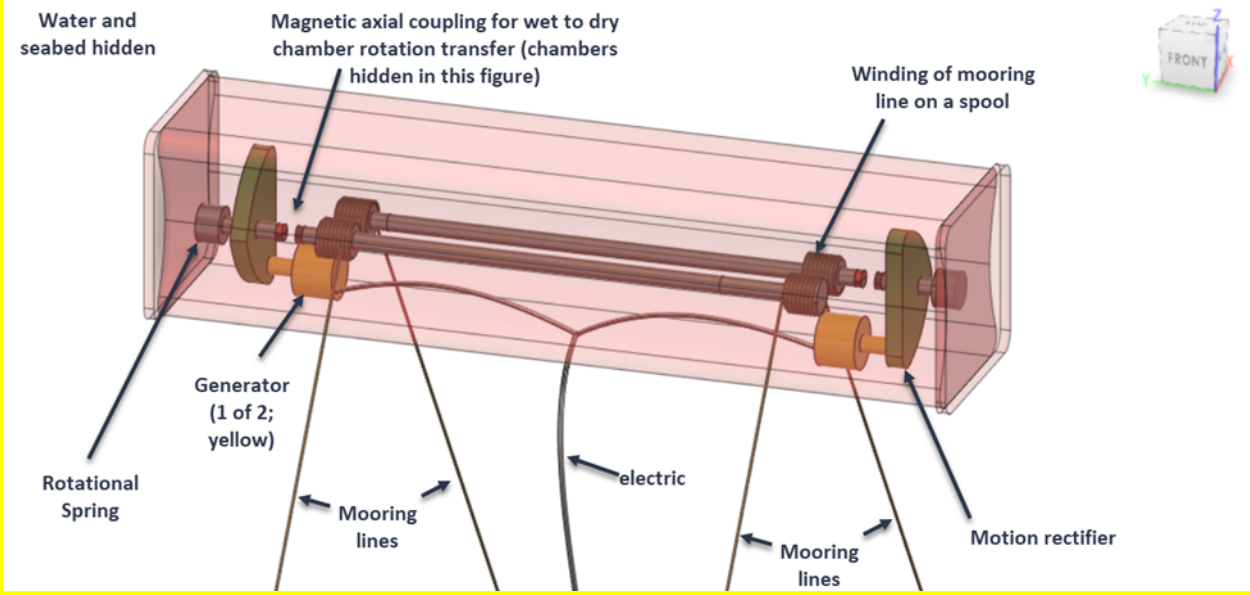

Figure 3: Closer look at standalone buoy configuration

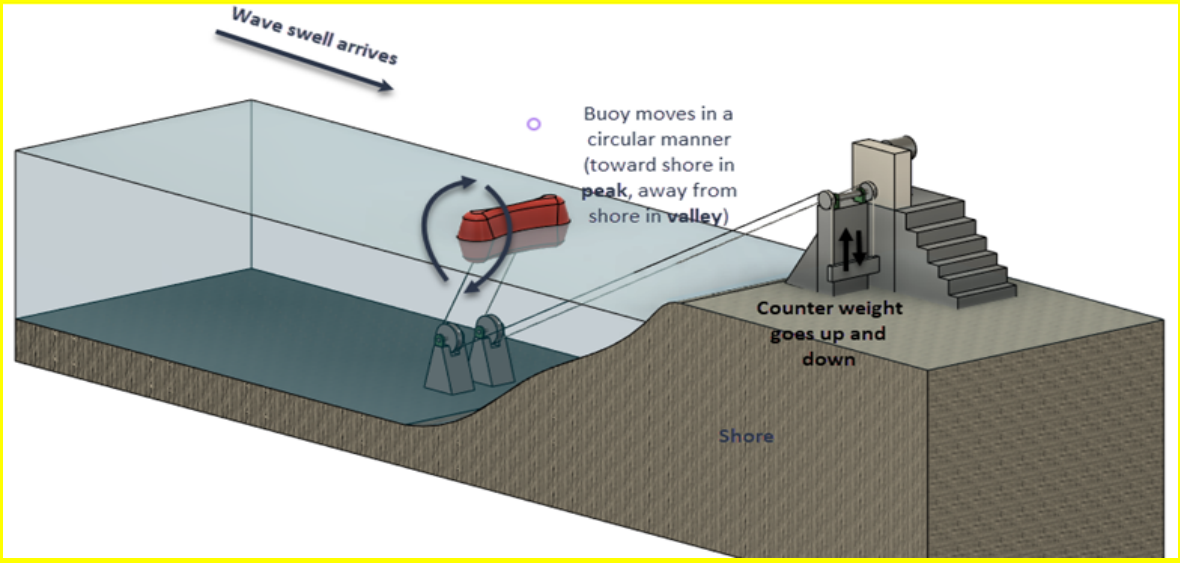

Figure 4: Shore configuration

9.3 APPENDIX C: LOAD RAOS

9.3.1 Base Model and Iteration 3

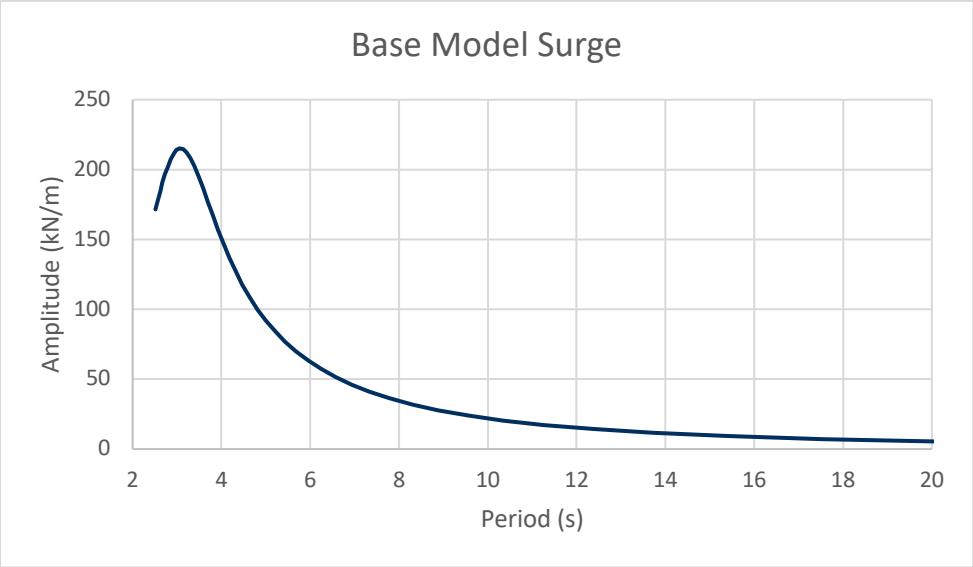

Figure C1: Base Model Surge RAO

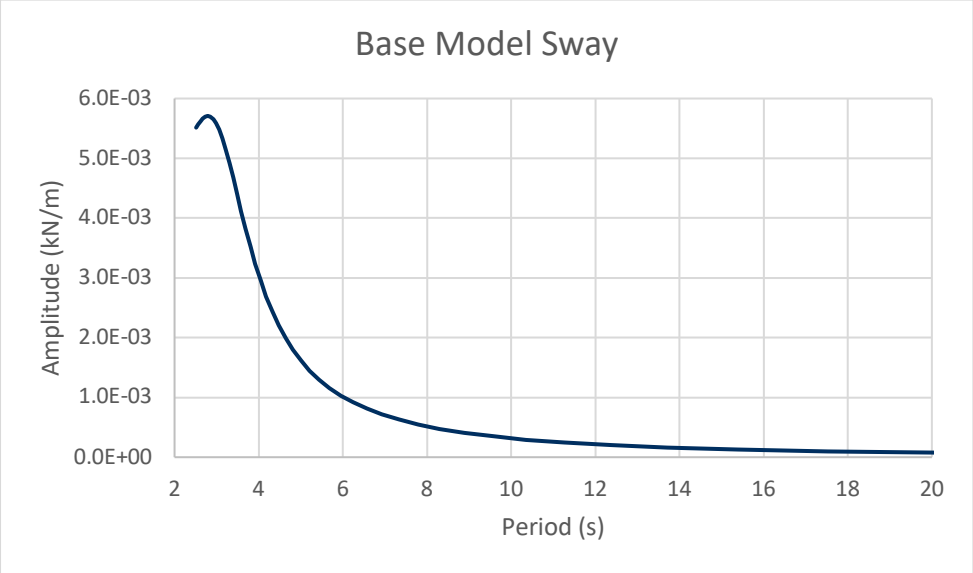

Figure C2: Base Model Sway RAO

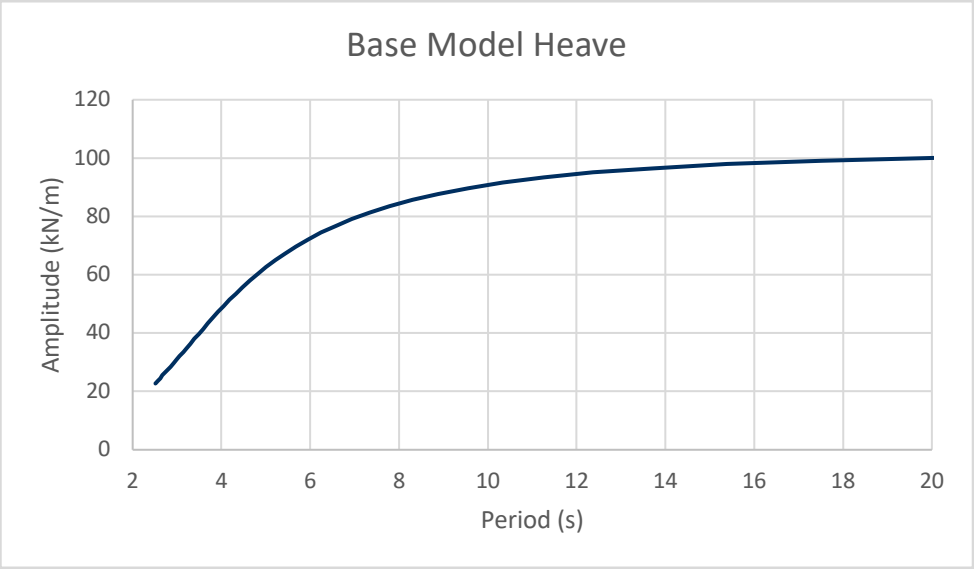

Figure C3: Base Model Heave RAO

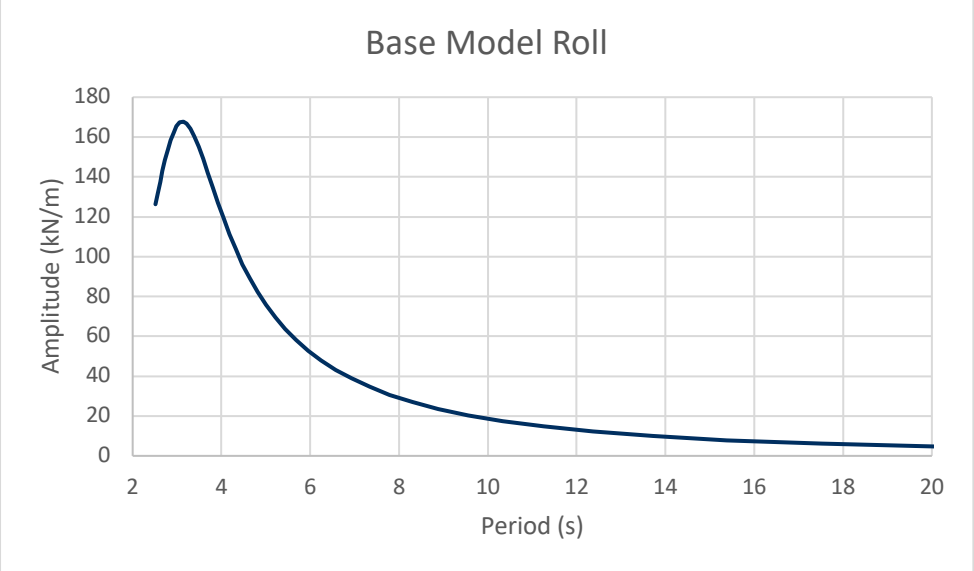

Figure C4: Base Model Roll RAO

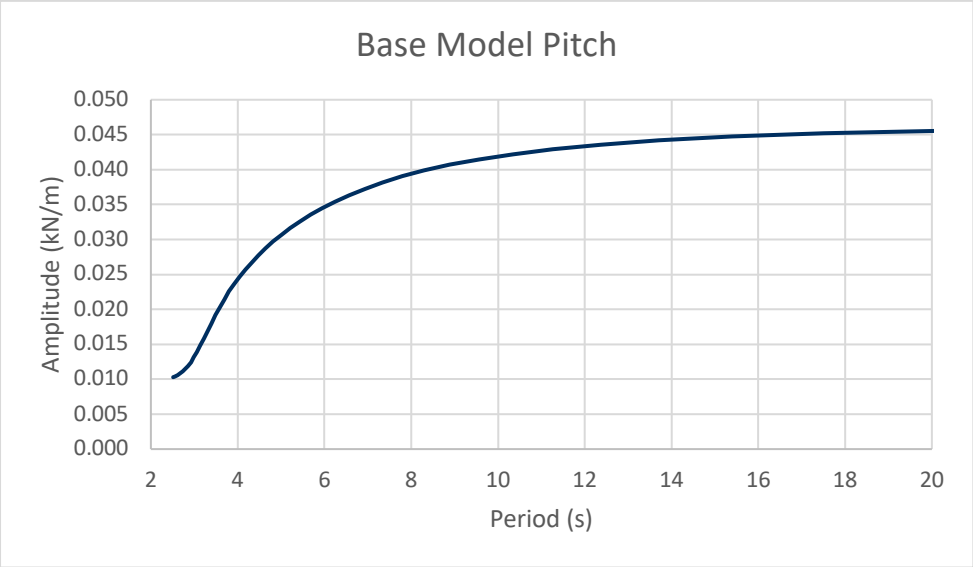

Figure C5: Base Model Pitch RAO

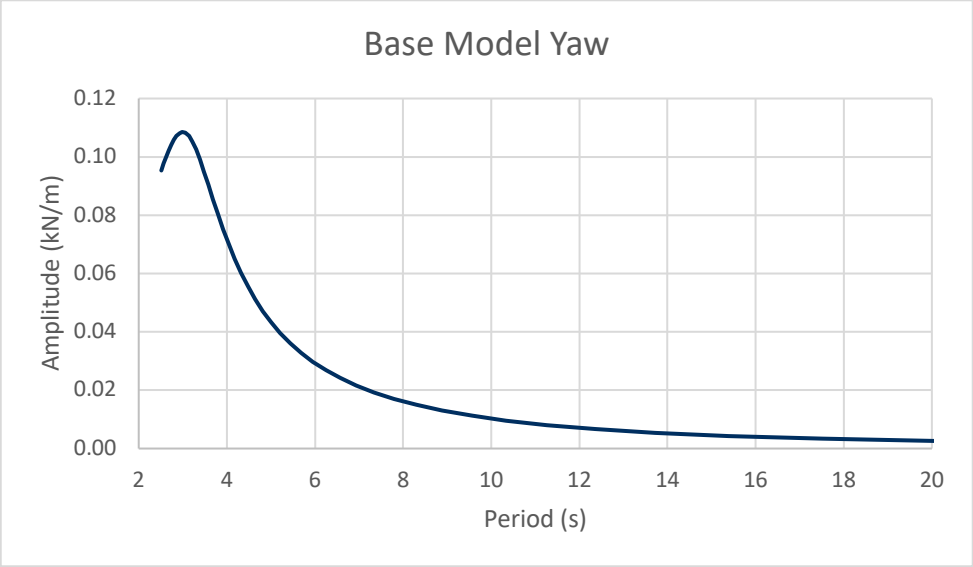

Figure C6: Base Model Yaw RAO

9.3.2 Iteration 1

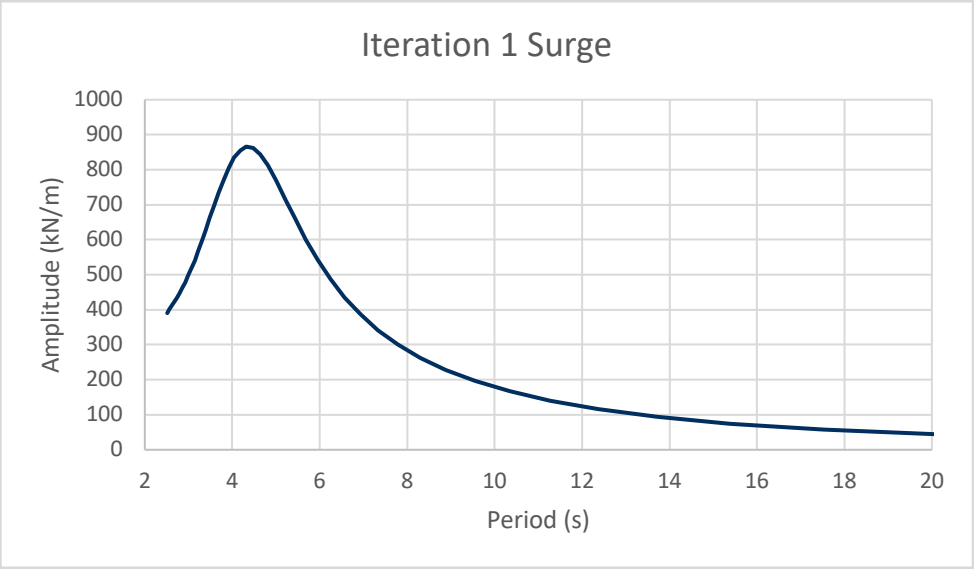

Figure C7: Iteration 1 Surge RAO

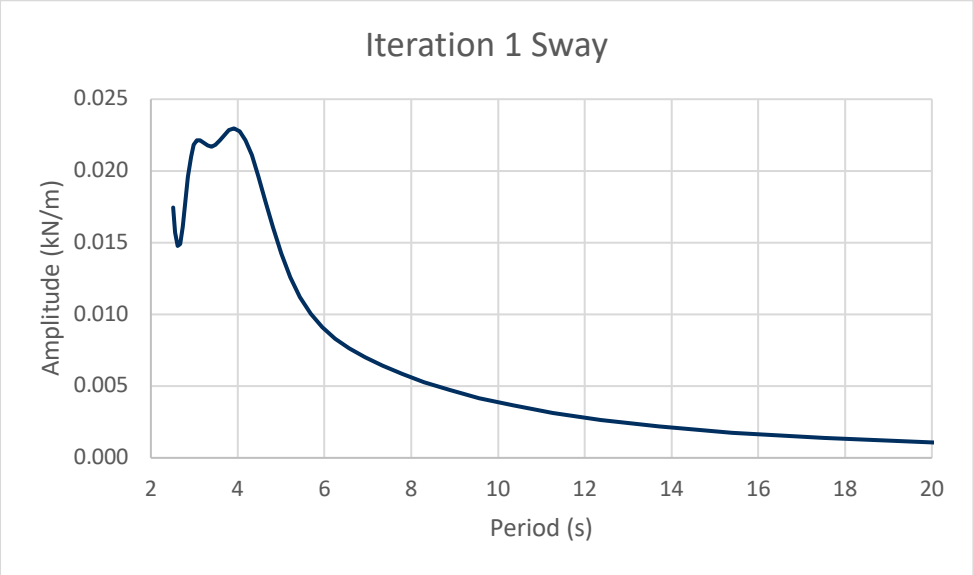

Figure C8: Iteration 1 Sway RAO

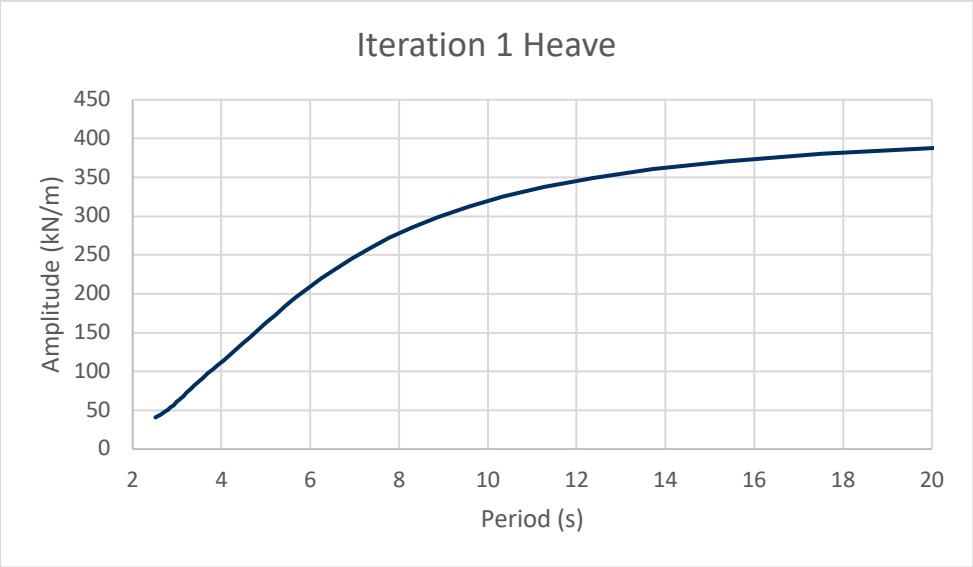

Figure C9: Iteration 1 Heave RAO

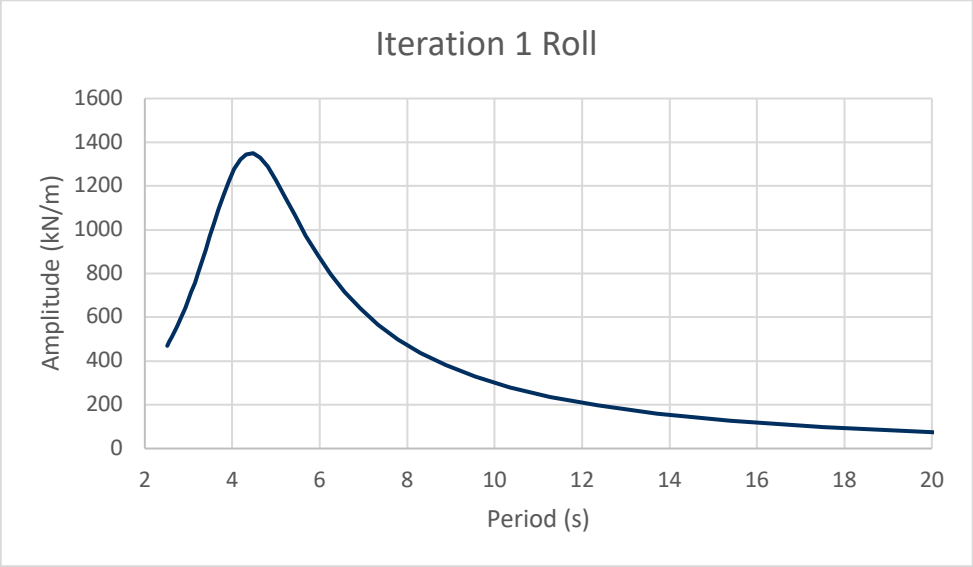

Figure C10: Iteration 1 Roll RAO

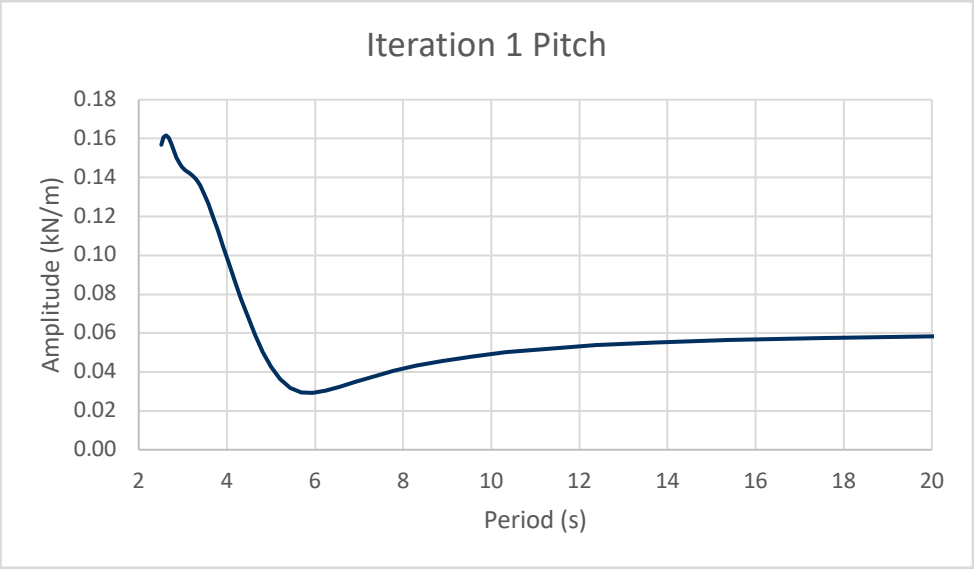

Figure C11: Iteration 1 Pitch RAO

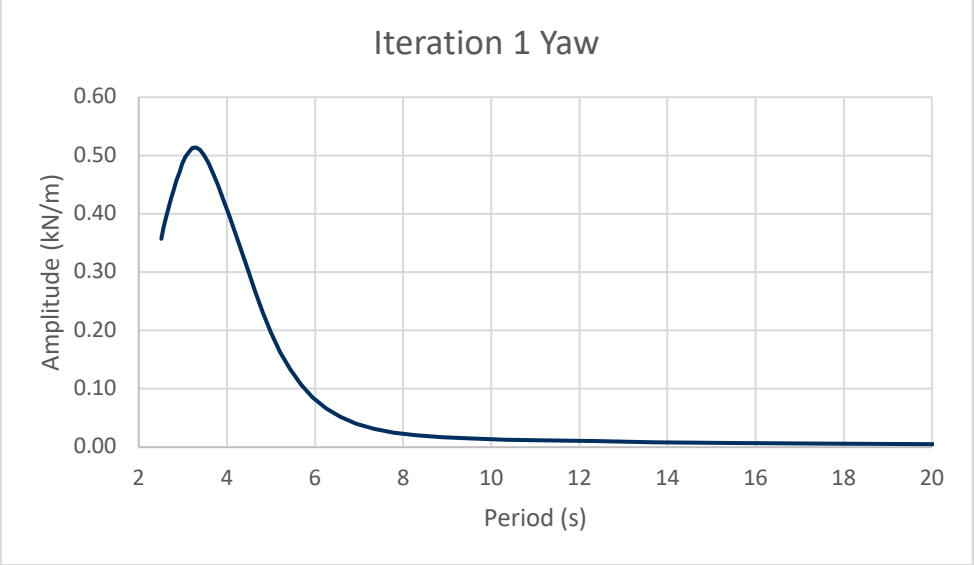

Figure C12: Iteration 1 Yaw RAO

9.3.3 Iteration 2

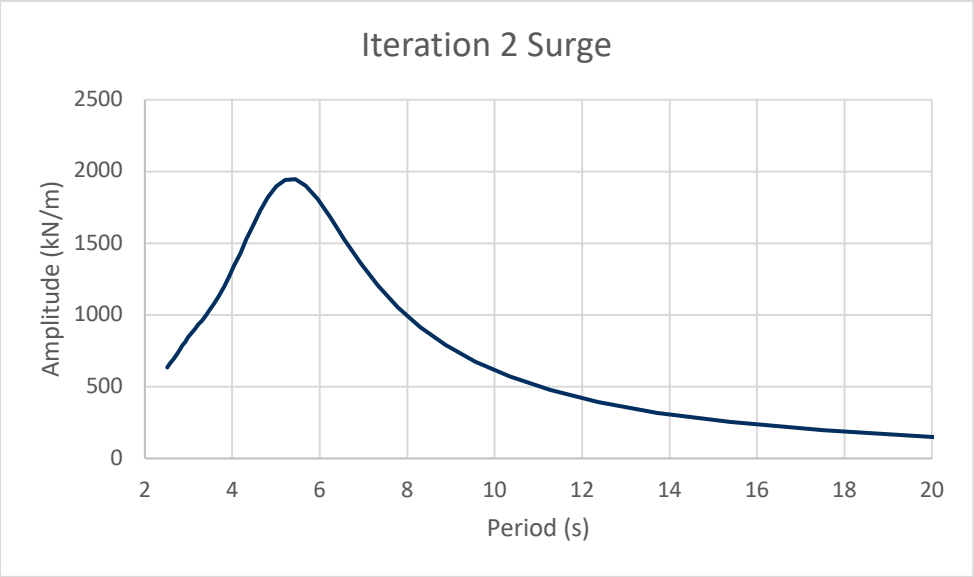

Figure C13: Iteration 2 Surge RAO

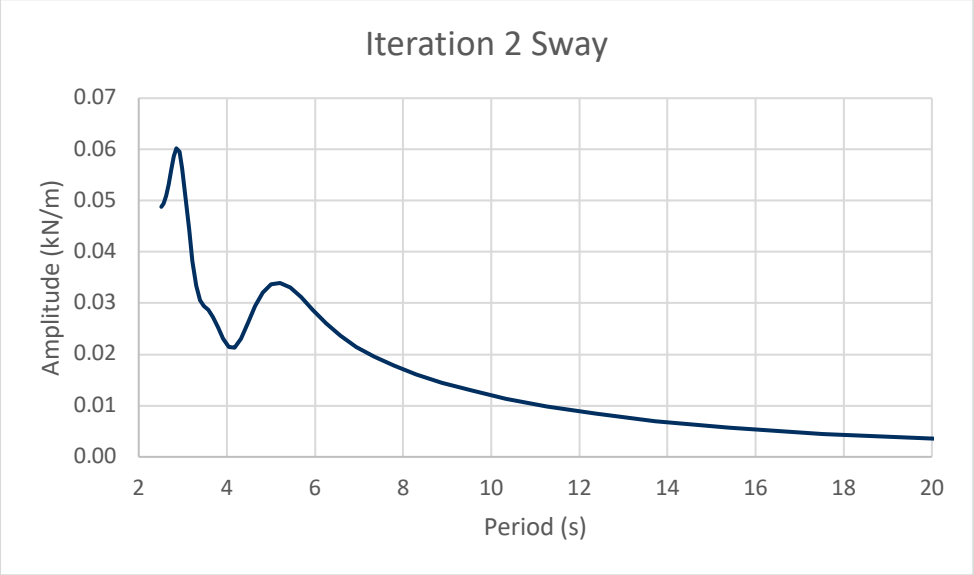

Figure C14: Iteration 2 Sway RAO

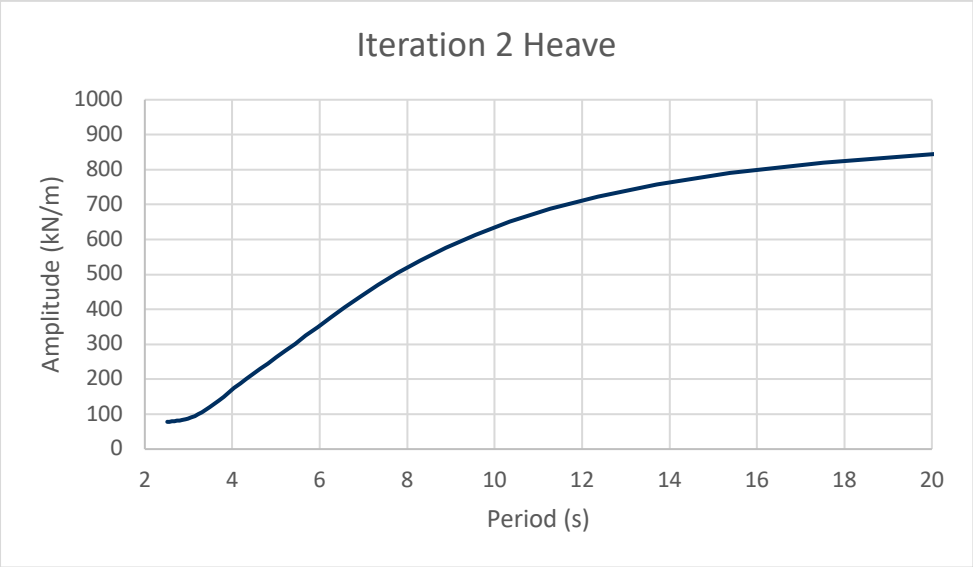

Figure C15: Iteration 2 Heave RAO

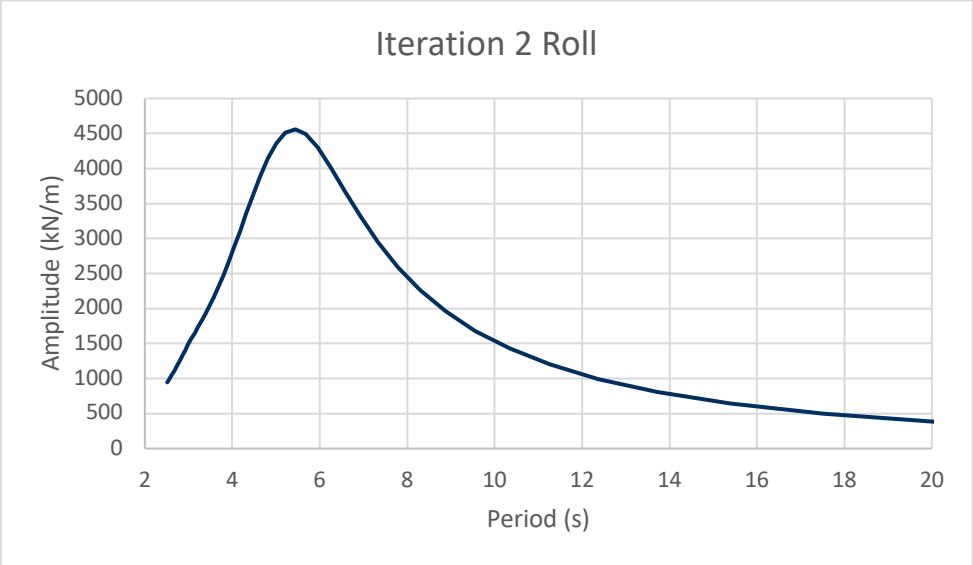

Figure C16: Iteration 2 Roll RAO

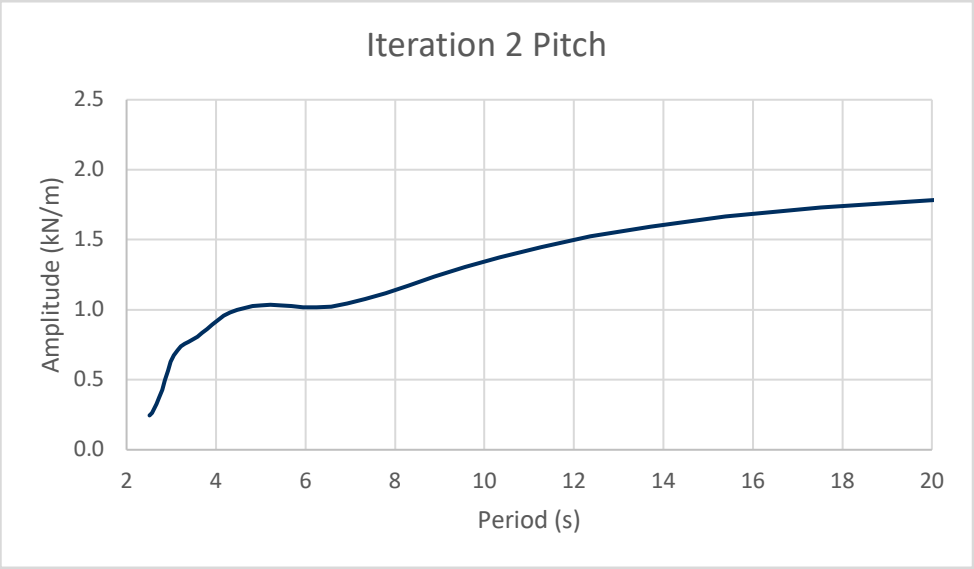

Figure C17: Iteration 2 Pitch RAO

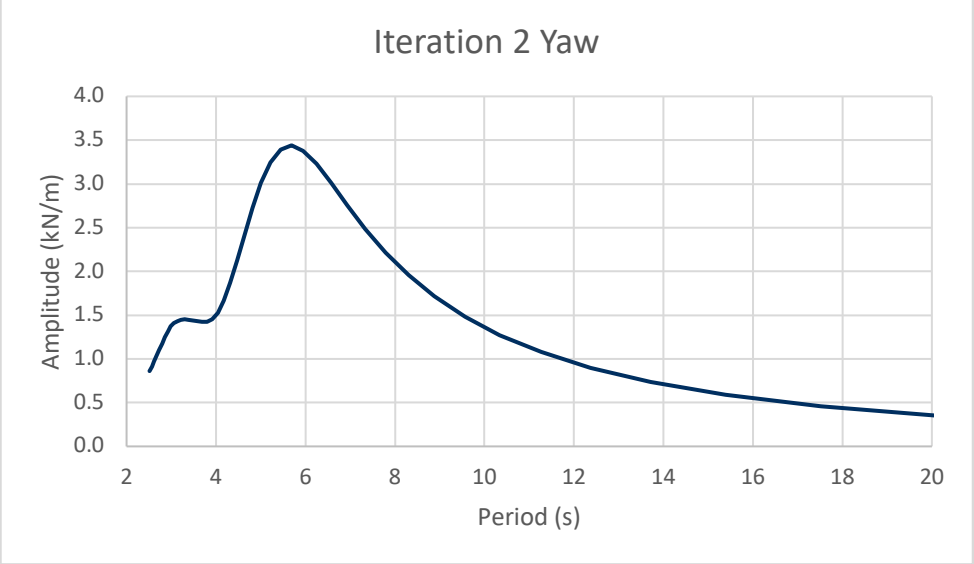

Figure C18: Iteration 2 Yaw RAO

9.3.4 Iteration 4

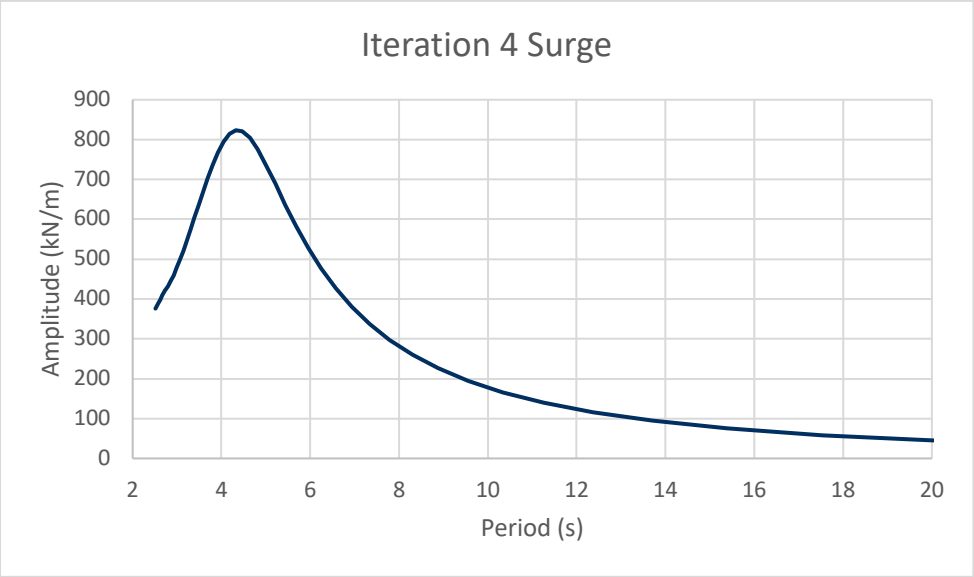

Figure C19: Iteration 4 Surge RAO

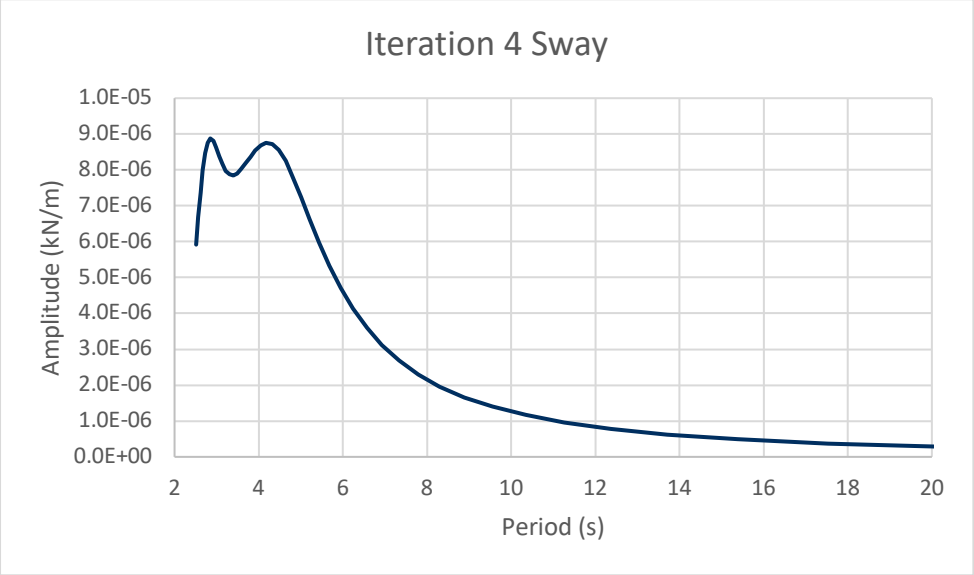

Figure C20: Iteration 4 Sway RAO

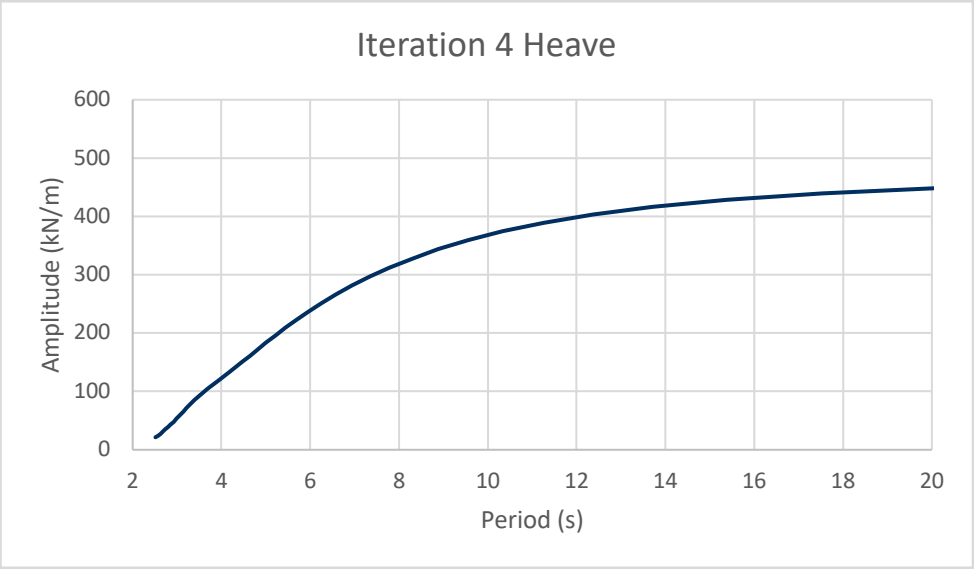

Figure C21: Iteration 4 Heave RAO

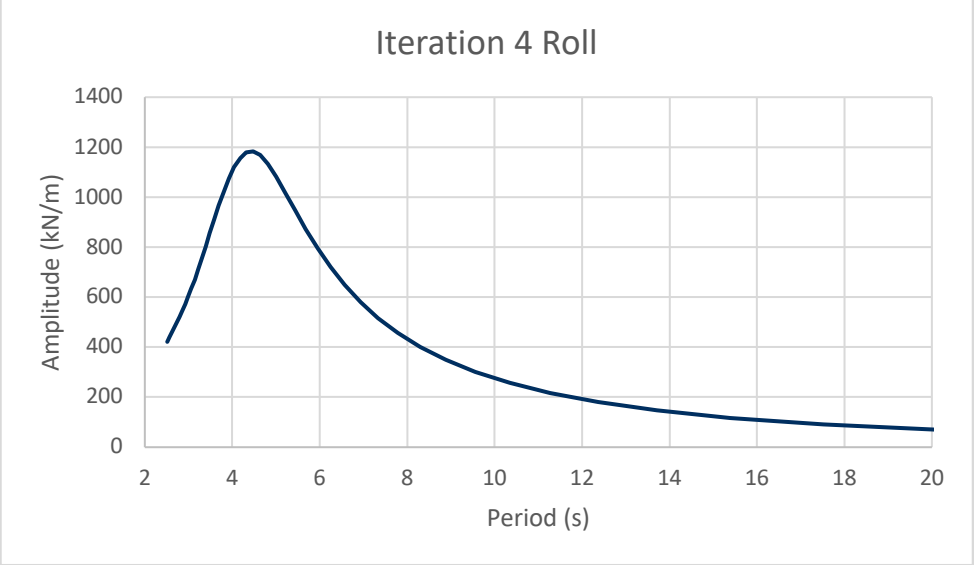

Figure C22: Iteration 4 Roll RAO

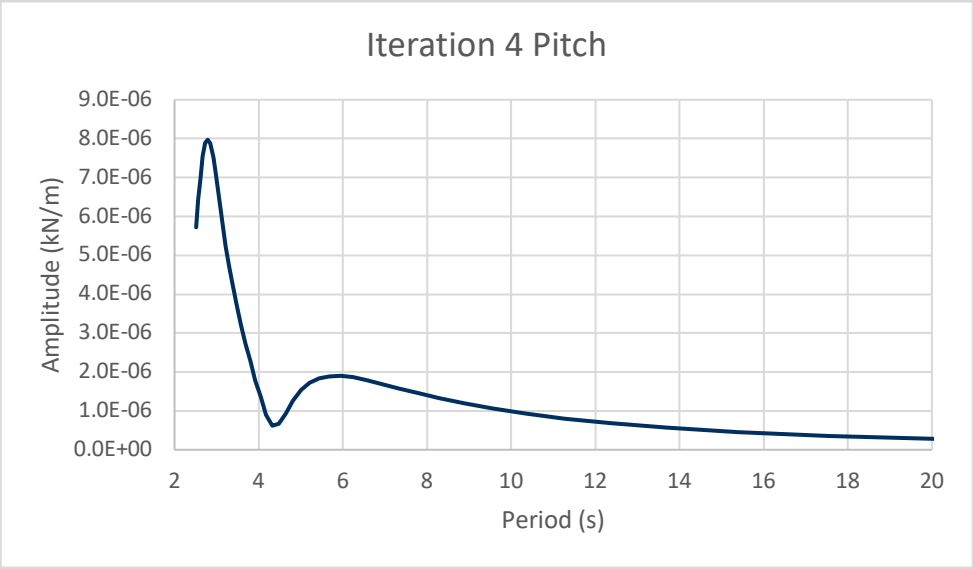

Figure C23: Iteration 4 Pitch RAO

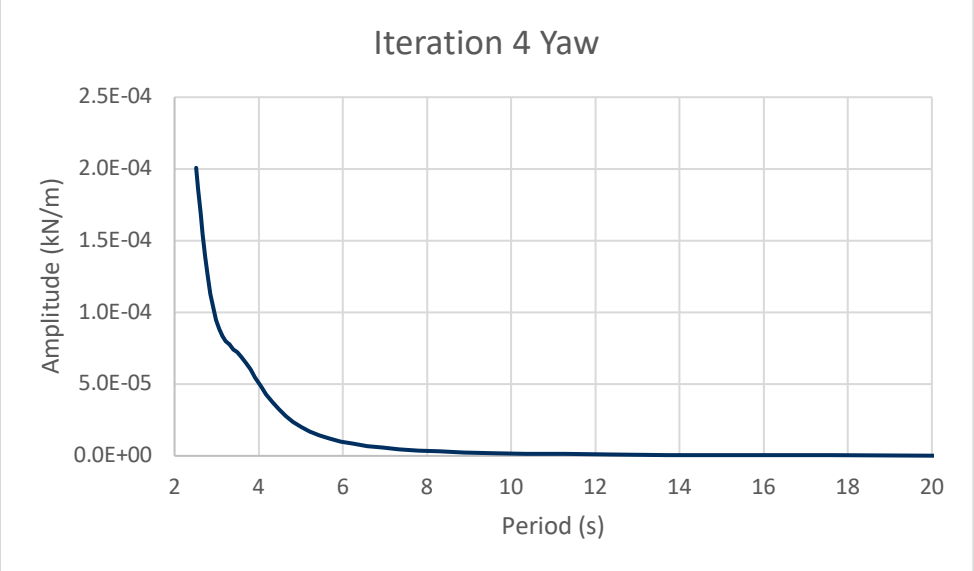

Figure C24: Iteration 4 Yaw RAO

9.4 Appendix D: Winch Line Velocities

The following tables show the maximum, minimum, mean positive, and mean negative velocities in the wave ward and leeward winches for the Base Model and all iterations. Since the system can generate power during both the pay out and the pay in of the mooring lines, means of the positive velocities and negative velocities were averaged separately. For the Iteration 2 model during the 4s period waves, Winch 1 saw no negative velocity and Winch 3 saw no positive velocity. Therefore, the mean negative velocity of Winch 1 and the mean positive velocity of Winch 3 have no value. All data in the following

tables was taken over the first five wave cycles for regular waves with a height of 1.75m and a winch damping constant of 0.068 kN s m^{-1}.

Table D1: Winch 1 Maximum Velocity

Wave Period [s]	Velocity [m/s]				
	Base Model	Iteration 1	Iteration 2	Iteration 3	Iteration 4
4	0.299	0.449	0.317	1.878	0.349
5	0.090	0.162	0.259	1.237	0.134
6	0.106	0.028	0.124	1.084	0.054
7	0.117	0.050	0.035	0.831	0.040
8	0.131	0.040	0.021	0.610	0.031
9	0.157	0.045	0.030	0.557	0.035
10	0.187	0.039	0.031	0.517	0.039
11	0.271	0.043	0.027	0.483	0.044
12	0.278	0.048	0.023	0.454	0.049
13	0.550	0.053	0.024	0.427	0.055
14	0.461	0.059	0.026	0.400	0.060

Table D2: Winch 1 Minimum Velocity

Wave Period [s]	Velocity [m/s]				
	Base Model	Iteration 1	Iteration 2	Iteration 3	Iteration 4
4	-0.161	-0.216	0.169	-1.830	-0.117
5	-0.114	-0.200	-0.095	-1.122	-0.124
6	-0.109	-0.084	-0.152	-1.350	-0.092
7	-0.120	-0.052	-0.069	-0.846	-0.061
8	-0.127	-0.048	-0.038	-0.732	-0.036
9	-0.153	-0.047	-0.028	-0.632	-0.036
10	-0.181	-0.041	-0.030	-0.573	-0.039
11	-0.220	-0.041	-0.027	-0.526	-0.043
12	-0.244	-0.047	-0.023	-0.488	-0.048
13	-0.362	-0.053	-0.023	-0.454	-0.054
14	-0.437	-0.058	-0.025	-0.428	-0.059

Table D3: Winch 3 Maximum Velocity

Wave Period [s]	Velocity [m/s]				
	Base Model	Iteration 1	Iteration 2	Iteration 3	Iteration 4
4	0.118	0.264	-0.143	1.088	0.160
5	0.102	0.157	0.164	0.878	0.099
6	0.094	0.081	0.130	1.032	0.079
7	0.106	0.051	0.066	0.652	0.048
8	0.119	0.046	0.038	0.662	0.032
9	0.147	0.040	0.028	0.593	0.033
10	0.175	0.036	0.029	0.544	0.037
11	0.227	0.041	0.023	0.498	0.041
12	0.238	0.047	0.020	0.461	0.046
13	0.445	0.052	0.023	0.433	0.052
14	0.404	0.058	0.025	0.405	0.057

Table D4: Winch 3 Minimum Velocity

Wave Period [s]	Velocity [m/s]				
	Base Model	Iteration 1	Iteration 2	Iteration 3	Iteration 4
4	-0.112	-0.374	-0.283	-1.424	-0.300
5	-0.089	-0.146	-0.233	-1.220	-0.118
6	-0.095	-0.040	-0.112	-0.815	-0.060
7	-0.101	-0.049	-0.025	-0.684	-0.030
8	-0.123	-0.039	-0.025	-0.539	-0.026
9	-0.151	-0.038	-0.030	-0.521	-0.033
10	-0.177	-0.036	-0.030	-0.493	-0.037
11	-0.208	-0.042	-0.024	-0.458	-0.043
12	-0.237	-0.047	-0.020	-0.426	-0.047
13	-0.324	-0.053	-0.024	-0.400	-0.052
14	-0.351	-0.059	-0.026	-0.378	-0.058

Table D5: Winch 1 Average Positive Velocity

Wave Period [s]	Velocity [m/s]				
	Base Model	Iteration 1	Iteration 2	Iteration 3	Iteration 4
4	0.205	0.297	0.271	0.928	0.218
5	0.043	0.100	0.187	0.748	0.080
6	0.061	0.014	0.072	0.643	0.027
7	0.070	0.020	0.018	0.531	0.019
8	0.082	0.019	0.009	0.399	0.018
9	0.097	0.023	0.011	0.367	0.021
10	0.115	0.024	0.013	0.338	0.024
11	0.128	0.027	0.013	0.314	0.027
12	0.147	0.030	0.013	0.293	0.030
13	0.240	0.033	0.014	0.275	0.034
14	0.209	0.037	0.016	0.258	0.038

Table D6: Winch 1 Average Negative Velocity

Wave Period [s]	Velocity [m/s]				
	Base Model	Iteration 1	Iteration 2	Iteration 3	Iteration 4
4	-0.086	-0.120	NaN	-1.006	-0.069
5	-0.052	-0.130	-0.040	-0.696	-0.075
6	-0.063	-0.047	-0.089	-0.808	-0.045
7	-0.073	-0.022	-0.040	-0.534	-0.025
8	-0.080	-0.021	-0.018	-0.451	-0.020
9	-0.096	-0.025	-0.013	-0.397	-0.021
10	-0.113	-0.024	-0.012	-0.361	-0.024
11	-0.132	-0.026	-0.014	-0.330	-0.027
12	-0.149	-0.030	-0.014	-0.307	-0.030
13	-0.159	-0.033	-0.014	-0.287	-0.034
14	-0.187	-0.037	-0.016	-0.270	-0.037

Table D7: Winch 3 Average Positive Velocity

Wave Period [s]	Velocity [m/s]				
	Base Model	Iteration 1	Iteration 2	Iteration 3	Iteration 4
4	0.050	0.188	NaN	0.654	0.113
5	0.053	0.090	0.086	0.601	0.053
6	0.054	0.037	0.080	0.637	0.039
7	0.064	0.023	0.036	0.415	0.020
8	0.075	0.022	0.017	0.413	0.017
9	0.093	0.021	0.013	0.374	0.020
10	0.110	0.022	0.014	0.341	0.023
11	0.129	0.026	0.013	0.313	0.026
12	0.146	0.029	0.012	0.291	0.029
13	0.177	0.033	0.014	0.272	0.033
14	0.189	0.037	0.016	0.254	0.036

Table D8: Winch 3 Average Negative Velocity

Wave Period [s]	Velocity [m/s]				
	Base Model	Iteration 1	Iteration 2	Iteration 3	Iteration 4
4	-0.039	-0.236	-0.237	-0.790	-0.186
5	-0.043	-0.080	-0.168	-0.733	-0.054
6	-0.056	-0.021	-0.070	-0.456	-0.027
7	-0.062	-0.021	-0.017	-0.427	-0.014
8	-0.077	-0.019	-0.011	-0.366	-0.015
9	-0.094	-0.020	-0.012	-0.346	-0.019
10	-0.112	-0.021	-0.013	-0.318	-0.023
11	-0.128	-0.026	-0.012	-0.297	-0.026
12	-0.147	-0.030	-0.012	-0.276	-0.029
13	-0.158	-0.033	-0.014	-0.258	-0.033
14	-0.182	-0.037	-0.016	-0.244	-0.037

The following tables present the maximum, minimum, mean positive, and mean negative velocities of the wave ward and leeward winches for the Iteration 1 model in the reduced wave height sea states. Separate means of the positive velocities and the negative velocities were taken since the system can generate power during both the pay out and pay in of the mooring lines. The data is taken from the entire three-hour simulation for each case.

Table D9: Irregular Wave Winch 1 Velocities

Significant Wave Height [m]	Peak Period [s]	Winch1 Velocity [m/s]			
		Maximum	Minimum	Mean Positive	Mean Negative
0.5	7.5	0.276	-0.268	0.080	-0.080
0.5	9.5	0.152	-0.160	0.050	-0.050
1.0	7.5	1.221	-1.237	0.464	-0.464
1.0	9.5	0.403	-0.388	0.137	-0.136

Table D10: Irregular Wave Winch 3 Velocities

Significant Wave Height [m]	Peak Period [s]	Winch3 Velocity [m/s]			
		Maximum	Minimum	Mean Positive	Mean Negative
0.5	7.5	0.255	-0.266	0.082	-0.082
0.5	9.5	0.160	-0.161	0.049	-0.050
1.0	7.5	1.082	-1.092	0.449	-0.448
1.0	9.5	0.511	-0.534	0.145	-0.144

9.5 APPENDIX E: UNIVERSITY OF IOWA WAVE TANK SPECIFICATIONS

Wave Basin Wave Generation and Beach Information

Deep-water wave generation:

Wavemaker type	6-segment plunger
Wave period	0.5 s – 2.5 s
Deep Water wave amplitude	0 – 250 mm

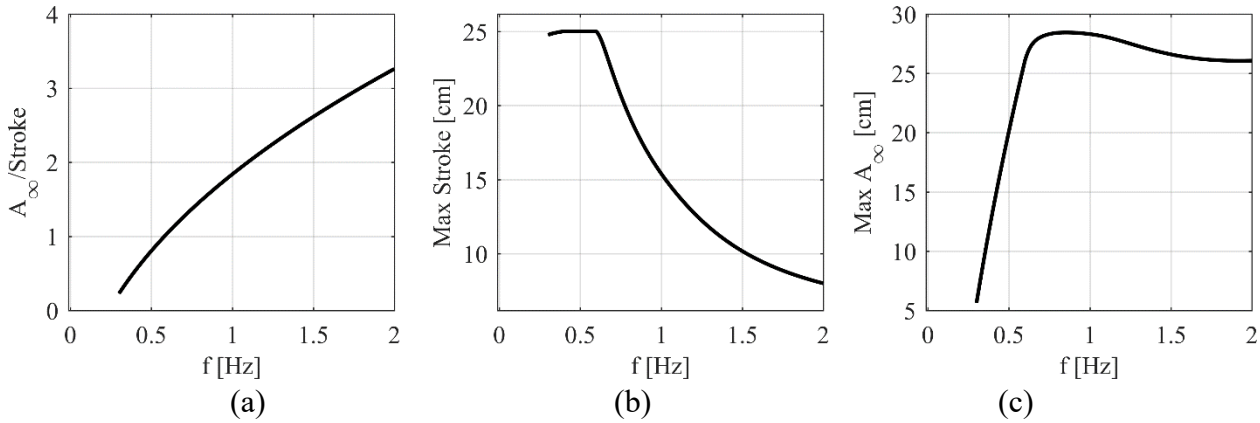

Figure 1 (a) Wavemaker transfer function; (b) Wavemaker excursion limits; (c) Maximum wave amplitude (deep water) as a function of frequency

Beach Geometry

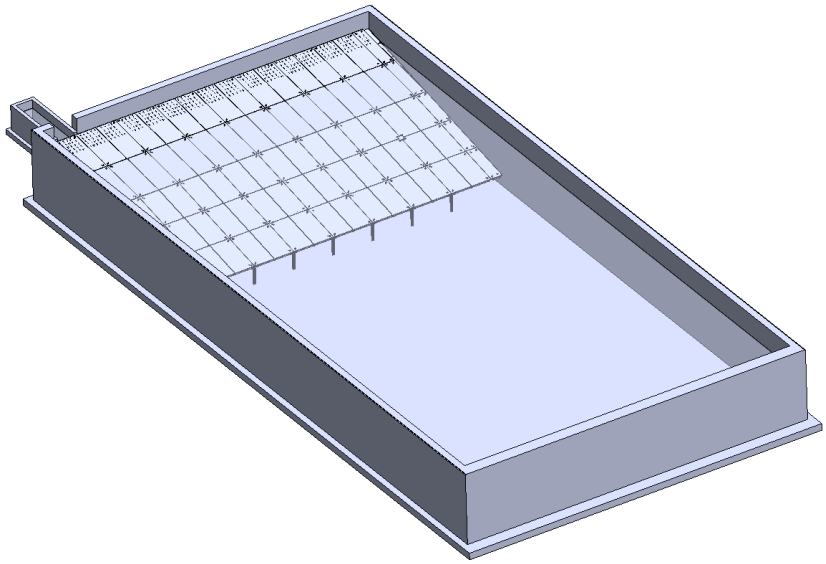

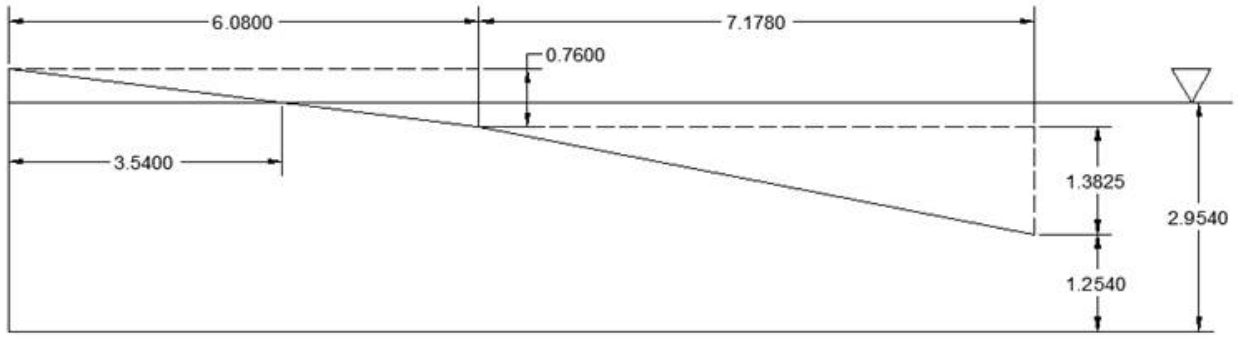

Breaking Wave Generation

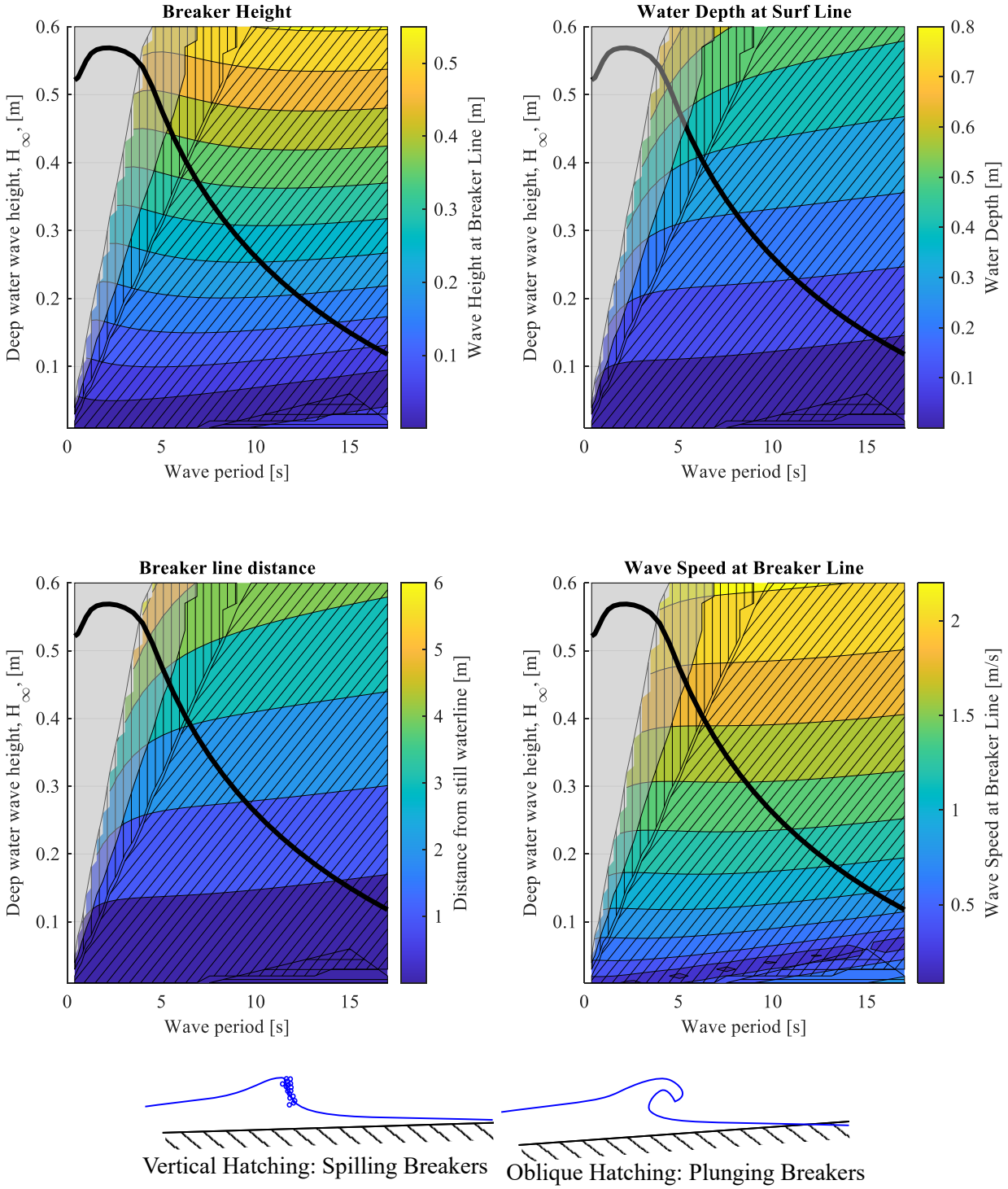

Figure 2: Modeled breaker height, water depth at the breaker line, breaker line distance, and breaker celerity. Bold black line indicates limit of deep-water wave generation by IIHR wavemaker.

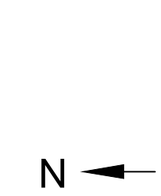

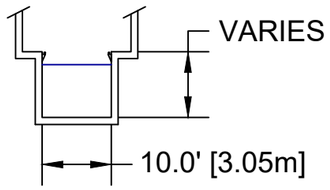

TYPICAL
CROSS SECTION